ENHANCED CONTROL OF PHOTOVOLTAIC POWER CONVERTERS UNDER MISMATCHING CONDITIONS

Thesis

Submitted in partial fulfillment of the requirements for the degree of

DOCTOR OF PHILOSOPHY

by

VANJARI VENKATA RAMANA

DEPARTMENT OF ELECTRICAL AND ELECTRONICS ENGINEERING,

NATIONAL INSTITUTE OF TECHNOLOGY KARNATAKA,

SURATHKAL, MANGALORE -575025

JULY, 2019

DECLARATION

by the Ph.D. Research Scholar

I hereby *declare* that the Research Thesis entitled Enhanced control of photovoltaic power converters under mismatching conditions which is being submitted to the National Institute of Technology Karnataka, Surathkal in partial fulfillment of the requirement for the award of the Degree of Doctor of Philosophy in Electrical and Electronics Engineering is a *bonafide report of the research work carried out by me.* The material contained in this Research Thesis has not been submitted to any University or Institution for the award of any degree.

....
Vanjari Venkata Ramana, 165022EE16F08
Department of Electrical and Electronics Engineering

Place: NITK-Surathkal
Date:

CERTIFICATE

This is to *certify* that the Research Thesis entitled Enhanced control of photovoltaic power converters under mismatching conditions submitted by Vanjari Venkata Ramana (Register Number: EE16F08) as the record of the research work carried out by him, is *accepted as the Research Thesis submission* in partial fulfillment of the requirements for the award of degree of Doctor of Philosophy.

Dr. B. Venkatesaperumal
(Research Guide)

Prof. K.N. Shubhanga
(Chairman-DRPC, EEE dept.)

Acknowledgements

Abstract

Exhausting fossil fuel, a huge increase in oil prices, global warming, damage to environment, increasing energy demand are major problems being faced. In order to avoid these problems, power generation is being done using renewable energy sources. Among the renewable energy sources, solar photovoltaic (PV) is dominant because of long operational life, lesser emission, decreasing cost of solar photovoltaic panels. Photovoltaic sources exhibit unique maximum power point under uniform conditions. Under mismatching conditions, there will be multiple peak points because of the presence of bypass diodes. Maximum power point tracking algorithm is used to track the maximum power from the PV source.

This thesis presents a literature review of maximum power point tracking (MPPT) algorithms for tracking the global peak. The methodology employed for tracking maximum power point is classified as empirical methods, perturbation methods, model-based methods, artificial intelligence methods, evolutionary computing methods, scanning-based methods, and modified perturbation methods. Based on the literature survey, research gaps are identified and are presented as objectives for this thesis.

Four maximum power point tracking algorithms capable of tracking global peak under mismatching conditions are proposed. The first algorithm is based on searching technique and bisection method in which zone wise division of characteristics is performed based on open circuit voltage and panel characteristics. It is a duty ratio based control method and the value of duty ratio is calculated based on bisection method until the global peak is detected. Once the global peak is detected, conventional perturb and observe method is used to retain the operating point at GP.

The second algorithm is based on current control in which reference current is moved in the forward and backward direction by multiplying or dividing PV current with 0.9. The movement of PV current is continued in the backward direction until the operating voltage is less than minimum voltage below which there is no chance of occurrence of global peak. After that, the perturbation of PV current is continued in the forward direction until the operating current is less than minimum current below

which there is no chance of occurrence of global peak. During the process of perturbation, the maximum power point is identified and a conventional algorithm is used to retain the operating point at that point.

The third algorithm uses reference voltage control and reference current control to track the global peak. The choice to use voltage or current control is made using a decision variable. The algorithm operates in the current control mode to find the nearest peak and operates in voltage control mode to identify the inflection point. Initially, the voltage below which there is no chance of occurrence of the global peak is identified and it is initialized as the reference voltage. Then the succeeding peak is identified using reference current control. Once the peak is determined, reference voltage control is used to identify the inflection point. This process is continued until the operating PV current is less than the minimum possible current.

The fourth algorithm tracks the global peak by sampling variations in the transient period during charging of the input capacitor. The algorithm operates in three stages viz., scanning, correcting and retaining the operating point at MPP. In the scanning stage, the maximum power and voltage at maximum power are identified by changing the value of duty ratio from maximum to minimum value. The correcting stages bring the operating point close to the voltage at maximum power point by varying the duty ratio and retaining stage maintains the operating point at MPP.

The simulation studies of all the four MPPT algorithms are performed in MATLAB. All the methods are compared with recent existing MPPT methods in the literature. Hardware implementation is performed using solar array simulator, the boost converter, and resistive load.

Contents

List of Figures

List of Tables

Nomenclature

AC	Alternating current
ABC	Artificial bee colony
ACO	Ant colony optimization
ADC	Analog to digital converter
ANN	Artificial neural network
DAC	Digital to analog converter
DC	Direct current
DE	Differential evolution
FF	Flashing fireflies
FOA	Firefly optimization algorithm
FOCV	Fractional open circuit voltage
FLC	Fuzzy logic controller
FSCC	Fractional short circuit current
GMPPT	Global maximum power point tracking
GP	Global peak
GPV	Global peak value
GPT	Global peak tracking
HC	Hill climbing
IC	Implementation complexity
INC	Incremental conductance
INP	Inflection point
NN	Neural Network
LPSO	Leader particle swarm optimization
MPP	Maximum power point
MPPT	Maximum power point tracking
LP	Local peak
OCP	Open circuit point
PSO	Particle swarm optimization
PV	Photovoltaic
PWM	Pulse width modulation
SCP	Short circuit point
TS	Tracking speed

TR	Transient response
SSR	Steady state response
STC	Standard test conditions
VCC	Voltage and current control
VWS	Voltage window search
δ_I	ratio of current at MPP to short circuit current
δ_V	ratio of voltage at MPP to open circuit voltage
ΔI	Change in current
ΔP	Change in power
ΔP_m	Change in maximum power
ΔV	Change in voltage
a	diode ideality factor
C_i	input capacitance of boost converter
C_o	output capacitance of boost converter
d	duty ratio
d_{min}	minimum value of duty ratio
d_{max}	maximum value of duty ratio
f_s	switching frequency of boost converter
G	Irradiance
I	PV current
I_{min}	minimum current of PV array below which there will be no GP
I_o	Output current
I_{omin}	minimum value of load current
I_{omax}	maximum value of load current
I_{sc}	Short circuit current
I_{scn}	Short circuit current at standard test conditions
I_{scm}	Short circuit current of single module
I_{sct}	Short circuit current of total array
I_{ph}	Light generated current
I_r	reverse saturation current of diode
I_{ref}	Reference current
k	Boltzmann constant
L	inductance of boost converter
N_{pp}	Number of strings in parallel

N_s	Number of cells in series in a module
N_ss	Number of series connected modules (string)
P_crit	critical value of power for detecting change in shading pattern
P_max	maximum power of PV array
q	electron charge
R_load	equivalent resistance of load
R_loadmin	minimum value of load resistance
R_loadmax	maximum value of load resistance
R_pvmax	maximum resistance of PV array
R_p	Parallel resistance
R_pv	equivalent resistance of PV array
R_pvmin	minimum resistance of PV array
R_pvmax	maximum resistance of PV array
R_s	Series resistance
T	Temperature
V	PV voltage
V_crit	critical value of voltage
V_min	minimum voltage of PV array below which there will be no GP
V_mp	Voltage at maximum power point
V_mpn	Voltage at maximum power point at standard test conditions
V_o	Output voltage
V_oct	Open circuit voltage of total array
V_oc	Open circuit voltage
V_ocn	Open circuit voltage at standard test conditions
V_ocm	Open circuit voltage of single module
V_oct	Open circuit voltage of total array
V_ref	Reference voltage

Chapter 1

INTRODUCTION

Contents

1.1 Background

The increase in energy demand, skyrocketing oil prices, greenhouse gases and environmental threats arising due to the generation of electricity from fossil fuels, led to finding out an alternative for the generation of power. Power generation from renewable energy is increasing abundantly. Various researchers explored renewable energy sources like solar, wind, and micro-hydro for production of electricity. Energy from the sun for the generation of electricity can be extracted using two technologies. They are solar thermal and solar photovoltaic. Solar thermal utilizes heat for the generation of thermal energy or electrical energy. On the other hand, solar photovoltaic (PV) generates electricity using light energy from the sun (Schellnhuber, 2004).

PV cell converts light energy into electrical energy based on the photovoltaic effect. PV cell is a semiconductor diode. The p-n junction of it is exposed to light (Sedra and Smith, 1998). Charge carriers are generated from the PV cell when the light is incident on it and the electric current will flow if the cell is short-circuited. When the energy of incident photon on the PV cell is greater than the band gap energy of the cell, then covalent electron of the semiconductor will get detached from the valence band. The wavelength of the incident light and semiconductor material are the crucial parameters in this process. Absorption of solar radiation, generation, and transportation of charge carriers in the device and collection of charge carriers at the terminals of the PV cell are the basic processes that happen in PV cell (Villalva et al., 2009).

The variants of PV cell are classified as shown in Fig. 1.1. PV cells are classified based on the material used for constructing them. They are crystalline silicon, thin film, multi-junction, dye-sensitized and organic solar cells. Crystalline silicon is classified as mono-crystalline and multi-crystalline PV cells. Mono-crystalline cells are manufactured from a single crystal of silicon. These are more efficient and expensive. Multicrystalline silicon solar cells are made from cast square ingots. These are less expensive and less efficient than monocrystalline solar cells.

Thin-film cells are done by reducing the active materials in the cell. Thin films are classified as amorphous and cadmium telluride solar cells. Amorphous cells as old as crystalline solar cells. These are easy for production and has lesser efficiency than crystalline solar cells. CdTe solar cells are easier to make and are less expensive. The efficiency of CdTe solar cells is very less. However, they are used in large scale

installations.

Multi-junction cells consist of multiple thin films. They are done by growing one solar cell on the other. The band gap energy of each layer is different allowing to absorb electromagnetic radiation over a different portion of the spectrum. The initial applications of these cells are specific to satellite and space exploration. Currently, these are used in terrestrial concentrator photovoltaic applications (CPV). Organic solar cells are built from thin films which include polymers. These are done in roll to roll printing process which leads to inexpensive large scale production. The cell efficiencies are low.
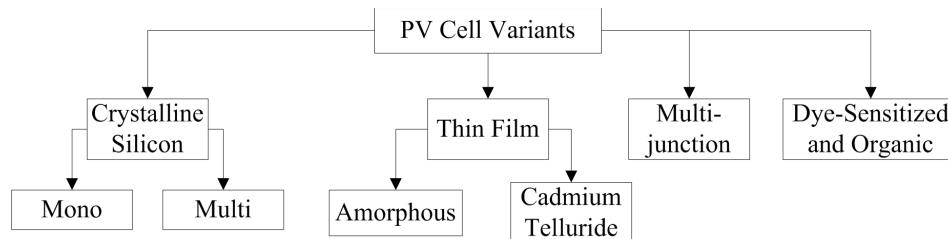
Figure 1.1: Classification of variants of PV cell

PV cell is the fundamental unit of PV power generation unit. A single PV cell produces around 0.7 V. In order to increase the voltage capability of the PV system, PV cells are connected in series to form modules. The modules are commercially available. For a further increase in voltage capability or current capability, PV modules are connected in series or parallel to form panels. PV panels are connected in series or parallel to form arrays. The output of the PV module is direct current (DC). For interfacing the PV module with grid-connected systems or standalone systems with alternating current (AC) load, power conversion to AC is inevitable. The power conversion is done using power electronic devices. The physical process of conversion of light energy into electrical energy in PV cell is less efficient. So, the electrical output of the PV system should be dealt with utmost care for utilizing it to the maximum extent (Villalva et al., 2009).

1.2   Photovoltaic System

The generalized block diagram of the complete PV system is presented in Fig. 1.2.

1. **PV Source:** PV source contains a PV module or a group of PV modules

connected either in series or parallel or both. Commercially PV modules are available in different types: monocrystalline, polycrystalline and thin-film.

2. **Power Interface:** Power Interface can be either a DC-DC converter or DC-AC converter. A DC-DC converter is used for DC loads. DC-AC is used for AC loads or grid connection. For AC loads or grid, either single stage (only DC-AC) or two stages (both DC-DC and DC-AC) can be employed.
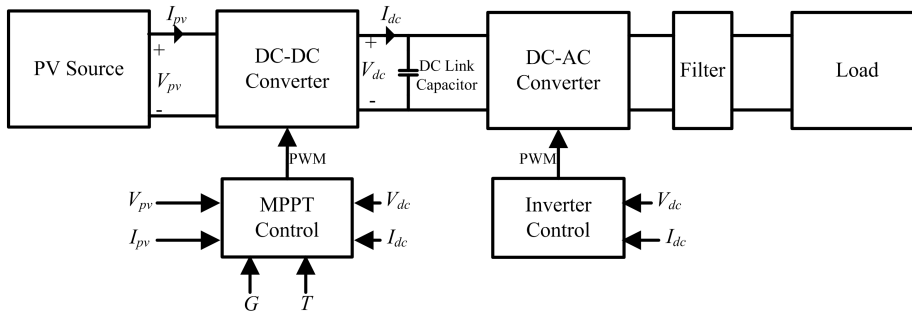
Figure 1.2: Generalized Block Diagram

3. **Load:** Load can be resistive, battery, ac loads and grid-connected system

4. **Controller:** For a single stage system, only one control can be employed. The control can be either for maximum power point or for constant DC link voltage. For two-stage, two separate controls are required. The inputs to the controller depend on the type of the algorithm and application. For maximum power point tracking either irradiance (G) and temperature (T) or PV voltage (V) and PV current (I) are used as inputs. For voltage control, the output voltage of the DC-DC converter (V_{dc}) or output current of the DC-DC converter (I_{dc}) can be used. The output of the controller is duty ratio which will be converted into pulses for switches of the converter.

1.3 PV Modeling

PV manufacturers provide a datasheet which contains a set of empirical data. This data can be used by the designers for mathematically modeling a PV module. The crucial parameters in the PV module datasheet are open circuit voltage (V_{ocn}), short circuit current (I_{scn}), voltage at the maximum power point (V_{mpn}), current at the

maximum power point (I_{mpn}), voltage temperature coefficient (K_v), current temperature coefficient (K_i) and the number of cells connected in series in a module. The datasheet also contains experimental curves for irradiance and temperature. All the data available in the datasheet are at standard test conditions (STC). The mathematical model can be adjusted based on the data available in the datasheet.

The inputs to the PV model are irradiance (G) and temperature (T) and the output is the equivalent circuit parameters of the PV module. The temperature dependence on output parameters is presented in (Skoplaki and Palyvos, 2009). Single diode model, two diode model, three diode model, and dynamic model, are the different types of equivalent circuit models available in the literature for representing the PV module. The equivalent circuit parameters of the PV model are photovoltaic current (I_{ph}), diode reverse saturation current (I_{r}), shunt resistance (R_{p}), series resistance (R_{s}) and diode ideality factor (a). The current obtained from the PV source depends on the amount of solar radiation falling on PV Surface. The amount of solar irradiation falling on PV source is proportional to the current produced by the PV source and it is represented by a current source (I_{ph}) in the equivalent circuit model. The recombinations taking place in the quasi-neutral region is represented by diode D. The resistance offered to the flow of current in the PV module is represented by series resistance (R_{s}). The resistance offered to the leakage current of the PV module is represented by shunt resistance (R_{p}). Single diode model is represented in Fig. 1.3. By applying KCL to Fig. 4.3(a), equation (1.1) is deduced.

$$ I = I_{\mathrm{ph}} - I_{\mathrm{r}} \left\{ exp\left(\frac{q\left(V + IR_{\mathrm{s}}\right)}{akTN_{\mathrm{s}}} \right) - 1 \right\} - \frac{V + IR_{\mathrm{s}}}{R_{\mathrm{p}}} \tag{1.1} $$

where k is the Boltzmann constant, q is electron charge, V is the output voltage of the PV module and I is the output current of the PV module.

A detailed review of modeling PV array is presented in (Jena and Ramana, 2015).

1.4 Characteristics of P-V Array

1.4.1 Uniform Conditions

Under uniform conditions, all the modules connected together exhibit the same electrical characteristics. If all the modules are in uniform condition and N_{ss} be the number of series connected modules (string) and N_{pp} is number of strings connected
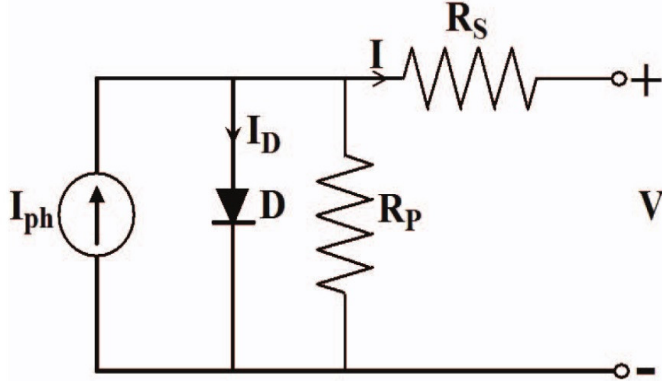
Figure 1.3: Single Diode Model

in parallel, then (1.1) is modified as (1.2).

$$I = I_{\mathrm{ph}}N_{\mathrm{pp}} - I_0 N_{\mathrm{pp}} \left\{ exp\left(\frac{q\left(V + IR_{\mathrm{s}}\frac{N_{\mathrm{ss}}}{N_{\mathrm{pp}}}\right)}{akTN_{\mathrm{s}}N_{\mathrm{ss}}} \right) - 1 \right\} - \frac{V + IR_{\mathrm{s}}\frac{N_{\mathrm{ss}}}{N_{\mathrm{pp}}}}{R_{\mathrm{p}}\frac{N_{\mathrm{ss}}}{N_{\mathrm{pp}}}} \qquad (1.2)$$

where N_{ss} is number of modules connected in series (string) ans N_{pp} is number of strings connected in parallel.

By solving (1.2) for I and V, the characteristics of the PV module are obtained. The current-voltage (I-V) characteristics of the PV module are presented in Fig. 1.4(a). The PV Power(P) is obtained as a product of PV voltage (V) and PV current (I). There are three important points in the I-V curve. They are open circuit point (OCP), short circuit point (SCP) and maximum power point (MPP). At OCP, $I{=}0$, $V = V_{\mathrm{oc}}$. At SCP, $V{=}0$, $I = I_{\mathrm{sc}}$. At MPP, $I{=}I_{\mathrm{mp}}$, $V = V_{\mathrm{mp}}$ i.e., at this point maximum power from the PV module can be obtained. For a PV module, there exists a unique maximum power point under uniform conditions.

1.4.2   Mismatching Conditions

Mismatching conditions refers to the exhibition of different electrical characteristics by different modules of the same specification that are connected either in series or in parallel. Causes of mismatching conditions are due to factors like shading, soiling, degradation, manufacturing errors, wiring losses, etc (Maghami et al., 2016).

During mismatching conditions, the derated module will limit the current flowing
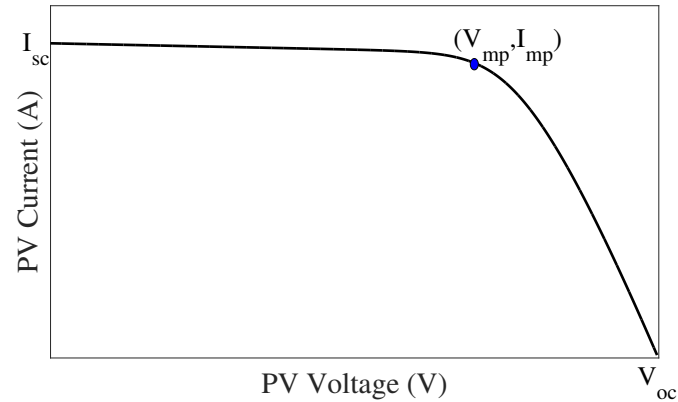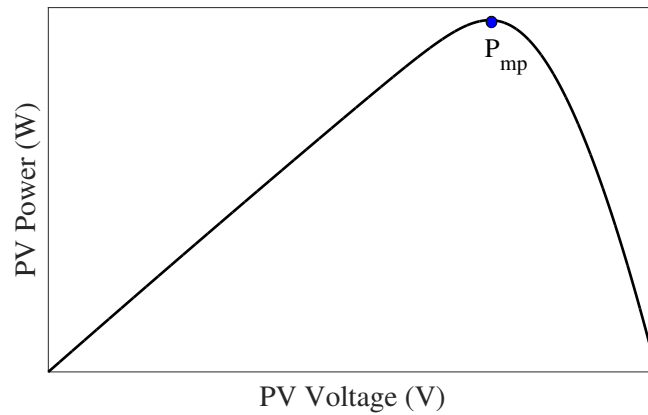
Figure 1.4: (a) *I-V* and (b) *P-V* characteristics of PV module

through the healthy module. The derated module will start acting as load and starts dissipating power. This could lead to the creation of hot-spots in the derated module which could damage it. In order to avoid these undesirable effects, the bypass diode is connected in anti-parallel across a PV module or a PV sub-module (groups of cells in series). The presence of bypass diodes leads to multiple steps in *I-V* curves and multiple peaks in *P-V* curves. Apart from the important operating points mentioned in uniform conditions, the other points are inflection points, local peaks, and global peak. Inflection points (INP) are those in which the step in *I-V* curve originates. Because of the presence of multiple steps in *I-V* curve, there will be multiple peaks in the *P-V* curve. All the peaks are referred to as local peaks. The maximum among the local peaks is the global peak.

In order to analyze the characteristics of the PV source, a PV string comprising

of four series-connected modules is considered. Each module is equipped with two bypass diodes. The practical data from the PV string comprising of four modules is obtained using IV-400 *I-V* tracer. The details of the *I-V* Tracer are presented in Appendix-B. When the four modules are uniformly irradiated, there will be a unique power point. The characteristics of uniform irradiance are presented in Fig. 1.5(a). Performance of PV string will be affected due to losses in the PV system. Predominant loss of power is due to shading, soiling, and degradation. Losses due to shading mainly occur because of trees, passing clouds and the shadow of one module on another module. Fig.1.5(b) shows the characteristics of the string due to the shading of two modules by surrounding buildings. It can be noticed that there are two stairs in *I-V* characteristics and two peaks in *P-V* characteristics. In large PV fields, because of the change in the direction of the sun, there will be shading on PV modules due to other PV modules. In order to study this effect, each of the four modules is shaded unequally by the shades of other PV modules. This led to five stairs in *I-V* characteristics and five peaks in *P-V* characteristics as shown in Fig. 1.5(c). The characteristics due to random human shade are presented in Fig. 1.6(a). Losses on PV array occurring due to deposition of dust, snow, dirt and other small materials on the surface of PV modules are termed as soiling losses. According to case studies presented in (Maghami et al., 2016), there is a significant loss of power due to soiling across the globe. Soiling can cause accumulation of dust blocks on the PV module. Power loss will be significant even if one cell is completely shaded or soiled. In the considered case of four modules, if one cell is completely blocked, the power generation of that particular module will be reduced to half as two bypass diodes are connected to each module. One possible solution to avoid power loss is to keep bypass diodes across each cell. But keeping bypass diodes across each cell is not a viable option as it increases the cost of the system. Fig. 1.6(b) shows the *I-V* and *P-V* characteristics of the PV string because of soiling on PV modules. In this case, two cells in two different modules are blocked with different thickness of soil because of which there are two stairs and two peaks in *I-V* and *P-V* characteristics respectively. There is a decrease in short circuit current because the string is under a cloud. The characteristics of a random shading pattern with the shading of buildings and soiling of panels under cloudy conditions are presented in Fig. 1.6(c).
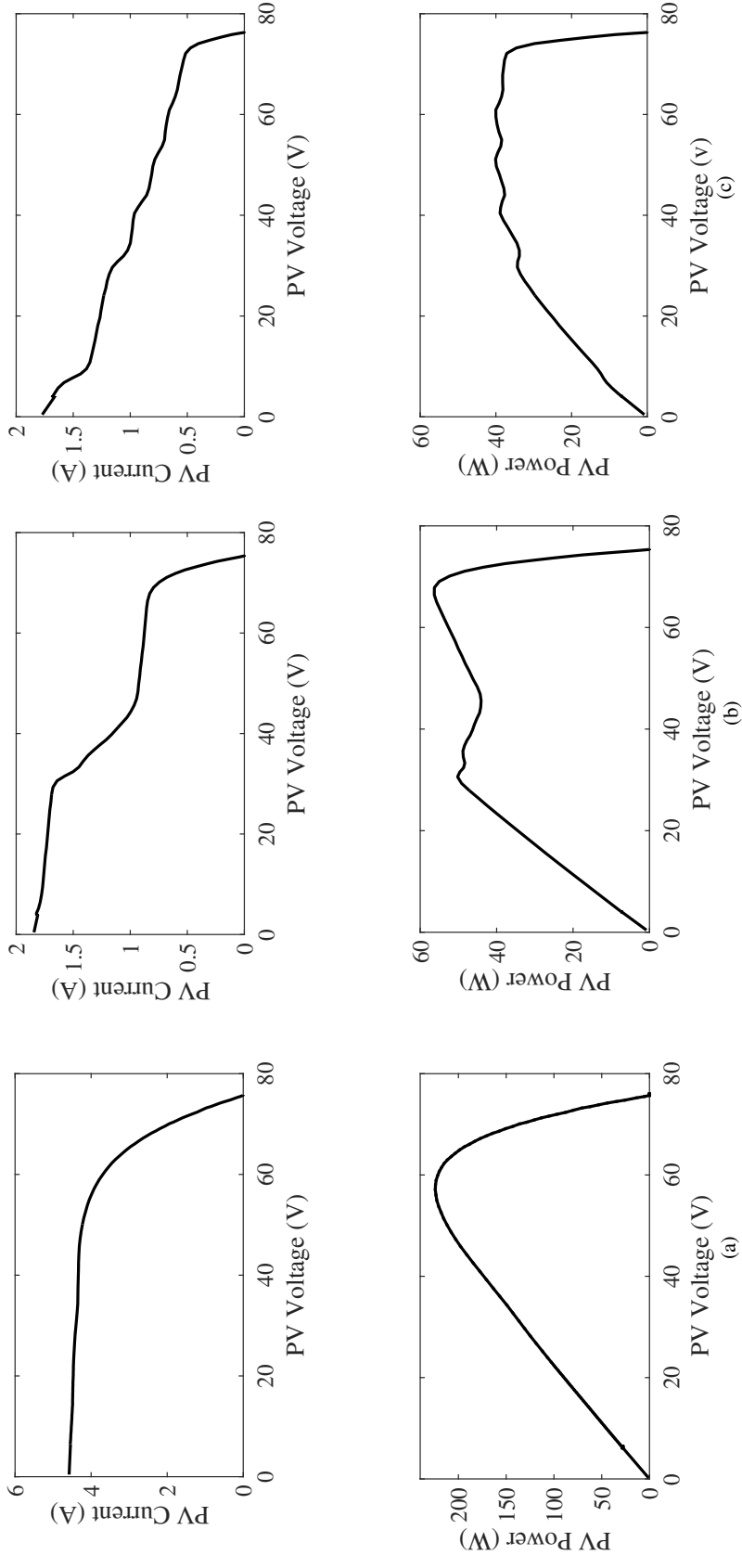
Figure 1.5: *I-V* and *P-V* characteristics: (a) Under uniform irradiance, (b) Shading due to buildings, (c) Modules shaded by other modules
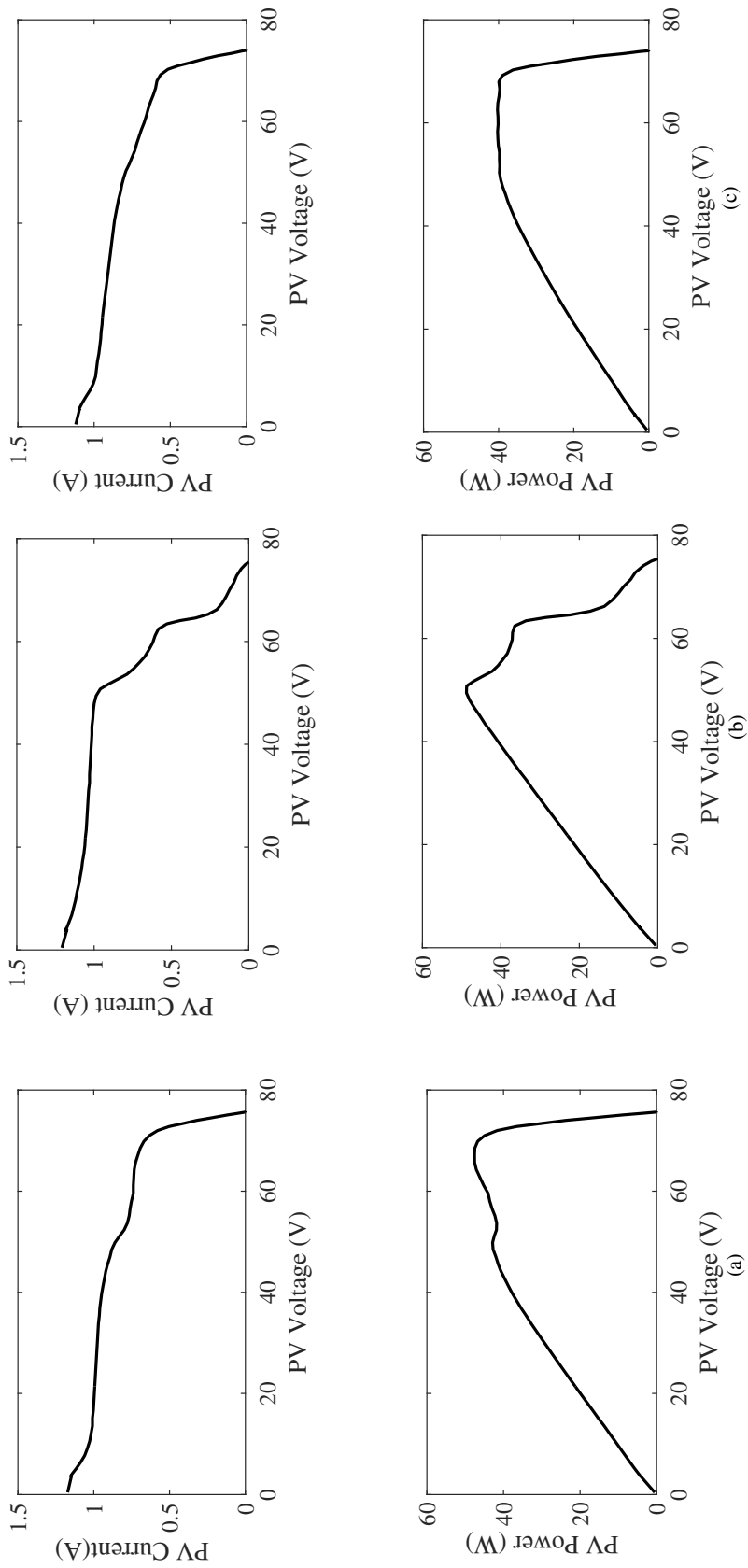
Figure 1.6: *I-V* and *P-V* characteristics: (a) Human shade on modules, (b) One cell in each sub-module blocked with the soil of different thickness under cloudy conditions, (c) Extension of (b) with shading of buildings

Apart from the mentioned losses, the performance of PV modules deteriorate due to aging. As per (Bastidas-Rodrguez et al., 2015), the modules are suffering from early degradation due to the problems like poor maintenance, maximum usage in outdoors and corrosive environments. Because of the degradation, the fill factor of the modules will be reduced (Nguyen and Low, 2010a). If a degraded module is present in the series connected string, then it can affect the performance of the whole string leading to change in characteristics which can be similar to characteristics during partial shading or soiling conditions.

It can be noticed from the P-V curves that there are multiple peak points out of which many are local peaks and one is the global peak. A maximum power point algorithm should be developed such that global peak is to be determined. The simulink model for obtaining the I-V and P-V characteristics under mismatching conditions is presented in Appendix-C.

1.5 Maximum Power Point Tracking

Maximum Power extraction from the PV source will not only depend on irradiance (G) and temperature (T) but also depends on the operating point of the PV source. The concept of maximum power point tracking is based on the operating point matching between the PV array and the power converter. In order to obtain the maximum power, the apparent resistance of the PV module is varied to match it to the resistance at maximum power point (Taghvaee et al., 2013a). Because of varying environmental conditions and non-linearity in characteristics, tracking of MPP becomes a challenging task. In the I-V characteristics there is a unique maximum power point under uniform irradiance. This maximum power point changes with changes in irradiance and temperature. So it is necessary to develop an MPPT algorithm to track the maximum power under varying atmospheric conditions (Nguyen and Low, 2010a).

For mismatching conditions, there exists multiple peaks in P-V curve. Many attempts are made to track maximum power under mismatching conditions. Although all the methods are designed for the same objective, they differ in flexibility, cost speed, and implementation complexity. An effective MPPT algorithm should have high accuracy, higher tracking speed, less complexity, lesser number of sensors, ability to track global peak and lesser oscillations in steady state.

The input to the maximum power point tracking control algorithm will be either

PV voltage and PV current or irradiance and temperature or a combination of any of those. The output will be either duty ratio or reference voltage or reference current. In case of direct duty ratio control, the duty ratio obtained will be sent to the pulse width modulation for the generation of pulses to the converter. In case of voltage or current reference control, the reference voltage or current is compared with respective PV voltage or PV current using a PI controller and the output of PI controller is fed as input to the PWM for the generation of pulses.

1.6 Literature Review

The literature presented on maximum power point tracking is classified as:

- Empirical methods

- Perturbation methods

- Model-based methods

- Artificial Intelligence methods

- Evolutionary computing methods

- Modified perturbation methods

- Scanning-based methods

1.6.1 Empirical Methods

These methods use approximate relationships to track the maximum power point. There are two empirical-based methods that are widely presented in the literature. They are:

- Fractional open circuit voltage (FOCV)

- Fractional short circuit current (FSCC)

1.6.1.1 Fractional Open Circuit Voltage (FOCV)

This method is based on the approximate relationship between the voltage at the maximum power point to open circuit voltage (Schoeman and Wyk, 1982). The relationship is given by (1.3).

$$V_{\mathrm{mp}} \quad \approx \quad \delta_{\mathrm{V}} \times \quad V_{\mathrm{oc}} \tag{1.3}$$

where δ_{V} is a constant and it depends on the PV module. Usually, the value of it varies between 0.65 and 0.9. The value of δ_{V} is selected before implementation based on the values of irradiance and temperature. In order to implement this method, the PV array has to get momentarily disconnected from the converter for measuring open circuit voltage. This could lead to loss of power. In order to avoid this, pilot cells are used in (Hart et al., 1984) to obtain V_{oc}.

1.6.1.2 Fractional Short Circuit Current (FSCC)

This method is based on the approximate relationship between the current at the maximum power point to short circuit current (Masoum et al., 2002b). The relationship is given by (1.4).

$$I_{\mathrm{mp}} \quad \approx \quad \delta_{\mathrm{I}} \times \quad I_{\mathrm{sc}} \tag{1.4}$$

where δ_{I} is a constant and it depends on the PV module. Usually, the value of it varies between 0.8 and 0.9. The value of δ_{I} is selected before implementation based on the values of irradiance and temperature. Similar to FOCV, δ_{I} should be selected based on the PV source. For measuring the short circuit current, the PV source should be momentarily short-circuited. This will lead to loss of power. In order to overcome this problem, an additional switch is connected to the PV panel to measure a short circuit which leads to an increase in the number of components and cost. A comparison of empirical-based methods is presented in Table 1.1.

Merits:

- Simple to implement

- Lesser number of sensors

- Negligible oscillations at steady state

Demerits:

- Cannot detect maximum power point in all cases

- Not suitable in mismatching conditions

Table 1.1: Comparison of Empirical Based Methods

#	Reference	Sensors Used	Contribution
1	(Schoeman and Wyk, 1982)	V	Empirically calculated value of V_{mp} using V_{oc}
2	(Hart et al., 1984)	V	Empirically calculated value of V_{mp} using V_{oc} using pilot cells
3	(Masoum et al., 2002b)	I	Empirically calculated value of I_{mp} using I_{sc}

1.6.2 Perturbation Methods

In these methods, the control variable is varied to track the MPP. The most popular perturbation based methods are:

- Perturb and Observe and Hill Climbing

- Incremental Conductance

1.6.2.1 Perturb and Observe/Hill Climbing

Perturb and observe (P and O) and hill climbing (HC) methods are extensively used for tracking the maximum power. The fundamental concept of the P and O and HC is the same. In the P and O method, a perturbation in the operating voltage of the PV module is used to track the global peak. Whereas, in the HC method, a perturbation in the duty ratio of the power converter is used to track the global peak. If the perturbation is positive and change in power is positive, then the next perturbation is negative. If the perturbation is positive and change in power is negative, then next perturbation is positive. If the perturbation is negative and change in power is positive, then next perturbation is positive. If the perturbation is negative and change in power is negative, then next perturbation is negative. The perturbation is

continued until the operating point reaches the maximum power point. This process is presented in Table 1.2 (Hua et al., 1998, Xiao and Dunford, 2004). The initial works on hill climbing methods are presented in (Bucciarelli et al., 1980, Teulings et al., 1993, Kim et al., 1996, Hashimoto et al., 2000, Koutroulis et al., 2001, Veerachary et al., 2001). The initial works on hill climbing method are presented in (Wasynezuk, 1983, Hua and Lin, 1996, Al-Amoudi and Zhang, 1998, Kasa et al., 2000, Hua and Lin, 2001, Hsiao and Chen, 2002, Jain and Agarwal, 2004, Femia et al., 2005, Wolfs and Tang, 2005, D'Souza et al., 2005, Kasa et al., 2005). In literature, perturb and observe method and hill climbing terminology are used interchangeably.

Table 1.2: Perturbation of Parameters for HC/P and O

Perturbation	Change in Power	Next Perturbation
Positive	Positive	Negative
Positive	Negative	Positive
Negative	Positive	Positive
Negative	Negative	Negative

For a small step size, the time taken to track the MPP is more. If the larger step size is considered, there will be huge oscillations in PV power at steady state. To overcome these problems, an adaptive step size for perturbation is presented in (Liu et al., 2008, Piegari and Rizzo, 2010). In these algorithms, the step size is large when the operating point is away from MPP and becomes small when the operating point is closer to MPP. In order to avoid problems in conventional and adaptive P and O algorithms occurring due to drift during a change in shading pattern, a modified P and O is presented in (Killi and Samanta, 2015) by incorporating current as sensing parameter apart from voltage and power. Hill climbing and P and O methods can fail under rapidly changing atmospheric conditions and mismatching conditions.

1.6.2.2 Incremental Conductance

The incremental conductance (INC) method is based on the following facts:

- Slope of PV power curve is zero at MPP

- Slope of the PV power curve is positive at the left of MPP

- Slope of the PV power curve is negative at the right of MPP

15

The above concept is described as an equation in (1.5).

$$dP/dV = 0 \quad ; \qquad\qquad at \quad MPP$$
$$dP/dV > 0 \quad ; \quad at \quad left \quad of \quad MPP \qquad (1.5)$$
$$dP/dV < 0 \quad ; \quad at \quad right \quad of \quad MPP$$

The derivative of power w.r.t. voltage is expressed in terms of voltage and current and is equated to zero in (1.6).

$$\frac{dP}{dV} = \frac{d(IV)}{dV} = I + V\frac{dI}{dV} \cong I + V\frac{\Delta I}{\Delta V} = 0 \qquad (1.6)$$

(1.6) can be written as in (1.7)

$$\Delta I/\Delta V = -I/V; \qquad\quad at \quad MPP$$
$$\Delta I/\Delta V > -I/V; \quad at \quad left \quad of \quad MPP \qquad (1.7)$$
$$\Delta I/\Delta V < -I/V; \quad at \quad right \quad of \quad MPP$$

The initial literature in the incremental conductance method are presented in (Boehringer, 1968, Costogue and Lindena, 1976, Harada and Zhao, 1993). Instantaneous conductance (I/V) is compared with incremental conductance($\Delta I/\Delta V$) to track the MPP (Hussein et al., 1995). The efficiency of this algorithm is the same as P and O and it yields good performance under rapidly changing environmental conditions. The problem of perturbation size exists in this algorithm like the P and O. An attempt with variable step size incremental conductance algorithm is done in (Enrique et al., 2010). The PV array is operated at a reference voltage (V_{ref}). The reference voltage is equal to the voltage at the maximum power point when the PV source is operating at maximum power. At the MPP, a reference voltage (V_{ref}) equals to the voltage at maximum power point (V_{mp}). The operating point is maintained at MPP until there is a change in the shading pattern. The algorithm increments or decrements V_{ref} to track the new MPP. A comparison of perturbation based methods is presented in Table 1.3

Merits:

- Implementation Complexity is less

Table 1.3: Comparison of Perturbation Based Methods

#	Reference	Sensors Used	Contribution
1	(Hussein et al., 1995)	V,I	implemented incremental conductance
2	(Hua et al., 1998)	V,I	implemented perturb and observe
3	(Xiao and Dunford, 2004)	V,I	implemented hill climbing method
4	(Liu et al., 2008, Piegari and Rizzo, 2010)	V,I	adaptive P and O
5	(Enrique et al., 2010)	V,I	adaptive incremental conductance
6	(Killi and Samanta, 2015)	V,I	improved P and O to avoid drift problems during rapidly changing environmental conditions

- Detects true peak

- PV array Independent

Demerits:

- Cannot track global peak in mismatching conditions

1.6.3   Model Based Methods

Model-based MPPT has recently appeared in the literature to improve the tracking speed and dynamic performance of the MPPT. Relying on the mathematical model of the PV system in addition to the temperature and irradiance measurements, the MPP point is analytically determined. In (Zhang et al., 2000), a full voltage scan is performed to find the MPP. This technique has the lowest possible tracking time but is highly CPU-intensive, and requires solar radiation sensors that are quite expensive. In (Cristaldi et al., 2012), the authors have used a single diode model to track the maximum power point. In (Tsang and Chan, 2013), a non-linear model is fitted to the PV system and maximum power points under different working conditions are derived based on fitting models. However, its efficiency is highly affected by the PV model accuracy which is not perfect and decreases with the aging of PV systems. To improve the accuracy of the model-based MPPTs while maintaining its high tracking speed, an MPPT method combining both the model-based and heuristic techniques is proposed

in (Hartmann et al., 2013). The method merges a heuristic method and the PV mathematical model to obtain accurate and high-speed tracking. A method based on model-based for mismatching conditions is presented in (Mahmoud and El-Saadany, 2016). Initially, the values of light generated current and reverse saturation current of each PV module are obtained using the values of irradiance and temperature. Then set of equations derived are used for calculation of maximum power point.

The authors in (Cristaldi et al., 2014) proposed an improved model based MPPT that does not require an irradiance meter. Their method relies on the PV model as well as the voltage and current measurements to estimate the irradiance received by the PV system mathematically. The PV model is utilized to find the MPP voltage. The disadvantage of this method in comparison to the heuristic techniques is the need for temperature measurement.

Methods based on thermal imaging are used in (Hu et al., 2014) for tracking global maximum power point. The thermal imaging technique is used for obtaining the value of temperature. Based on temperature, voltage, and current, the characteristics are formulated and the global peak is determined. A method based on image technique is used in (Mahmoud and El-Saadany, 2017) for tracking GP. The irradiance of each PV module is estimated using the image of a PV module captured by an optical camera. The temperature in this paper is estimated based on the method presented in (Cristaldi et al., 2014). Based on the values of irradiance and temperature, the mathematical model is used to analytically obtain the value of the maximum power point. These methods require additional equipment which increases the cost of the system drastically.

A method is proposed in (Jedari and Fathi, 2017) by measuring three values of voltage and current at three different points around the operating point. A polynomial equation developed based on single diode model is used to estimate the PV characteristics and thereby obtaining the global peak from the estimated characteristics. A comparison of model based methods is presented in Table 1.4.

Merits:

- Better tracking speed

18

Table 1.4: Comparison of Model Based Methods

#	Reference	Sensors Used	Contribution
1	(Zhang et al., 2000)	G, T	full Voltage scan is performed to track the MPP
2	(Cristaldi et al., 2012)	G, T	single diode model of module is used to obtain the characteristics and to track MPP
3	(Tsang and Chan, 2013)	G, T	non-linear models are fitted to PV system and MPP is obtained from the fitted models
4	(Hartmann et al., 2013)	G, T, V, I	combined model based methods with conventional methods
5	(Mahmoud and El-Saadany, 2016)	G,T	extended above method for mismatching conditions by measuring irradiance and temperature of each individual module
6	(Cristaldi et al., 2014)	V,I,T	estimates the value of irradiance using the values of voltage and current. Temperature is measured. Using G and T PV model is used to obtain V_{mp}.
7	(Hu et al., 2014)	V,I,T	used thermal imaging technique for measuring temperature
8	(Mahmoud and El-Saadany, 2017)	G, T	used optical camera and digital imaging to obtain the irradiance of each module
9	(Jedari and Fathi, 2017)	V,I	used three different operating points to estimate the global peak by plotting the characteristics

Demerits:

- Highly dependent on PV array characteristics

- Cannot always track the true peak

- Implementation complexity is high

- Usage of irradiance and temperature sensors increases the cost of the system

1.6.4 Artificial Intelligence Methods

Artificial Intelligence MPPT techniques are basically of two types. They are:

- Artificial Neural Network

- Fuzzy Logic

1.6.4.1 Artificial Neural Network

Neural networks are being used widely for non-linear systems. Parameter approximations are performed for solving difficult problems with neural networks. An input layer, hidden layers, and the output layer comprise a neural network as shown in Fig. 1.7. The input layer consists of either irradiance and temperature of the PV module or the voltage and current of the PV module. The output layers consist of either the reference voltage, reference current or the duty cycle of power converters operated at or near the MPP. The input signals are propagated to the output layer by means of a hidden layer based on the transfer function applied to the input signal. There is no particular rule for the identification of the number of neurons in the hidden layer. In most cases, the number of hidden layers is chosen empirically. The decision to use the transfer function is user specific and is decided based on the array configuration. The tangent sigmoid function is widely used as the transfer function for the hidden layer in the literature and pure linear function is used at the output layer. The main advantage of this technique is that, it provides accurate MPP.

An artificial intelligence based neural network MPPT algorithm is presented in (Karatepe et al., 2009) using radial bias function. Another algorithm is presented in (Subiyanto et al., 2012) by combining hopfield neural network with fuzzy logic controller. A method based on the artificial neural network in combination with P and O is proposed in (El-Helw et al., 2017) for tracking the global peak. ANN takes irradiance and temperature as input and produces duty ratio as output. Usage of ANN brings the operating point to the vicinity of global peak. From there P an O is used to retain the operating point at the global peak. Here the tracking of GP depends on training the neural network. For accurate tracking, a large amount of data needs to be used. Also, the neural network MPPT takes irradiance and temperature as an input. Using irradiance and temperature sensors for each module increases the cost of the system. A comparison of ANN-based methods is presented in Table 1.5.
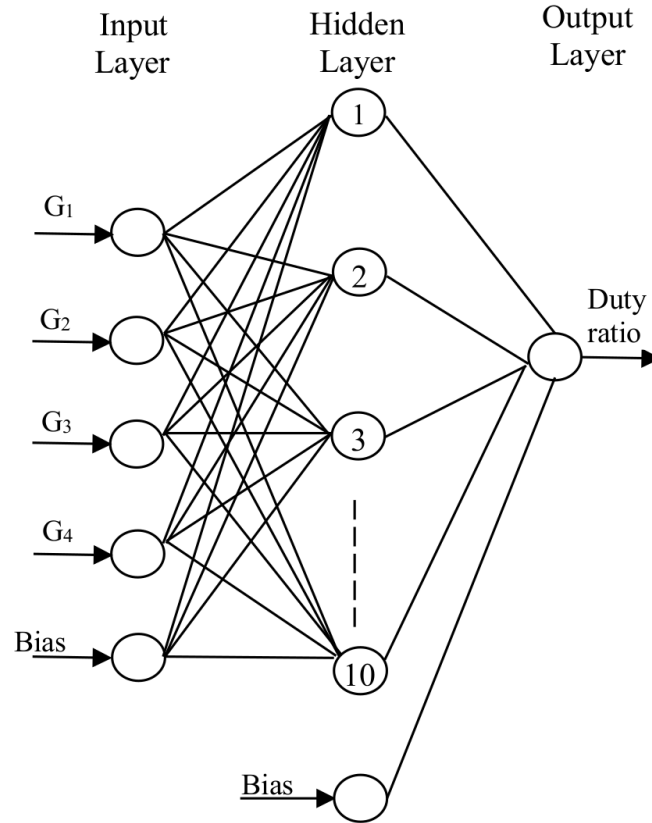
Figure 1.7: Input, Output and Hidden Layer of Neural Network

Table 1.5: Comparison of Artificial Neural Network Methods

#	Reference	Sensors Used	Contribution
1	(Karatepe et al., 2009)	G, T	used radial bias function of neural network
2	(Subiyanto et al., 2012)	G, T	used hopfield neural network in combination with fuzzy logic controller
3	(El-Helw et al., 2017)	G, T	used NN in combination with P and O

Merits:

- Tracking speed is high

Demerits:

- Highly dependent on PV array characteristics

- Huge amount of data need to know for training the neural network

- Usage of irradiance and temperature sensors increases the cost of the system

- In case of improper tuning, MPP cannot be achieved.

1.6.4.2 Fuzzy Logic

Fuzzy logic controller (FLC) have been frequently used for MPPT. Every FLC contains three parts; fuzzification, inference rules and defuzzification. For MPPT, the inputs of FLC are error (e) and the change in error (Δe). They are given by (1.8) and (1.9) respectively.

$$e\left(k\right) = \frac{P(k) - P(k-1)}{V(k) - V(k-1)} \tag{1.8}$$

$$\Delta e = e(k) - e(k-1) \tag{1.9}$$

The output of FLC is the change in voltage ΔV or the change in duty cycle Δd.

An MPPT using FL algorithm to track the MPP under varying environmental conditions is presented in (Ahmed and Miyatake, 2008). A method combining a modified Fibonacci search and the fuzzy logic algorithm is presented in (Ramaprabha et al., 2012). The proposed approach makes use of a wide search range to track the GMPP (Ramaprabha et al., 2012). An adaptive fuzzy controller with a modified incremental conductance algorithm is presented in (Punitha et al., 2013) for tracking the global peak in mismatching conditions. Takagi-Sugeno fuzzy-based method is used to extract maximum power for the fluctuating weather and mismatching conditions (Chiu, 2010). A method based on Takagi-Sugeno fuzzy based incremental conductance is proposed in (Sekhar and Mishra, 2014).

A modified FL controller for MPPT was proposed in (Alajmi et al., 2013) to improve the performance of the PV system during mismatching conditions as a replacement for P and O method. In this, the FL algorithm scans and stores the maximum power during the operation of perturb and observe the algorithm. The variables used are the change in power (ΔP), change in current (ΔI) and deviation in maximum power from the actual power (ΔP_{m}). An extension to (Alajmi et al., 2013) is presented in (Boukenoui et al., 2016) to enhance its performance. A new control loop is added to scan and store the data. A method based on fractional order in combination with fuzzy logic control is presented in (Tang et al., 2017). A polynomial fuzzy based modeling approach is presented in (Rakhshan et al., 2017). All these

fuzzy based algorithms can track GP accurately but for tracking a rule base need to be formulated, for which complete idea of the system is required. A comparison of fuzzy logic based algorithms is presented in Table 1.6.

Table 1.6: Comparison of Fuzzy Logic Based Methods

#	Reference	Sensors Used	Contribution
1	(Ahmed and Miyatake, 2008)	V, I	conventional fuzzy logic algorithm is used
2	(Ramaprabha et al., 2012)	V, I	adaptive fuzzy logic control with modified incremental conductance method is used
3	(Chiu, 2010)	V, I	Takagi-Sugeno fuzzy based method is employed
4	(Sekhar and Mishra, 2014)	V, I	Takagi-Sugeno(TS) fuzzy based method with incremental conductance method is used
5	(Alajmi et al., 2013)	V, I	uses fuzzy logic with scanning and storing method to track global peak
6	(Boukenoui et al., 2016)	V, I	extension of (Alajmi et al., 2013) by adding a new control loop.
7	(Tang et al., 2017)	V, I	fractional order in combination with fuzzy logic controller is used
8	(Rakhshan et al., 2017)	V, I	polynomial based fuzzy logic function is used

Merits:

- Tracks true MPPT

Demerits:

- Highly dependent on PV array characteristics

- Implementation complexity is high

- Complete knowledge of the PV system is required for forming the rule base.

1.6.5 Evolutionary Computing Methods

1.6.5.1 Particle Swarm Optimization

Particle Swarm Optimization (PSO) is a population-based search method, model based on the the behavior of bird flocks (Eberhart and Kennedy, 1995). A swarm of individuals also known as particles is used in this algorithm. A candidate solution is represented by each particle. The behavior of the particles is emulating the success of neighboring particles and achieving their own success. The position of each particle is determined by the best particle of the whole system. The position of the particle is also determined by the best solution found by the particular particle. It is determined using (1.10).

$$x_i^{k+1} = x_i^k + v_i^{k+1} \tag{1.10}$$

where v_i is velocity component representing the step size. The velocity component is given by (1.11).

$$v_i^{k+1} = wv_i^k + c_1 r_1 \left\{ P_{\text{best,i}} - x_i^k \right\} + c_2 r_2 \left\{ G_{\text{best}} - x_i^k \right\} \tag{1.11}$$

where c_1 and c_2 are the acceleration coefficients, w is the inertia weight, r_1, r_2 are random numbers in the range of 0 and 1, $P_{\text{best,i}}$ is the personal best of the particle i, and G_{best} is the best of the particle in the whole system. A pivotal role is played by inertia weight in balancing local search and global search. A smaller value of w improves the local search and a larger value of w accelerates the global search process.

A direct control based particle swarm optimization algorithm for PV system under mismatching conditions is proposed in (Ishaque et al., 2012a). Three different duty ratios are used as particles. The particles are initialized for every change in irradiance using power-duty ratio characteristics. A deterministic PSO proposed in (Ishaque and Salam, 2013a) eliminates the random number in the acceleration factor of velocity equation in order to improve the tracking capability. The algorithm is implemented on a buck-boost converter and is compared with the HC algorithm. This method uses direct duty ratio control. The three particles (duty cycles) are initialized between the minimum and maximum values of duty ratio (d_{min} and d_{max}). A modified PSO is proposed in (Babu et al., 2015) to track the global peak under mismatching conditions. This work is a modification of work proposed in (Ishaque et al., 2012b), where the middle particle (d_{middle}) between d_{min} and d_{max} is proposed for optimization in tracking

time. It is given by (1.12)

$$d_{\text{middle}} = 1 - \frac{\sqrt{R_{\text{pv}}}}{\sqrt{R_{\text{load}}}} \qquad (1.12)$$

where, $R_{\text{pv}} = (V_{\text{mp}}/I_{\text{mp}})$ is the resistance of PV module and R_{load} is equivalent load resistance of the output. This method exhibited a faster dynamic response with slight steady state oscillations.

In another work, (Chao et al., 2015) proposed an improved PSO algorithm. The authors presented an exponential form parameter control to improve the performance of conventional PSO. A PSO algorithm based on the window based search to reduce the search space and improve the convergence time is presented in (Manickam et al., 2016). It also reduces the power oscillations in the transient period. An algorithm to differentiate uniform and mismatching condition is proposed in this paper. A leader

Table 1.7: Comparison of Particle Swarm Optimization Based Methods

#	Reference	Sensors Used	Contribution
1	(Ishaque et al., 2012b)	V, I	used conventional PSO with three duty ratios as particles
2	(Ishaque and Salam, 2013b)	V, I	acceleration factor is used to eliminate random numbers in PSO
3	(Babu et al., 2015)	V, I	implemented (Ishaque et al., 2012b) with duty ratio initialization using input and output resistance of power converter
4	(Chao et al., 2015)	V, I	exponential form parameter control is used to improve the performance of conventional PSO
5	(Manickam et al., 2016)	V, I	proposed window based search to reduce the search space of PSO and to reduce the power oscillation
6	(Ram and Rajasekar, 2017)	V, I	used leader PSO with exclusive mutation strategies.
7	(Pragallapati et al., 2017)	V, I	AVPSO adjusting adaptive weight factor and adaptive cognitive factor is proposed

PSO (LPSO) is employed in (Ram and Rajasekar, 2017). In this paper, exclusive mutation strategies are employed to obtain the best leader that helps the algorithm to differentiate between local and global MPP. An adaptive velocity PSO (AVPSO) is

proposed in (Pragallapati et al., 2017). This algorithm continuously adjusts individual particles weight factor and cognitive acceleration coefficient based on its the operating point during the tracking process. Thus, the adaptive nature of the particles velocity improves the global maximum power point tracking (GMPPT) time and power yield. A comparison of PSO based techniques is presented in Table 1.7.

1.6.5.2 Differential Evolution

Differential evolution (DE) is one of the existing stochastic parameter optimization methods which is being widely used in engineering applications (Das and Suganthan, 2011). The computational stages of this algorithm are the same as that of the standard evolutionary algorithm. It uses scaled differences of random numbers, but uses distinct population members as a search mechanism. A one to one selection approach is used to direct the search towards the prospective region. The process is continued until termination criteria are met.

A DE-MPPT algorithm is proposed in (Taheri et al., 2010), for a boost converter to track the GP under mismatching conditions. A global peak tracking algorithm is proposed for a high gain boost converter in (Tey et al., 2014). In this process, the convergence of the optimal point is achieved by forcing the particles by means of changing the direction of mutation.

Table 1.8: Comparison of Differential Evolution Based Methods

#	Reference	Sensors Used	Contribution
1	(Taheri et al., 2010)	V, I	differential evolution based MPPT technique is proposed
2	(Tey et al., 2014)	V, I	DE algorithm is modulated so that the mutation always forces the particle in generation to converge towards optimal point
3	(Ramli et al., 2015)	V, I	modified differential evolution with only one tuning parameter
4	(Kumar et al., 2017b)	V, I	combination of whale optimization and differential evolution is presented
5	(Kumar et al., 2017a)	V, I	combination of Jaya and differential evolution is presented

A modified differential evolution (MDE) algorithm is proposed for mismatching

26

condition in (Ramli et al., 2015). This method uses only mutation factor as tuning paramter and is given by (1.13).

$$V_{i,G} = X_{i,G} + \Phi \qquad (1.13)$$

where, Φ is the perturbation in duty cycle given by (1.14).

$$\Phi = F\left(X_{best,G} - X_{i,G}\right) \qquad (1.14)$$

The integration of Jaya algorithm and DE is done in (Kumar et al., 2017b). A simulation study is carried out where the results showed that it tracked global MPP for different cases. A hybrid approach combining Whale optimization (WO) and DE is introduced for tracking the global peak faster with reduced oscillation at steady state in (Kumar et al., 2017a). A comparison of DE techniques is presented in Table 1.8.

1.6.5.3   Ant Colony Optimization

Ant colony optimization (ACO) uses a stochastic problem with a probabilistic algorithm for searching global maximum. The algorithm is based on the behavior of the ants that find the best path towards the food (Dorigo and Gambardella, 1997). This algorithm is modified into an optimization algorithm by (Shen et al., 2005) and (Dorigo et al., 2006). Initially all the ants (individuals) search for food. If any of the ants find the food, the size of the food is determined. If the size of the food is large, then ants bring a small portion of it to the nest. In their way to its nest, the pheromones are left in its path which enables other ants to find its source. The quantity of pheromones in the path is directly proportional to numbers of ants traveling in that path. The pheromones get vaporized over time. There will be a decrease in the density of pheromones if the ants are not traveling in the path. In this manner, the shortest possible way from the nest to the food source is determined by the ants.

An ACO based MPPT algorithm is proposed in (Adly and Besheer, 2012) with a battery load. It is used in conjunction with the fractional open circuit voltage method. The parameters of the PI controller are optimized using the ACO algorithm. A novel ACO algorithm under mismatching conditions is proposed in (Jiang et al., 2013). An ACO algorithm with a New Pheromone Updating strategy (ACO NPU MPPT)

saving the computation time and with high accuracy, zero steady-state oscillations, and high robustness is proposed in (Titri et al., 2017).

1.6.5.4 Artifcial Bee Colony (ABC)

Artificial Bee Colony algorithm uses three types of bees for identifying the solution. They are employed bee, onlookers, and scout bee (Sundareswaran et al., 2015). The identification of food source and sharing the information with other bees is done by employer bees. The information from the employer bees is taken by onlooker bees. Based on the information, they spot the optimal food location. A random search for the new food source is performed by the scout bee. The optimal solution with reduced time is achieved by proper cooperation and communication among these three groups. During the tracking of the global peak, the duty cycle is denoted for the position of food. The optimal power is denoted for the source of food. The algorithm tracks the target using (1.15).

$$x_\mathrm{i} = d_\mathrm{min} + \frac{(i-1)\left[d_\mathrm{max} - d_\mathrm{min}\right]}{N_\mathrm{b} - 1} \tag{1.15}$$

The number of bees is denoted by N_b, the number of iterations is denoted by i, minimum and maximum values of the duty ratio of boost converter are denoted by d_min and d_max respectively. In order to check the new food location, the employed bees act as scout bees. The employed bees and onlooker bees are used for tracking the global peak of the PV system. Compared to PSO and enhanced PSO, the ABC algorithm has better tracking response in mismatching conditions.

An artificial bee colony optimization algorithm for tracking the global peak of a standalone PV system containing DC motor is proposed in (Oshaba et al., 2015). In this method, two PI controllers are used. One is for global peak tracking and the other is for controlling the speed of DC motor. The parameters of the two controllers are optimized by ABC. A variant of ABC with changes in inertia weight is proposed in (Fathy, 2015) and is named as modified ABC. Conventional ABC technique has limited number of controlling parameters and it sometimes gets trapped at local peak. Modified ABC mentioned in the above lines is used to solve this problem. The accelerated food position in modified ABC is calculated as given by (1.16).

$$v_\mathrm{ij} = w_\mathrm{ij} x_\mathrm{ij} + \varphi_\mathrm{ij}\left(x_\mathrm{ij} - x_\mathrm{kj}\right) + \varphi_\mathrm{ij}\left(y_\mathrm{j} - x_\mathrm{ij}\right) \tag{1.16}$$

where,

$$w_{ij} = \frac{\left| x_e^k - x_{ij} \right|}{max\left(x_e^k, x_{ij} \right)} \tag{1.17}$$

where, x_{ij} is the present food source, v_{ij} is the new food source and it depends on its previous value x_{ij}, w_{ij} is the inertia weight use to control the x_{ij}, y_j is the jth position of the global optimal solution, φ_{ij} is a random number, φ_{ij} is the random number for next food position, x_{kj} is next food position to the previous solution, x_e^k is the position of global best optimal solution for iteration k, and $\left| x_e^k - x_{ij} \right|$ is the Euclidean norm. A solution with high computation speed, reduced number of iterations is obtained by the modified ABC algorithm when compared to PSO, conventional ABC and genetic algorithm under mismatching conditions.

1.6.5.5 Fireflies Optimization Algorithm

Fireflies optimization algorithm (FOA) is a population-based optimization method similar to PSO. The inspiration for this obtained from illuminated bugs. The mathematical representation of this algorithm is presented in (Yang, 2009) and (Yang, 2010). FOA has fewer parameters for tuning compared to PSO. The key parameter for the behavior of fireflies is the flashing light. It is used for attracting the potential prey and mating partners and also a mechanism for a protective warning. The important parameter is the brightness which is used for determining the new position of the particles in the search space (Yang, 2009). In case, if the brightness of firefly p is less than firefly q, the new position of firefly p is determined by (1.18).

$$x_p^{t+1} = x_p^t + \beta\left(r \right)\left(x_p - x_q \right) \tag{1.18}$$

The position of the fireflies are represented by x_p and x_q , distance between these two fireflies is denoted by r, level of attractiveness is denoted by β. The degree of attractiveness (β) is calculated using (1.19).

$$\beta\left(r \right) = \beta_0 e^{-\gamma\left(x_{pq} \right)^n} \quad , n > 1 \tag{1.19}$$

where, γ is the absorption coefficient that controls the light intensity and β_0 is initial attractiveness. In the FOA MPPT, the position of firefly is represented by duty ratio, brightness of each butterfly is represented by PV power. The FOA-MPPT is implemented in (Sundareswaran et al., 2014) and exhibited a better performance

than PSO in terms of tracking accuracy, tracking speed and dynamic response. A comparison of ACO, ABC and FF techniques is presented in Table 1.9.

Table 1.9: Comparison of Evolutionary Computing Based Methods

#	Reference	Sensors Used	Contribution
1	(Adly and Besheer, 2012)	V, I	used FOCV method to track the MPP and ACO is used to optimize the parameters of PI controller
2	(Jiang et al., 2013)	V, I	used ACO to track the global peak
3	(Titri et al., 2017)	V, I	ACO with new pheromone udpating strategy is used
4	(Sundareswaran et al., 2015)	V, I	used artificial bee colony to track the global peak
5	(Oshaba et al., 2015)	V, I	ABC is used to control the parameters of PI controller that is used to track the global peak
6	(Fathy, 2015)	V, I	modified ABC with changes in inertia weight
7	(Sundareswaran et al., 2014)	V, I	firefly optimization algorithm is used to track the global peak

Merits:

- Tracks the global peak accurately

- lesser dependence on PV array datasheet

Demerits:

- Implementation complexity is high

- Tracking speed is less

1.6.6 Modified Perturbation Methods

The derivative characteristics i.e., $(dP/dV < 0)$ or $(dP/dI > 0)$ are the same for local and global peaks. This is the reason for the perturbation based algorithms to

get trapped in local peaks. Several authors modified conventional perturbation based algorithms to track the global peak under mismatching conditions.

A two stage IC based method is proposed in (Kobayashi et al., 2006) for tracking the global peak under mismatching conditions. In the first stage, the operating point is made to operate in the vicinity of global peak using the resistance at maximum power point as in 1.20.

$$R_{\mathrm{mp}} = k\frac{V_{\mathrm{mp}}}{I_{\mathrm{mp}}} \tag{1.20}$$

where k is the correction factor, while V_{mp} and I_{mp} are voltage and current at MPP. In the second stage, INC algorithm is used to retain the operating point at MPP. A two-stage modified P and O is proposed in (Patel and Agarwal, 2008). The algorithm contains two parts: a) main program and b) GP tracking routine. It is based on the fact that the distance between two consecutive peaks is 0.8 times open circuit voltage of the module (V_{ocm}). The algorithm initially uses a conventional algorithm to track the peak. Once a local peak is tracked, the operating point is incremented or decremented by 0.8 V_{ocm} and another local peak is tracked. The maximum among the local peaks is the global peak. With this algorithm, almost 80% of the curve need to be scanned for tracking the global peak. This leads to a decrease in tracking speed. The conditions pertaining to the failure of this method is presented in (Ahmed and Salam, 2015). Another algorithm is presented in (Ahmed and Salam, 2015) with simplified equations.

An alternative P and O is presented in (Carannante et al., 2009) which uses the comparison of two instantaneous power value for tracking the GP. The comparison is given by (1.21).

$$\frac{P_{\mathrm{m}}\left(t\right) - P_{\mathrm{ref}}\left(t\right)}{P_{\mathrm{m}}\left(t-1\right)} < \epsilon \tag{1.21}$$

$P_{m}\left(t\right)$ is the instantaneous measured power and $P_{\mathrm{ref}}\left(t\right)$ is the instantaneous maximum power reference. Apart from this equation, there are various equations which complicate the MPPT algorithm. This method is tested for only one shading pattern, thus its effectiveness cannot be validated. A method based on dividing rectangles algorithm is presented in (Nguyen and Low, 2010b). This method has high tracking speed, but as per (Wang et al., 2016), there are chances that the operating point gets trapped in a local maximum.

A duty cycle sweep method based on modified HC method is presented in (Lei

et al., 2011) for mismatching conditions. The initial value of the duty cycle is given by (1.22).

$$D = 1 - \sqrt{\frac{R_{\mathrm{mp}}}{R_{\mathrm{load}}}} \tag{1.22}$$

where R_{load} is the load resistance and R_{mp} is the resistance at maximum power point. The duty cycle is swept from 0 to 90 %. Then sweep duty cycle is carried out for the range of 0 to 90%. This method needs to scan over 80% of curve which leads to increase in tracking time.

A voltage sweep method is presented in (Koutroulis and Blaabjerg, 2012) to periodically change the voltage of PV array from its maximum value to minimum value. The operating current and voltage are stored in microcontroller memory at each sampling cycle. The global maximum identified based on the values of voltage and current stored in the microcontroller. Once GP is identified conventional P and O is used to retain the operating point at MPP.

A voltage window search (VWS) algorithm is presented in (Boztepe et al., 2014) to reduce the tracking time by reducing the search space of the voltage window. This method can track the global peak accurately with lesser computational time. This method uses a single termination criterion to reduce the search space of the algorithm. A method based on slopes of P-V curve to track global peak is presented in (Balasankar et al., 2017). The area of P-V curve is divided into zones and tracking is done based on slopes of P-V curve. This method requires the measurement of open circuit voltage for every shading pattern.

An algorithm presented in (Wang et al., 2016) operates in three stages. In the first stage, the incremental conductance algorithm to track the leftmost peak of the P-V curve. This is called the searching stage. In the second stage, a part of the curve is skipped where there is no chance of occurrence of global peak and is referred to as skipping stage. The third step is to judge whether the algorithm will go to searching stage or skipping stage. Usage of this method leads to a decrease in tracking speed. A jumping method is proposed in (Chen et al., 2016) based on the observation of P-V characteristics. Initially, the duty ratio is made equal to zero and the open circuit voltage of array is determined. From the open circuit voltage of array, the open circuit voltage of the module is derived. Then an auto-scaling variable step size algorithm presented in (Chen et al., 2014) is used to determine the rightmost peak. Once the rightmost peak is detected, the algorithm tracks the leftmost peak by initializing duty

ratio to 0.95 for the boost converter. The algorithm then tracks every local peak by making a jump in the operating voltage based on the fact that MPP occurs after $(0.8 \times V_{\text{ocm}})$ from the current peak. Conventional P and O is modified and implemented for mismatching conditions using a checking algorithm in (Alik and Jusoh, 2017). The purpose of the checking algorithm is to determine the global peak by comparing all existing local peak points.

The authors in (Ramyar et al., 2017) proposed a technique based on measuring the photovoltaic current at specific points to identify the shading pattern. Once the shading point is identified, the hill climbing method is applied for tracking the local maxima and the global peak is identified. The process for identifying the shading pattern and tracking the local peaks is time-consuming and it decreases the tracking speed. A method based on sampling, an approximation of I-V curve and dividing the voltage region into sub-regions to track the GP is proposed in (Ghasemi et al., 2018).

A comparison of modified perturbation based methods is presented in Table 1.10.

Merits:

- Lesser implementation complexity

- could track global peak accurately

- lesser dependence on PV array

Demerits:

- Lesser Tracking speed compared to ANN and model-based algorithms

1.6.7   Scanning-Based Methods

Recently scanning based MPPT algorithms are drawing much attention because of less tracking time and high efficiency. Scanning of the PV curve based on capacitor charging is presented in (Spertino et al., 2015, Parlak, 2014) to track the global peak. In this method, for a change in shading pattern, the PV module is isolated from the DC-DC converter and connected to the capacitor so that it gets charged. During charging of the capacitor, the capacitor voltage and the capacitor current are

Table 1.10: Comparison of modified perturbation Based Methods

#	Reference	Sensors Used	Contribution
1	(Kobayashi et al., 2006)	V, I	modified incremental conductance for mismatching conditions
2	(Patel and Agarwal, 2008)	V, I	modified P and O is proposed
3	(Carannante et al., 2009)	V, I	modifed P and O with instantaneous powers are proposed
4	(Nguyen and Low, 2010a)	V, I	method based on dividing rectangles algorithm is proposed
5	(Koutroulis and Blaabjerg, 2012)	V, I	proposed method based on voltage sweep
6	(Wang et al., 2016)	V, I	an algorithm by searching, scanning and jumping procedures is used to track the GP
7	(Chen et al., 2016)	V, I	method based on jumping the operating voltage to track the maximum power is proposed
8	(Alik and Jusoh, 2017)	V, I	modified P and O with checking algorithm is used
9	(Ramyar et al., 2017)	V, I	measures PV current at specific points to identify the shading pattern
10	(Ghasemi et al., 2018)	V, I	method based on sampling and approximation of I-V curve is proposed to track GP using set of equations

sampled and the global peak is determined. Tracking speed for obtaining global peak is less, but isolating the module form DC-DC converter leads to a discontinuity in supply to the load for systems without storage. Also, this arrangement needs extra circuit comprising of switches leading to an increase in the number of components. A scanning based approach is proposed in (Kotti and Shireen, 2015), in which the PV panel is short-circuited using the controlled switch of the boost converter. For tracking GP, initially the switch is closed, i.e., the duty cycle is one. Because of this, the PV voltage declines to zero and the current rises to short-circuit current. In this period, the values of PV voltage (V), PV current (I) are sensed. From the detected values of voltage and current, maximum power and voltage at maximum power are determined. By setting the duty ratio at 1, the stress across the switch increases

during rapid changing irradiance conditions. This operation may lead to failure of the switch. As duty ratio is made equal to one, while tracking the maximum power point, there is a chance that the inductor of the boost converter will go to saturation under rapidly changing irradiance conditions. If the higher switching frequency is considered to avoid the inductor saturation, the settling time of the converter will decrease. This leads to a decrease in the number of samples taken for obtaining the maximum power. Another problem is that of missing maximum power point. Consider a shading pattern in which the global peak is located to the left of all the local peaks say at voltage V_1. If the shading pattern is now changed such that global peak occurs at voltage $V_2 > V_1$, the algorithm presented in (Kotti and Shireen, 2015) sweeps the curve from V_1 to zero. However, the actual peak lies at V_2. This leads to a considerable loss of power.

Another algorithm based on ramp based scanning technique is presented in (Ghasemi et al., 2016). Once the change in power is detected, the algorithm checks for the occurrence of mismatching condition. If no mismatching condition is detected, the P and O method is used to retain the operating point at MPP. If mismatching condition is detected, a ramp voltage is applied to the converter in both positive and negative directions, and corresponding values of maximum power and voltage are detected. It is presented in (Ghasemi et al., 2016) that the step changes in duty ratio will lead to an increase in oscillations, overshoot and settling time of the system. The authors described the disadvantage of a step change in irradiance from the point of view of implementing metaheuristic algorithms like PSO. The problem of overshoot and oscillations are minimum if the step size is large and duty ratio varies from a higher value to lower value for a boost converter. A comparison of scanning based methods is presented in Table 1.11.

Table 1.11: Comparison of Scanning Based Methods

#	Reference	Sensors Used	Contribution
1	(Parlak, 2014)	V, I	method based on capacitor charging by using an auxiliary circuit is presented
2	(Kotti and Shireen, 2015)	V, I	method based on capacitor charging by giving a step change in duty ratio
3	(Ghasemi et al., 2016)	V, I	method of scanning based on ramp cahneg in duty ratio

Merits:

- High Tracking speed

- Lesser Implementation complexity

Demerits:

- Stress on switches will be more for a step change in the duty ratio

1.7   Motivation

The maximum power point tracking algorithms implemented for mismatching conditions are generally comprised of two stages. In the first stage, a specialized technique (NN, EA, model-based, modified perturbation based, scanning based) is used to bring the operating point to the local peak. In the second stage, the conventional perturbation based algorithm is used to retain the operating point at the global peak. The advantage of perturbation-based algorithms is they are system independent. In perturbation based algorithms, in the tracking phase, if any change in irradiance occurs then the algorithm tracks the peak without the need of reinitialization of initial parameters. But the GPT algorithms are system dependent. The algorithms operating in the first stage for reaching the vicinity of the global peak cannot detect the change in the shading pattern. If the time of operation of the algorithm in the first stage is high, then there is a chance of detection of the false peak. The objective is to reduce the time of operation of the algorithm in stage-1 with reduced complexity and lesser system dependence. The change in shading pattern can be detected in the second stage where the conventional perturb based MPP will be operating.

1.8   Objectives

1. To develop a maximum power point tracking algorithm that tracks the global peak (GP) under mismatching conditions using the modified perturbation based algorithm.

2. To develop a maximum power point tracking algorithm that tracks the GP under mismatching conditions using scanning based approach.

1.9   Thesis organization

There are six chapters in this thesis document. Chapter 1 presents a brief introduction to the state-of-the-art global maximum power point tracking algorithms through a detailed literature survey. Based on the review of the work carried out, the objectives of the thesis are presented. Chapter 2 proposes a modified perturbation global peak tracking algorithm using direct duty ratio control. Chapter 3 proposes a modified perturbation algorithm for tracking global peak using current control. Chapter 4 proposes a modified perturbation algorithm for tracking global peak using voltage and current control. Chapter 5 proposes a scanning based algorithm for tracking global peak using direct duty ratio control. Chapter 6 summarizes the thesis major contributions and includes some discussions on possible future research.

Chapter 2

Global Peak Tracking Using Searching Technique and Bisection Method

Contents

2.1   Introduction

A two-stage global maximum power point tracking algorithm is proposed in this chapter. In the first stage, the algorithm reaches to the proximity of global peak by

sub-dividing the panel characteristics. The subdivisions are referred to as zones. The number of zones in the PV panel is equal to the number of bypass diodes connected in all the modules that are in series. The division of zones is done based on open circuit voltage of complete string at standard test conditions. The algorithm checks for the possibility of a global peak in each zone by measuring PV voltage and PV current and storing them in an array. The possibility of occurrence of a global maximum in each zone is checked using a simple searching technique. If there is a possibility of occurrence of the global peak in at least two zones, the bisection method is used to update the duty ratio based on estimated values of maximum powers in each zone. An iterative process is followed in which, if the possibility of occurrence of a global maximum in zones is at most one, then conventional hill climbing method maintains the operating point at maximum power which is the second stage of the algorithm. Simulation studies are performed using MATLAB for different patterns. Experimental validations are performed using PV modules, the boost converter, resistive load, and dSpace 1202 controller.

The following assumptions are considered in this chapter.

- The value of cell temperature is considered constant

- The ratio of V_{mp} to V_{oc} and I_{mp} to I_{sc} will not exceed 0.9.

- The minimum irradiance falling on the PV panel is 100W/m^2 and the maximum irradiance falling on the PV panel is 1000W/m^2.

- The effects of degradation on PV modules are not considered.

2.2 Methodology

2.2.1 Minimum and Maximum values of duty ratio

I-V curves and *P-V* curves for three different shading patterns are presented in Fig. 2.1(a) and Fig. 2.1(b) respectively. A method presented in (Nguyen and Low, 2010b) for buck-boost converter is adopted for boost converter for selecting the minimum and maximum values of duty ratio. The global peak may occur in three different regions as shown in Fig. 2.1(b). The voltage corresponding to the minimum and maximum values of peaks are denoted by V_{pmin} and V_{pmax} respectively. The corresponding values

are given by equations (2.1) and (2.2).

$$V_{\text{pmin}} \approx \delta_{\text{V}} \times V_{\text{ocm}} \tag{2.1}$$

$$V_{\text{pmax}} \approx \delta_{\text{V}} \times V_{\text{oct}} \tag{2.2}$$

where V_{ocm} is open circuit voltage of the single module and V_{oct} is open circuit voltage of the whole array. The value of δ_{V} is chosen as 0.9 in this work.

The approximate values of current corresponding to minimum and maximum values of peaks (I_{pmin} and I_{pmax}) for series connected modules are given by equations (2.3) and (2.4).

$$I_{\text{pmax}} \approx \delta_{\text{I}} \times I_{\text{scm}} \tag{2.3}$$

$$I_{\text{pmin}} \approx \delta_{\text{I}} \times (\gamma_{\text{m}} \times I_{\text{scm}}) \tag{2.4}$$

where I_{scm} is the short circuit current of the module. γ_{m} is a factor which is decided by the lowest possible irradiance occurring. This is chosen as ratio of minimum value of irradiance (say $100 \ W/m^2$) to irradiance at STC($1000 \ W/m^2$). The value of it (γ_{m}) is user-defined based on ambient conditions. The value of δ_{I} is chosen as 0.9 in this work. For parallel connected modules, (2.3) is replaced by equation (2.5).

$$I_{\text{pmax}} \approx \delta_{\text{I}} \times I_{\text{sct}} \tag{2.5}$$

I_{sct} is the sum of short circuit currents of all the strings connected in parallel. The minimum and maximum value of equivalent resistances (R_{pvmin} and R_{pvmax}) seen from source side are given by equations (2.6) and (2.7).

$$R_{\text{pvmin}} = \frac{V_{\text{pmin}}}{I_{\text{pmax}}} \tag{2.6}$$

$$R_{\text{pvmax}} = \frac{V_{\text{pmax}}}{I_{\text{pmin}}} \tag{2.7}$$

The points on I-V curve corresponding to equations (2.6) and (2.7) are denoted by points (i) and (ii) (indicated as GP occurrence region) in Fig. 2.1. The minimum and maximum values of duty ratio viz., d_{min} and d_{max} are derived based on (Veerachary et al., 2002). Equivalent resistance seen from PV panel R_{pv} is given by equation (2.8).
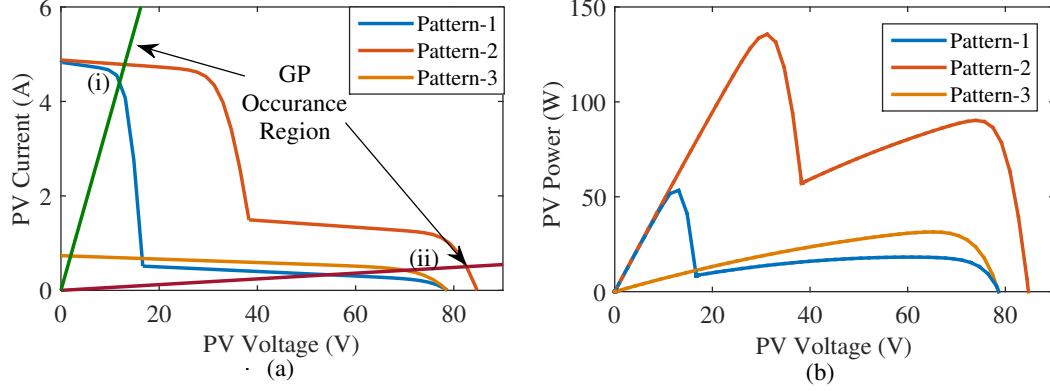
Figure 2.1: (a) *I-V* and (b) *P-V* characteristics indicating GP occurrence region (Section 2.2.1)

$$R_{\text{pv}} = \eta(1-d)^2 R_{\text{load}} \tag{2.8}$$

where R_{load} is load resistance, η is efficiency of the boost converter and d is duty ratio of boost converter. Equations (2.8) is rearranged as (2.9).

$$d = 1 - \sqrt{\frac{R_{\text{pv}}}{\eta \times R_{\text{load}}}} \tag{2.9}$$

From (2.9), minimum and maximum values of duty ratio are presented in equations (2.10) and (2.11).

$$d_{\text{min}} = 1 - \sqrt{\frac{R_{\text{pvmax}}}{\eta \times R_{\text{loadmin}}}} \tag{2.10}$$

$$d_{\text{max}} = 1 - \sqrt{\frac{R_{\text{pvmin}}}{\eta \times R_{\text{loadmax}}}} \tag{2.11}$$

The minimum and maximum values of duty ratio can be chosen close to (2.10) and (2.11). R_{loadmax} and R_{loadmin} are the maximum and minimum value of load resistance. The equations (2.10) and (2.11) presented for minimum and maximum values of duty ratio are derived by keeping the resistive load into consideration. However, these equations are applicable to constant voltage loads. For constant voltage loads, the value of output voltage (V_o) of the converter is constant and current varies. If the minimum and maximum output currents are I_{omin} and I_{omax} respectively, the minimum and maximum value of load resistance (R_{loadmin} and R_{loadmax}) are given by (2.12) and (2.13).

42

$$R_{\text{loadmin}} = \frac{V_{\text{o}}}{I_{\text{omax}}} \tag{2.12}$$

$$R_{\text{loadmax}} = \frac{V_{\text{o}}}{I_{\text{omin}}} \tag{2.13}$$

Equations (2.12) and (2.13) are substituted in (2.10) and (2.11) to get the respective minimum and maximum value of duty ratio. The minimum and maximum limits of duty ratio are d_{min} and d_{max} and the middle values of duty ratio (d_1 and d_2) will be values that are equally distributed between d_{min} and d_{max}. Duty ratio array dd is given by (2.14).

$$dd = [d_{\text{max}} \quad d_1 \quad d_2 \quad d_{\text{min}}] \tag{2.14}$$

2.2.2 Selection of Zone Voltages

For a single module, the voltage at maximum power(V_{mp}) is approximately represented by (2.15).

$$V_{\text{mpm}} \approx 0.9 \times V_{\text{ocm}} \tag{2.15}$$

where V_{ocm} is open circuit voltage of module. Before selection of the zone voltage, the number of zones needs to be selected. The number of zones is equal to the number of bypass diodes in the modules that are connected in series. Selection of zone voltages is based on the open circuit voltage of total series connected modules at STC. Based on (2.15), the zonal voltages are calculated using (2.16).

$$V_{\text{zo1}} = \frac{V_{\text{oct}} \times 0.9}{N_{\text{bd}}} \tag{2.16a}$$

$$V_{\text{zo2}} = \frac{2 \times V_{\text{oct}} \times 0.9}{N_{\text{bd}}} \tag{2.16b}$$

$$V_{\text{zo3}} = \frac{3 \times V_{\text{oct}} \times 0.9}{N_{\text{bd}}} \tag{2.16c}$$

$$V_{\text{zon}} = \frac{n \times V_{\text{oct}} \times 0.9}{N_{\text{bd}}} \tag{2.16d}$$

N_{bd} refers to number of bypass diodes connected in series connected modules. Here n is number of sub-modules in series which is equal to N_{bd}. So V_{zon} transforms to (2.17).

$$V_{\text{zon}} = 0.9 \times V_{\text{oct}} \tag{2.17}$$
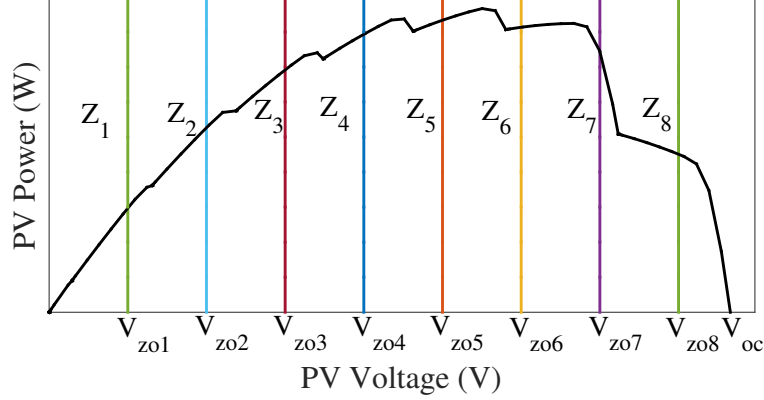
Figure 2.2: Zonewise distribution of voltages

After zonal voltages are identified, zones are divided. Zone 1 is from 0 to V_{zo1}, zone 2 is from V_{zo1} to V_{zo2}, zone n is from $V_{zo(n-1)}$ to V_{zon}. Fig. 2.2 indicates the zonewise distribution of voltages in P-V curve. As each module is equipped with two bypass diodes there are eight zones. The zones are indicated as Z_1, Z_2,...,Z_8 and the corresponding voltages are from V_{zo1} to V_{zo8}.

2.2.3 Approximation of I-V Curve

The usual procedure to approximate the I-V curve is with constant current and constant voltage (constant approx.) as shown in Fig. 2.3. The estimated power is very high compared to the actual power of the PV system. If the value of maximum power estimated from the approximated curve is closer to the actual value of maximum power, then the search time to track the global peak can be reduced. So, a new approximation is proposed in this work based on the concept of the equation for a line segment. This approach decreases the error in maximum power between the approximated curve and actual curve.

In Fig. 2.3, points (a) and (b) are the samples whose values of voltages and currents are known. The idea here is to estimate the maximum power between these two points. The maximum power is estimated by assuming the fact that the P-V curve is uniform between two operating points (a and b). This is because the maximum power has to be estimated for the worst possible condition. As the power obtained is maximum in uniform irradiance, this condition is used for estimation.

Let PV voltages at point (a) and (b) are V_a and V_b respectively. The corresponding currents are I_a and I_b. The estimated maximum power is computed at point (c) and
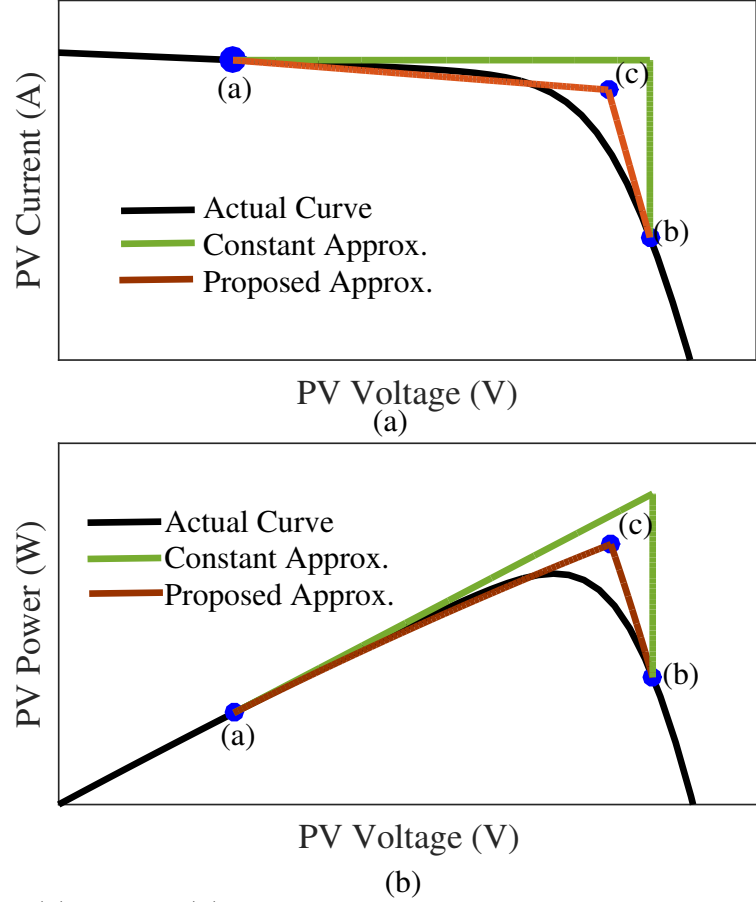
Figure 2.3: (a)*I-V* and (b) *P-V* curves for approximation using Proposed Method

are given by (2.18) and(2.19).

$$V_e = V_b - (0.1\,(V_b - V_a)) \tag{2.18}$$

$$I_e = 0.9I_a \tag{2.19}$$

The estimated value of maximum power is at point (c) as in (2.20).

$$P_e = V_e \times I_e \tag{2.20}$$

The values of power between points (a) and (c) and between (c) and (b) are estimated using slope of line. If a straight line is drawn between a and c, the equation of it is presented in (2.21).

$$I_{est} = mV_i + C_i \tag{2.21}$$

Where V_i is any voltage between points a and c, m is the slope of line connecting points a and c, C_i is constant, I_{est} is estimated value of current. The value of estimated power at voltage V_i is given by (2.22).

$$P_{est} = V_i \times I_{est} \tag{2.22}$$

In this manner, the power is estimated between two points in the *I-V* curve.

2.2.4 Terminologies Used for Implementing Proposed Approach

Four different matrices are used for implementing the proposed approach. They are:

1. Actual Matrix

2. Estimated Matrix

3. Zone Matrix

4. Total Matrix

2.2.4.1 Actual Matrix

The size of the actual matrix is 4 x n. The first row contains voltage information and it is termed as actual voltage array. The second row contains current information and it is termed as the actual current array. The third row contains power information and it is termed as actual power array. The fourth row contains duty cycle information and it is termed as actual duty array. n is the number of columns and it is equal to a number of samples taken. The maximum value of n is equal to the number of bypass diodes because there is no chance of occurrence of more than one peak in one zone (number of zones are equal to the number of bypass diodes). Each column has an information of PV voltage (V), PV current(I), PV power(P) and duty ratio (d). It means if the duty ratio, d is applied to power converter the values of V, I, P are obtained. The values of the actual matrix are arranged in the increasing order of voltages. The first column of this array is at short-circuit point and the last column is at open circuit point.

2.2.4.2 Estimated Matrix

The size of the estimated matrix is (3 x (2n-1)). If the number of columns in the actual matrix is n, then, there will be (2n-1) columns in the estimated array. It contains the data of V, I, P in first, second and third rows respectively. The estimated array is formed by combining actual voltage array, actual current array and actual power array with the estimated values of voltage, current, and power in increasing order of values. These are termed as estimated voltage array (V_e), estimated current array(I_e) and estimated power array(P_e). These values are calculated between two consecutive columns in the actual voltage array. The values of estimated voltage is calculated using (2.18) and the value estimated current is calculated using (2.19).

Estimated power array is obtained as a product of estimated voltage array and estimated current array.

2.2.4.3 Zone Matrix

The size of matrix is 3 x N_{bd}. Where N_{bd} is number of bypass diodes. Similar to previous matrices, the row in these array are termed as zone voltage array(V_z), zone current array (I_z) and zone power array (P_z) . The values of zone voltage array are calculated in section 2.2.2. The zone current array is an estimated which is obtained using the procedure described in section 2.2.3 using the concept of slope of line ((2.21) and (2.22)). The zone power array is a product of zone voltage array and zone current array.

2.2.4.4 Complete Matrix

It is the combination of estimated matrix and zone matrix arranged in increasing order of voltages. V_x is complete voltage array, I_x is complete current array and P_x is complete power array.

2.2.5 Description of Proposed Approach

The flowchart of the proposed methodology is presented in Fig. 2.4. Initially the panel structure is decided i.e., the number of modules in series (N_{ss}), number of strings (N_{pp}) are given as initial condition to the MPPT algorithm and calculate the number of bypass diodes in series (N_{bd}). The characteristic region is divided into

zones and zone voltage array is formulated using section 2.2.2. The duty ratio array is initialized using section 2.2.1 by calculating the minimum and maximum value of duty ratio. The duty ratio array is presented in (2.23).

$$dd = [dd\,(1) \quad dd\,(2) \quad dd\,(3) \quad dd\,(4)] \tag{2.23}$$

where $dd(1)$ is $d_{\max}$ and $dd(4)$ is $d_{\min}$ whose values are computed as in section 2.2.1. The values of $dd(2)$ and $dd(3)$ are equally between $dd(1)$ and $dd(4)$.

Then other default parameters viz., P_{crit} and k are initialized. Initially, $d_{\max}$ $(dd(1))$ is initialized as duty ratio to power converter. Once the steady state is reached, voltage (V) and current (I) are obtained. Power (P) is calculated.

These values of voltage(V), current(I), power(P) and duty ratio(d) are stored in an arrays V_a, I_a, P_a and d_a are termed as actual voltage array, actual current array, actual power array and actual duty cycle array respectively. All these are arranged in each row to form a actual matrix. The estimated matrix is calculated as per the procedure described section 2.2.4. The zone matrix is calculated using the slope of the line equation as per the procedure described in section 2.2.4. The total matrix comprising of voltage array (V_x), current array (I_x) and power array (P_x) are formulated as per section 2.2.4.

From the obtained values of V_{x} and P_{x}, zones are divided w.r.t zonal voltages. The value of the zone (z) is incremented if the maximum power of actual power array (P_a) is greater than the estimated power of the corresponding zones. If the number of zones (z) is greater than the (Number of bypass diodes in string-2) then the hill climbing method is operated. Else the duty ratio is estimated for the next iteration using the bisection method. For estimating the duty ratio, the following steps are followed.

- Find the maximum value of the estimated power(P_{me}) and its corresponding voltage (V_{me})

- Check the nearest value to V_{me} in actual voltage array which is less than which is less than V_{me} and designate it as $V_{\min}$.

- If V_{me} is one of the values of actual voltage, designate it as $V_{\max}$. If V_{me} is in the zonal voltage array, check the nearest maximum of V_{me} in actual voltage array and it is designated as $V_{\max}$.
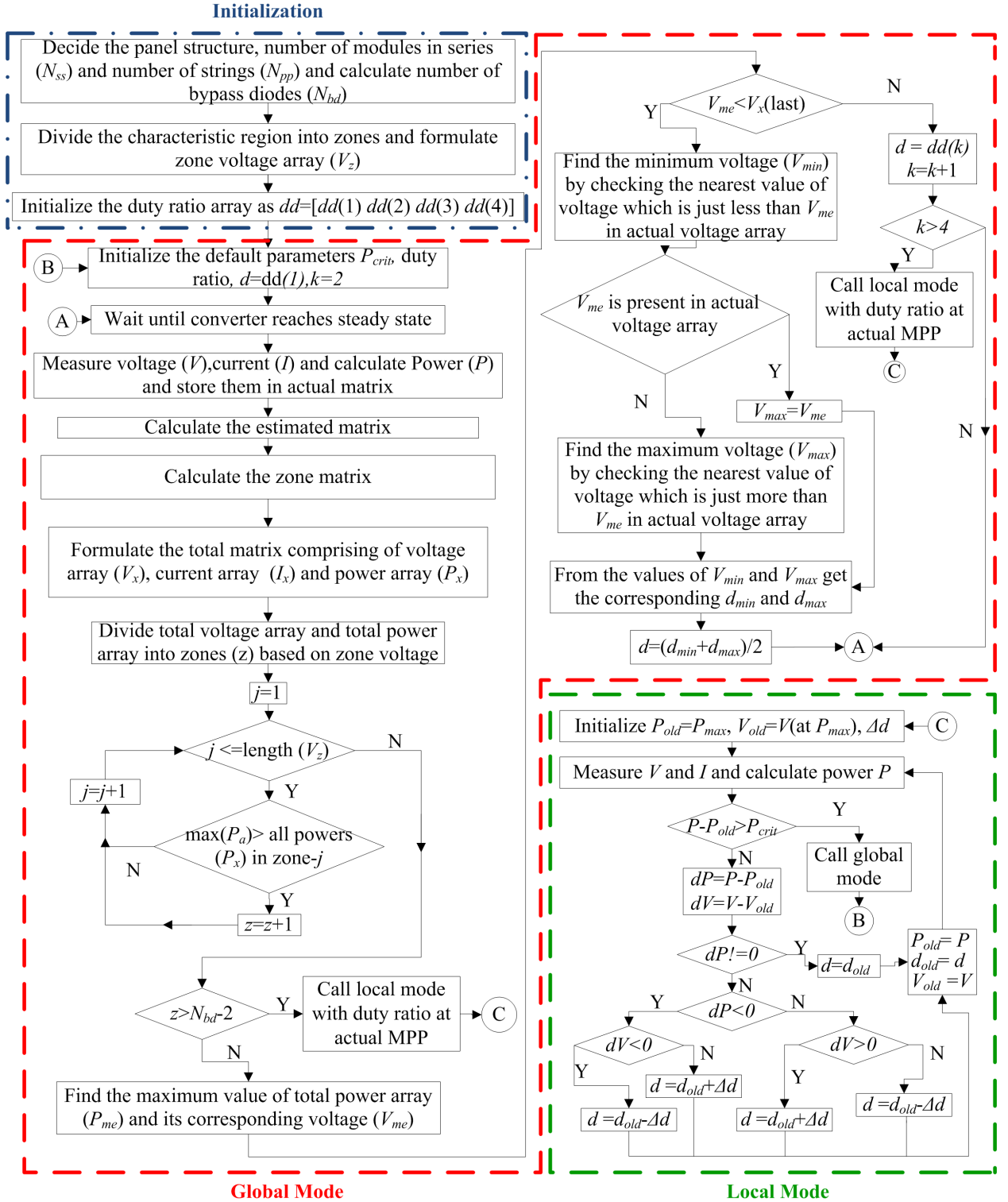
Figure 2.4: Flowchart of Proposed Method

- The corresponding duty ratios of $V_{\min}$ and $V_{\max}$ are denoted by $d_{\min}$ and $d_{\max}$ respectively. Obtain duty ratio by applying bisection method for $d_{\min}$ and $d_{\max}$ as in (2.24).

$$d = \frac{d_{\min} + d_{\max}}{2} \tag{2.24}$$

If the voltage corresponding to maximum estimated power is the last element of zonal voltage then

$$d = dd\,(k)\,; \qquad k = k + 1 \tag{2.25}$$

If $k > 4$ (initial value of k is 2), then operate the hill climbing method with duty ratio whose power is maximum is actual power array. The value of k is chosen to be four because the number of elements in dd array is four. If all the three values are initialized, then the hill climbing method will be operated at the point where maximum power is obtained. Else new duty ratio is obtained.

2.3   Simulation Results

The proposed global peak tracking algorithm is evaluated using simulations. Complete setup of simulation is represented as the block diagram in Fig. 2.5. PV panel is the source and is comprised of four modules in series. Two bypass diodes are connected for each module. So effectively there are eight submodules. The maximum power point algorithm is implemented in the MPPT block. This MPPT block takes PV voltage (V) and PV current (I) as input and generates duty cycle (d) as output. Pulse width modulation (PWM) block converts duty ratio into pulses required for the boost converter. Simulations are performed in MATLAB with a personal computer of 8 GB RAM, i74720HQ CPU.

The datasheet parameters of the module are presented in Table 2.1. Resistance is used as load. Boost converter is connected between source and load. Boost converter specifications are presented in Table 2.2.

Four different shading patterns are used for validating the proposed approach. The first shading pattern (P1) of G=[600 600 600 600 600 600 600 600]W/m^2 is given to eight sub modules at t=0s. At t=2s, the second shading pattern (P2) of [515 515 600 600 148 148 900 900] W/m^2 is applied. Shading Pattern-3 (P3) of G= G=[900 900 900 222 222 222 222 222] W/m^2 is applied at t=4s. Shading Pattern-4 (P4) of G=[700 700 750 750 413 413 623 623] W/m^2 is applied at t=6s. The I-V characteristics and P-V
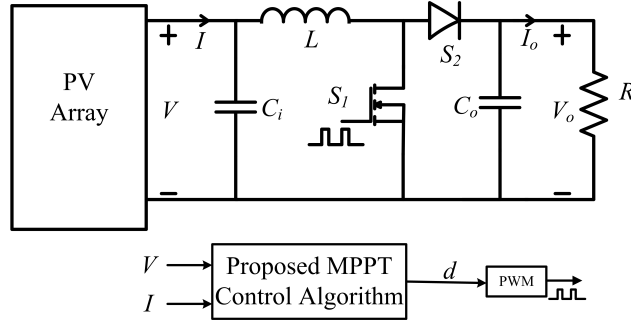
Figure 2.5: Block diagram for implementing proposed approach

Table 2.1: Datasheet Parameters of PV sub-module at STC

Parameter	Notation	Value
Maximum Power	P_{mpn}	37.5 W
Open Circuit Voltage	V_{ocn}	10.9 V
Short Circuit Current	I_{scn}	4.9 A
Voltage at maximum power	V_{mpn}	8.5 V
Current at maximum power	I_{mpn}	4.4 A
Number of cells in module	N_{s}	18

characteristics of shading patterns considered are shown in Fig. 2.6. The simulations results are compared with (Boztepe et al., 2014) and (Ghasemi et al., 2018).

The initial parameters viz., k and P_{crit} are set to 2 and 10W respectively. For Pattern-1(P1), it took four iterations for the proposed algorithm to reach the global maximum. From there, the hill climbing method maintains the operating point at the global maximum. The algorithm took 0.32s to reach the global peak. This can be noticed from PV Voltage, PV Current and PV power presented in Fig. 2.7. From Fig. 2.6, it can be noticed that the simulated power is in close agreement with the actual value of maximum power (P_{max}). The method in (Boztepe et al., 2014) takes 1.2s to reach the global peak and the method in (Ghasemi et al., 2018) takes 0.85s to

Table 2.2: Simulation Parameters of Boost Converter

Parameter	Notation	Value
Input Capacitance	C_{i}	300 μF
Output Capacitance	C_{o}	300 μF
Inducatnce	L	1 mH
Switching Frequency	f_{s}	25 kHz
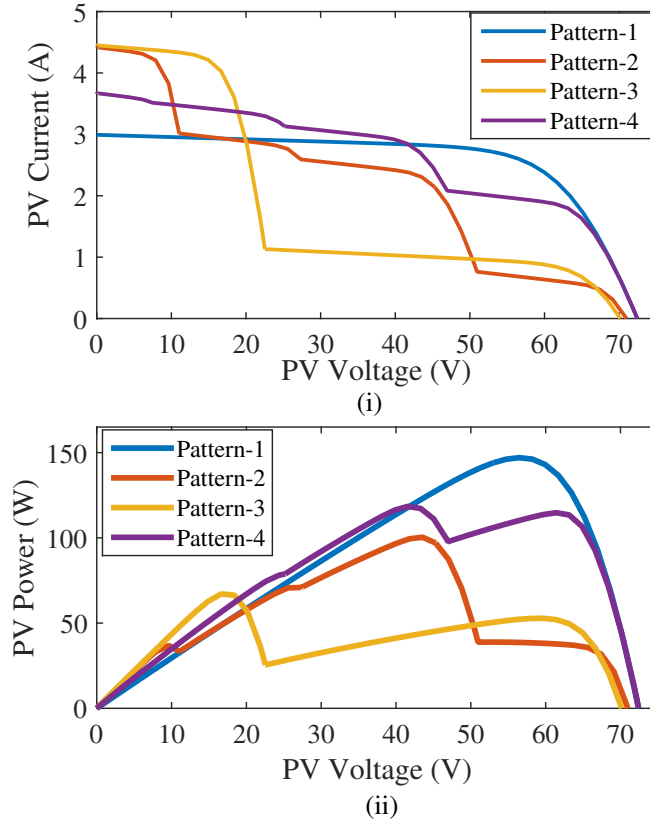
Figure 2.6: *I-V* and *P-V* curves of three shading patterns

reach the global peak. This can be noticed from Fig.2.8 and Fig. 2.9.

At t=2s, shading pattern is changed from P1 to P2. For this case, the maximum peak occurs at around 44V. The proposed algorithm took five iterations to track the global peak within a period of 0.46s as shown in Fig. 2.7. The method in (Boztepe et al., 2014) takes 1.05s and method in (Ghasemi et al., 2018) takes 0.62s to reach the global peak as depicted in Fig. 2.8 and Fig. 2.9. Shading pattern is changed from P2 to P3 at t=4s. The proposed algorithm took five iterations to reach the proximity of the global peak. It can be noticed from Fig. 2.7 that it took 0.54s to track the peak. The maximum power tracked is very close to the actual values of maximum power. But the method in Boztepe et al. (2014) has taken 0.62s to reach the global peak. The method in (Ghasemi et al., 2018) has taken 0.59s to reach the global peak. Shading pattern is changed from P3 to P4 at t=6s. The proposed algorithm took seven iterations to reach the proximity of the global peak. It can be noticed from Fig. 2.7 that it took 0.72s to track the peak. The method in Boztepe et al. (2014) has
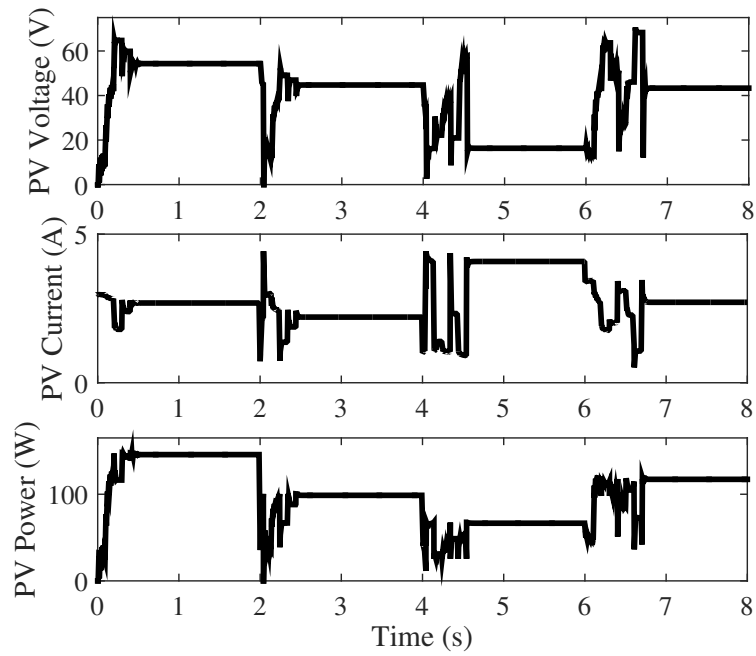
Figure 2.7: Simulations of PV Voltage, PV Current and PV power of the proposed method
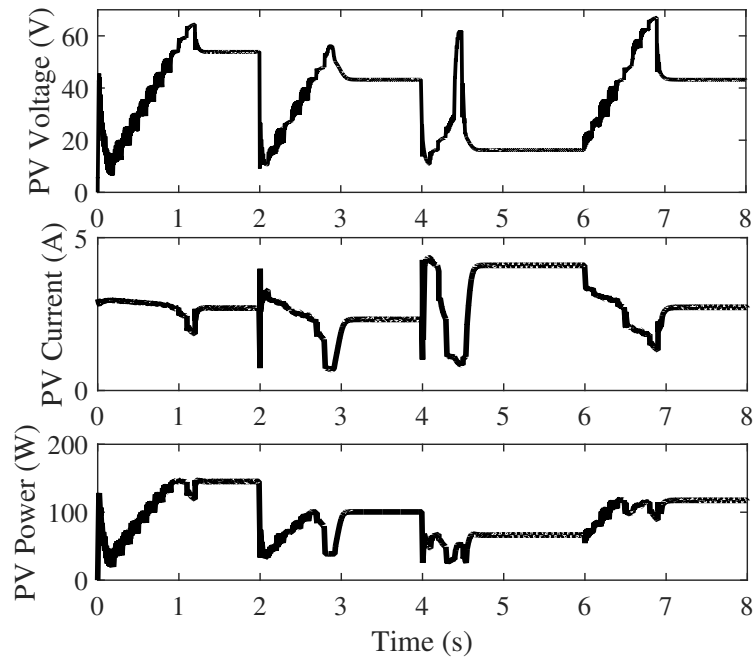
Figure 2.8: Simulations of PV Voltage, PV Current and PV power of the method presented in (Boztepe et al., 2014)
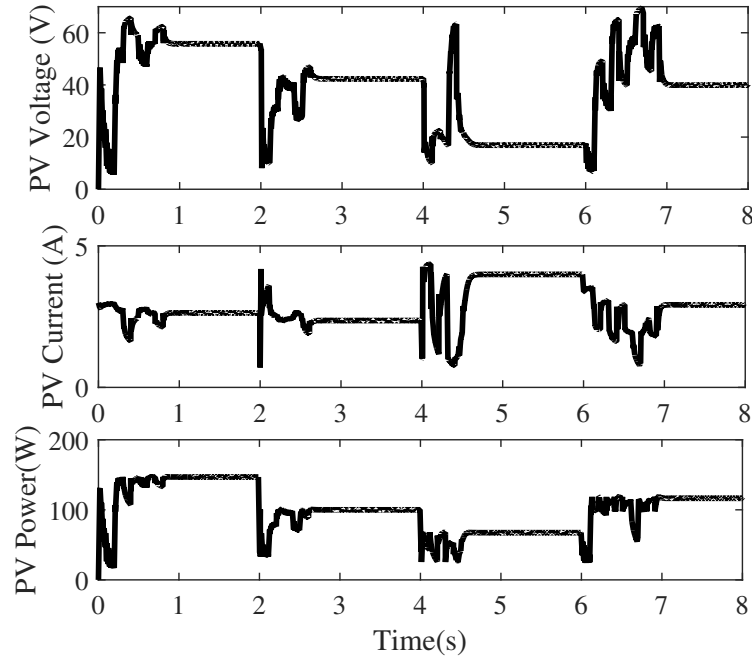
Figure 2.9: Simulations of PV Voltage, PV Current and PV power of the method presented in (Ghasemi et al., 2018)

Table 2.3: Tracking Time in simulation

Algorithm	Tracking Time (s)			
	P1	P2	P3	P4
Proposed	0.32	0.46	0.54	0.72
(Ghasemi et al., 2018)	0.85	0.62	0.59	0.95
(Boztepe et al., 2014)	1.2	1.05	0.62	1.05

taken 1.05s to reach the global peak. The method in (Ghasemi et al., 2018) has taken 0.95s to reach the global peak. The simulation times of proposed method, methods presented by (Boztepe et al., 2014) and (Ghasemi et al., 2018) are summarized in Table 2.3. On comparison with methods in (Boztepe et al., 2014) and (Ghasemi et al., 2018), the proposed method tracks global peak faster with good accuracy.
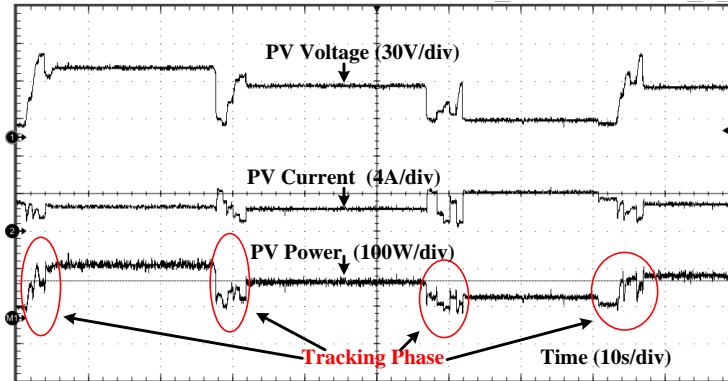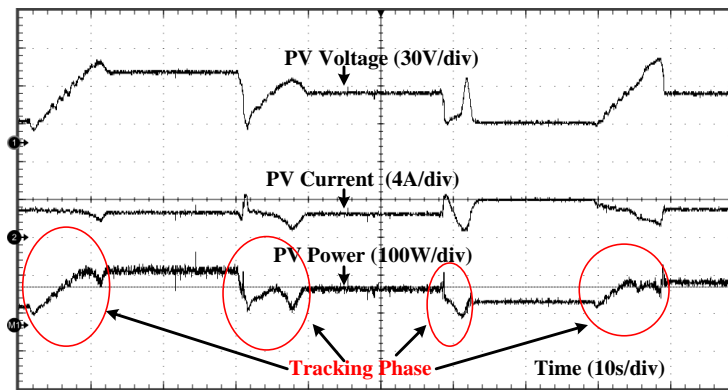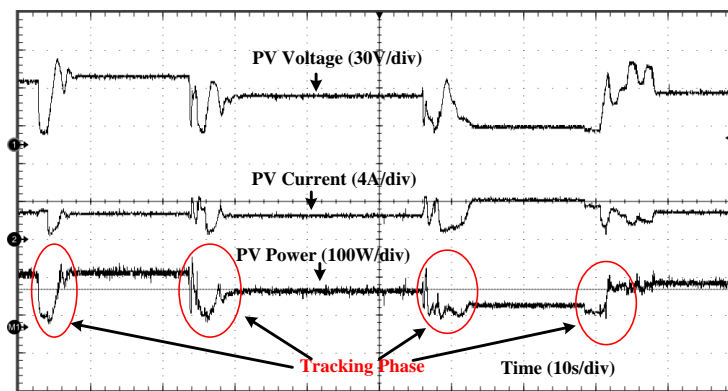
Figure 2.10: Experimental results of PV voltage (30V/div), PV current(4A/div) and PV power(100W/div) of all the four shading patterns (P1,P2,P3,P4) presented in Fig. 2.6 for (a) proposed method (b) method proposed in Boztepe et al. (2014) (c) method proposed in Ghasemi et al. (2018) Time scale: 10s/div

Table 2.4: Tracking Time in Hardware

Algorithm	Tracking Time (s)			
	P1	P2	P3	P4
Proposed	4.2	4.9	5.5	6.6
Ghasemi et al. (2018)	5.8	6.3	7.9	10.2
Boztepe et al. (2014)	10.9	10	5.7	10.3

2.4 Experimental Validations

The hardware setup used is presented in the Appendix. The proposed algorithm is verified using four different shading patterns presented in Fig. 2.6 using hardware setup. The algorithm is compared with two other existing algorithms presented in (Boztepe et al., 2014) and (Ghasemi et al., 2018). The waveforms of PV voltage, PV current and PV power for all the four shading patterns obtained using the proposed method, method in (Boztepe et al., 2014) and (Ghasemi et al., 2018) are presented in Fig. 2.10(a), (b) and (c) respectively. For pattern-1 (P1), it took 4.2s to track the peak. But the method in (Ghasemi et al., 2018) took 5.8s and method in (Boztepe et al., 2014) took 10.9s to track the peak. The tracking time for pattern-2 (P2) is 4.9s using the proposed method and the tracking time using (Boztepe et al., 2014) and (Ghasemi et al., 2018) for P2 are 6.3s and 10s respectively. For P3, the proposed algorithm took 5.5s to track the peak, the method in Boztepe et al. (2014) took 5.7s to track the peak and the method in (Ghasemi et al., 2018) took 7.9s to track the peak. The proposed took 6.6s to track the peak for pattern-4 (P4). The methods in (Ghasemi et al., 2018) and (Boztepe et al., 2014) took 10.2s and 10.3s to track the peak respectively. The tracking time of all these algorithms in hardware is summarized in Table 2.4. It can be validated from the experimental results that the proposed method tracks the global peak accurately with lesser tracking time.

2.5 Conclusion

A maximum power point tracking algorithm capable of tracking global peak under mismatching conditions is presented in this report. It operates in two stages. In the first stage, zone wise division of characteristics is performed based on open circuit voltage and panel characteristics. The possibility of occurrence of the global peak in

each zone is checked. The value of duty ratio is estimated based on bisection method. This stage brings the operating point to the proximity of the global maximum. In the second stage, the hill climbing algorithm maintains the operating point at MPP. For testing the algorithm boost converter is connected between source and load. The proposed algorithm is compared with an existing method. It is found that the proposed algorithm tracks the global maximum accurately in lesser time. Experimental validation is performed using solar modules, a boost converter, resistive load, and dSPACE controller. The proposed algorithm is found to be more reliable and efficient.

Chapter 3

Global Peak Tracking Using Current Control

Contents

3.1 Introduction

In this chapter, a current control technique is used for tracking the global peak. This method searches for the global peak by either multiplying or dividing the PV current by 0.9. The multiplication or division depends on the phase in which it is operating. There are two phases: backward phase and forward phase. The search is done both in the forward and backward direction of current obtained after the change in shading pattern. In the backward phase, the reference current is updated by dividing PV current with 0.9 until the PV voltage is less than the minimum voltage beyond which
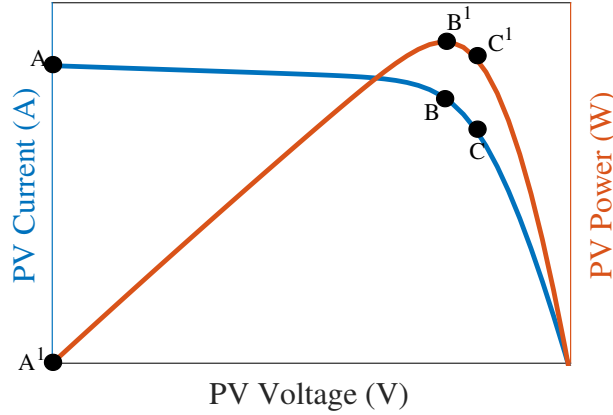
Figure 3.1: *I-V* and *P-V* characteristics under uniform Irradiance

there is no chance of occurrence of GP. In the forward phase, the reference current is updated by multiplying PV current with 0.9 until the PV current is less than the minimum value of current beyond which there is no chance of occurrence of the global peak. Simulations are performed in MATLAB to analyze the performance of the proposed algorithm. The proposed algorithm is experimentally validated using a solar simulator, boost converter, resistive load, and dSPACE MicroLabBox 1202 controller. The following assumptions are considered in this chapter.

- The value of cell temperature is considered constant

- The ratio of V_{mp} to V_{oc} and I_{mp} to I_{sc} will not exceed 0.9.

- The minimum irradiance falling on the PV panel is $100W/m^2$ and the maximum irradiance falling on the PV panel is $1000W/m^2$.

- The effects of degradation on PV modules are not considered.

3.2   PV Characteristics

For performing the detailed analysis of characteristics of the PV module in simulations, an equivalent circuit model is required. In this chapter, the single diode model is employed as an equivalent circuit of the PV module because of its simplicity and accuracy. It is depicted in Fig. 4.3(a). The expression for PV current (I) from the single diode model is given by (3.1) (Villalva et al., 2009).

$$I = I_{\text{ph}} - I_{\text{o}} \left\{ exp \left(\frac{q(V + IR_{\text{s}})}{akTN_{\text{s}}} \right) - 1 \right\} - \frac{V + IR_{\text{s}}}{R_{\text{p}}} \tag{3.1}$$

where I_{ph} is the light generated current , I_{o} is the diode reverse saturation current, R_{s} is the series resistance, R_{p} is the parallel resistance, a is the diode ideality factor, q is the electron charge, k is the Boltzmann constant, T is the cell temperature, N_{s} is the number of series connected cells in a module. *I-V* and *P-V* characteristics of PV module are presented in Fig. 3.1. The three important points in the curves are open circuit point ($V=V_{\text{oc}}$, $I=0$), short circuit point ($V=0$, $I=I_{\text{sc}}$) and maximum power point ($V=V_{\text{mpm}}$, $I=I_{\text{mpm}}$). Voltage at MPP for one module (V_{mpm}) and current at MPP for one module (I_{mpm}) are approximately given by (3.2) and (3.3) (Subudhi and Pradhan, 2013).

$$V_{\text{mpm}} = \delta_{\text{V}} V_{\text{ocm}} \tag{3.2}$$

$$I_{\text{mpm}} = \delta_{\text{I}} I_{\text{scm}} \tag{3.3}$$

V_{ocm} and I_{scm} are the open circuit voltage and short circuit current for a single module. δ_{V} and δ_{I} are constants and are PV module dependent. The values of δ_{V} and δ_{I} are considered as 0.9 (Masoum et al., 2002a). An approximate relation of (3.3) is presented in (3.4).

$$I_{\text{mpm}} \simeq 0.9 \times I; \quad I_{\text{scm}} \geq I \geq I_{\text{mpm}} \tag{3.4}$$

where I is the current at any operating point between I_{scn} and I_{mpn}. In Fig. 3.1, A, B, and C are the points on the *I-V* curve. A^1, B^1 and C^1 are corresponding points on the *P-V* curve. Point A is at short circuit point. By applying (3.4) at point A, the operating point close to the maximum power point is obtained. This is because the current at MPP is 0.9 times short circuit current (As per(3.4)). The obtained operating point from (3.4) is marked as point B in Fig.3.1. If the operating point is at point B, and (3.4) is applied to it, then the new equation becomes as shown in (3.5).

$$I_{\text{mpm}} \simeq 0.9 \times I_{\text{B}} \tag{3.5}$$

The operating point corresponding to (3.5) is at point C. The value of power at point C and C' is very close to the operating point at B which is very close to MPP. Similarly, for operating current at any point between points A and B, the I_{mpm} calculated from

(3.4) will lie in the vicinity of the peak. This fact is used for developing the global peak tracking algorithm in this chapter.

3.3   Proposed Methodology

3.3.1   Crucial Parameters for Implementing Proposed Approach

The important parameters for implementing the proposed approach are $V_{\min}$ and $I_{\min}$. $V_{\min}$ is the minimum value of voltage, below which there is no chance of occurrence of global peak. $I_{\min}$ is the minimum value of current below which there is no chance of occurrence of global peak. $V_{\min}$ and $I_{\min}$ are presented in (3.6) and (3.7)(Boztepe et al., 2014).

$$V_{\min} = \frac{P_{\max}}{I_{\mathrm{mp@STC}}} \tag{3.6}$$

$$I_{\min} = \frac{P_{\max}}{0.9 V_{\mathrm{oct}}} \tag{3.7}$$

Where $I_{\mathrm{mp@STC}}$ is the PV current at maximum power at a standard test condition. V_{oct} is the open circuit voltage of the complete array. The values of $V_{\min}$ and $I_{\min}$ are updated for every change in the value of maximum power ($P_{\max}$). These values are used for termination of a global peak tracking algorithm. In the backward phase, if the value of PV voltage (V) is less than $V_{\min}$, the backward phase is terminated, and the forward phase is initiated. In the forward phase, if PV current (I) is less than $I_{\min}$, then global peak tracking is terminated. The terminologies of the backward phase and forward phase are mentioned in section 3.1 and the operation of the algorithm in these phases are elaborated in the subsequent section (Section 3.3.2).

3.3.2   Procedure of Proposed Approach

The procedure for the proposed approach is presented as a flowchart in Fig. 3.2. For understanding the operation of the proposed algorithm, a PV array operating in mismatching condition is considered. Eight PV modules connected in series is used as PV array. The datasheet of the module used is presented in Table 2.1.
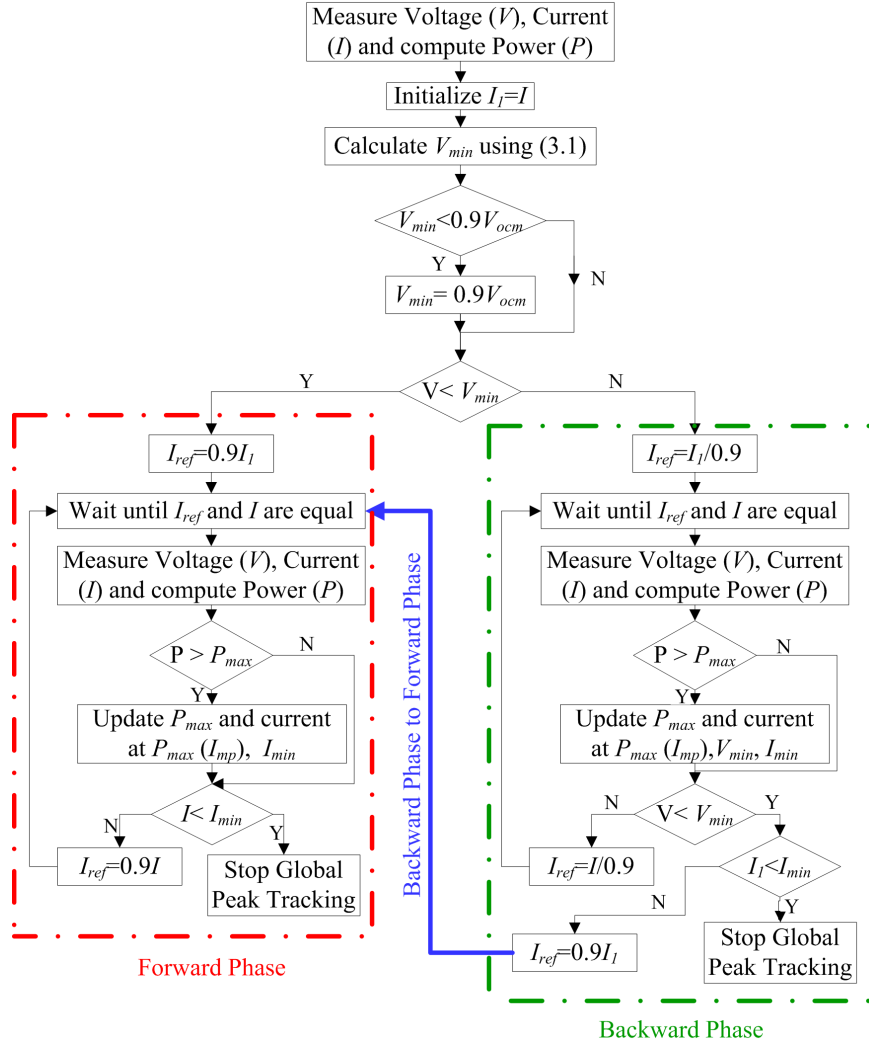
Figure 3.2: Flowchart of Proposed Method

Two irradiance patterns with four modules at 1000 W/m^2 and the other four at 300 W/m^2 are considered. The temperature is considered as 318K. The *I-V* and *P-V* characteristics of the pattern during a particular mismatching condition is presented in Fig. 3.3. Points A to L correspond to *I-V* curve, A^1 to L^1 correspond to *P-V* curve. The initial value is chosen at the middle of *I-V* curve (point A) in order to demonstrate the movement of the operating point in the backward and forward phase.

When a change in shading pattern is detected, the procedure in Fig. 3.2 is initiated. The initial value of current is assigned as I_1 (A in Fig. 3.3). The value of (V, I, P) at this point are (31.25V, 3.218A, 100.56W). The value of $V_{\min}$ calculated from (3.6) is 22.85V.
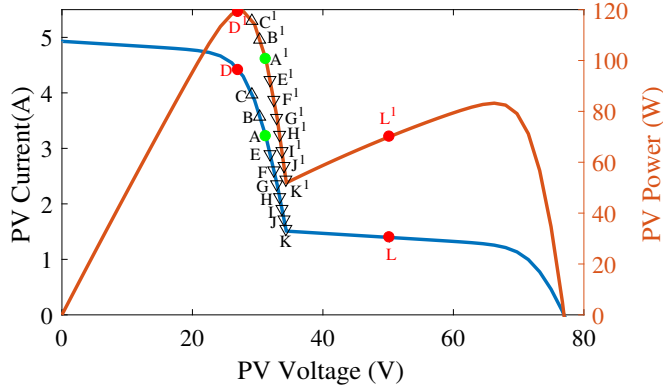
Figure 3.3: *I-V* and *P-V* characteristics under mismatching conditions

In a PV array with series connected modules, the value of $V_{\min}$ cannot be less than the voltage at the maximum power point of a single module ($0.9V_{\text{ocm}}$). So the condition $V_{\min} < 0.9V_{\text{ocm}}$ is checked. If it is satisfied then $V_{\min}$ is initialized as $0.9V_{\text{ocm}}$. The next condition $V < V_{\min}$ is checked. This condition decides whether the algorithm should operate in the backward phase or forward phase. If the value of the voltage (V) is less than $V_{\min}$, then the algorithm operates in the forward phase. Else the algorithm will operate in the backward phase. From Fig. 3.3, as the value of V at the initial point, is 31.25V and it is greater than $V_{\min}$, the algorithm operates in backward phase.

In backward phase, the value of current is divided by 0.9 to get the reference current (I_{ref}) as shown in (3.8).

$$I_{ref} = \frac{I}{0.9} \tag{3.8}$$

For every change in the value of I_{ref}, the corresponding PV voltage (V), PV current (I) are measured, and PV power (P) is computed. If the present value of power (P) is greater than $P_{\max}$, then $P_{\max}$ is updated as P. For every update in the value of $P_{\max}$, the values of current at maximum power (I_{mp}) is updated. The values of $V_{\min}$ and $I_{\min}$ are also updated using (3.6) and (3.7). In Fig. 3.3, the updation of reference current starts from point A (as it is the initial point). As the backward phase is initiated, the value of the reference current is updated using (3.8). The new value of reference current is 3.57A. It is denoted by point B in *I-V* curve and B^1 in *P-V* curve of Fig. 3.3. The value of (V,I,P) at this point B is (30.3V, 3.57A, 108.21W). As the value of power at point B is greater than the maximum power ($P_{\max}$), then $P_{\max}$ is updated, the values of $V_{\min}$ and $I_{\min}$ are also updated to 24.59V and 1.378A respectively as per

(3.6) and (3.7). The operating point will continue its perturbation in the backward direction until the value of PV voltage is less than $V_{\min}$. At point B in Fig. 3.3, the value of the PV voltage is greater than $V_{\min}$. So the algorithm is retained in backward phase, and the reference current is calculated. The updated value of reference current according to (3.8) is 3.97A which corresponds to the operating point C in I-V curve and C^1 in P-V curve of Fig. 3.3. The value of (V,I,P) at this point is (29.11V, 3.97A, 115.58W). As the power is greater than $P_{\max}$, $P_{\max}$ is updated as 115.58W. The value of $V_{\min}$ and $I_{\min}$ are computed as 26.27V and 1.472A respectively. As $V > V_{\min}$ (29.11 V > 26.27 V), the algorithm is retained in the backward phase, and new reference value of current is calculated as 4.41A and is denoted as point D in I-V curve and D^1 in P-V curve of Fig. 3.3. The value of (V,I,P) at this point is (27.78V, 4.41V, 122.5W). As $P > P_{\max}$, $P_{\max}$ is updated to 122.5W. The updated values of $V_{\min}$ and $I_{\min}$ are 27.84V and 1.56A respectively. At this point the PV voltage is less than $V_{\min}$ (27.78V < 27.84V).

If the condition $V < V_{\min}$ is satisfied, a decision should be made on whether the algorithm should go to forward phase or to stop the global peak tracking. Stoppage of global peak tracking indicates the algorithm has identified the global peak region. If $V < V_{\min}$, the algorithm checks whether the initial value of current (I_1) is less than minimum value of current below which there is no chance of occurrence of GP ($I_{\min}$). If I_1 is less than I_{min}, then global peak tracking is stopped. Else the operating point will move in the forward phase. As $V<V_{\min}$ at point D in Fig. 3.3, the backward phase is terminated and the condition $I_1<I_{\min}$ is checked. The value of I_1 is greater than $I_{\min}$ (3.218A > 1.56A). As I_1 is greater than $I_{\min}$, the algorithm moves from the backward phase to the forward phase.

During the start of the forward phase, the reference current is assigned as 0.9 times the initial value of current. From the next perturbation, the reference current in the forward phase is given by (3.9).

$$I_{ref} = 0.9I \tag{3.9}$$

The values of P_{max} and I_{min} are updated in a similar manner as described in the backward phase. The perturbation of reference current in the forward direction is continued until I is less than I_{min}. Once $I < I_{min}$, the global peak tracking is terminated, and the reference current is shifted to current at the maximum power

point (I_{mp}). In Fig. 3.3, the forward phase in initiated after the termination of the backward phase. As the initial value of reference current is $0.9I_1$, its value is 2.896A (0.9×3.218A), and it is denoted by point E in I-V curve and E^1 in P-V curve of Fig. 3.3. The values of (V,I,P) at this point are (31.89V, 2.896A, 92.35W). As the power is less than P_{max} , P_{max} is not updated. As there is no change in the value of maximum power (P_{max}), the values of V_{min} and I_{min} does not change. Since PV current is greater than I_{min}, the reference current is updated using (3.9). The new value of reference current is 2.604A, and it is denoted by point F in I-V curve and F^1 in P-V curve of Fig. 3.3. The (V,I,P) at point F is (32.47V, 2.604A, 84.55W). The value of PV power is less than P_{max}, and the value of PV current is more than I_{min}. So the reference current is updated using (3.9). This process is continued until point L. In Fig. 3.3, the points between F and L are G, H, I, J and K. The reference currents at points G, H, I, J and K in Fig. 3 are 2.35A, 2.12A, 1.91A, 1.72A and 1.55A respectively. At all these points the value of powers is less than P_{max}. This is evident from point G^1, H^1, I^1, J^1 and K^1 in Fig. 3.3. The current at point K is less than I_{min}. As the value of the current is less than the value of the current below which there is no chance of occurrence of GP (I_{min}), the forward phase is terminated. The value of I_{ref} is set to I_{mp} (at point D) which is the current at the maximum power point. After global peak tracking is terminated, the operating point is retained at global peak using a conventional MPPT algorithm.

The conventional MPPT algorithm will be operated until there is a change in the shading pattern. Once there is a change in the shading pattern, the proposed global peak tracking algorithm will be operated. The change in the shading pattern is detected if the change in power is greater than the pre-specified value of critical power (P_{crit}).

3.4   Simulation Results

The performance of the proposed algorithm is verified using simulations in MATLAB. The circuit diagram for implementing the proposed algorithm is shown in Fig. 3.4. PV array is connected to a resistive load with a boost converter as a power interface. PV array with eight modules connected in series is used for simulations. The specifications of the module used are presented in Table 2.1. The parameters of the boost converter are calculated using the procedure mentioned in (Mohan and Undeland, 2007) and are
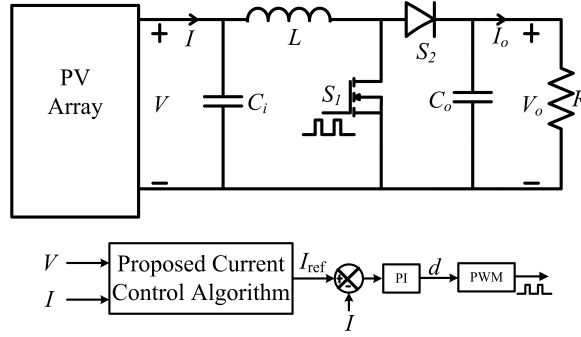
Figure 3.4: Circuit Diagram for Implementing the Proposed Approach
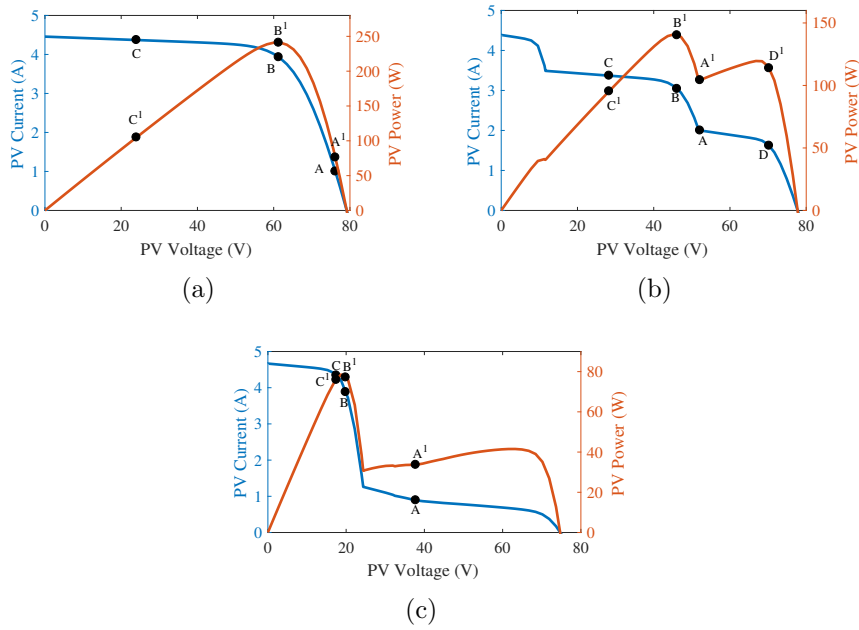
Figure 3.5: *I-V* and *P-V* characteristics for (a) Pattern-1 (b) Pattern-2 (c) Pattern-3

presented in Table 2.2. The MPPT controller takes PV voltage (V) and PV current (I) as inputs and gives reference current (I_{ref}) as output. The difference between the reference current and PV current ($I_{\text{ref}} - I$) is given as input to the PI controller, and the duty ratio is obtained as output. Pulse Width Modulator (PWM) converts the duty ratio into pulses for switch S_1. The proposed algorithm is compared with the search-skip-judge method presented in (Wang et al., 2016).

Three different shading patterns are used for verifying the effectiveness of the proposed algorithm. The *I-V* and *P-V* characteristics of shading pattern-1 (P1), shading pattern-2 (P2) and shading pattern-3 (P3) are presented in Fig. 3.5(a), Fig.
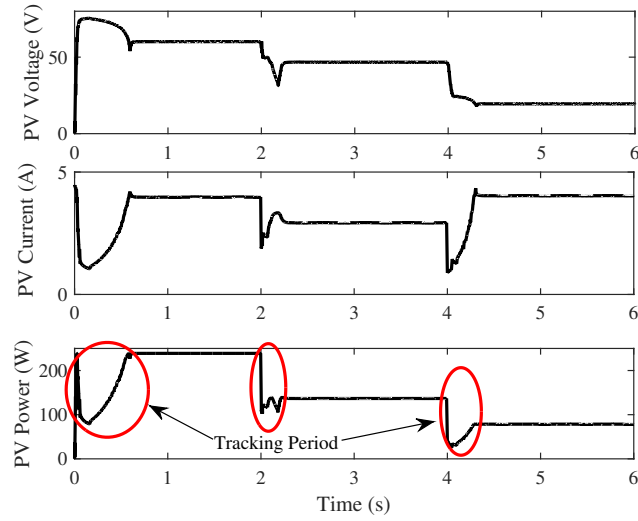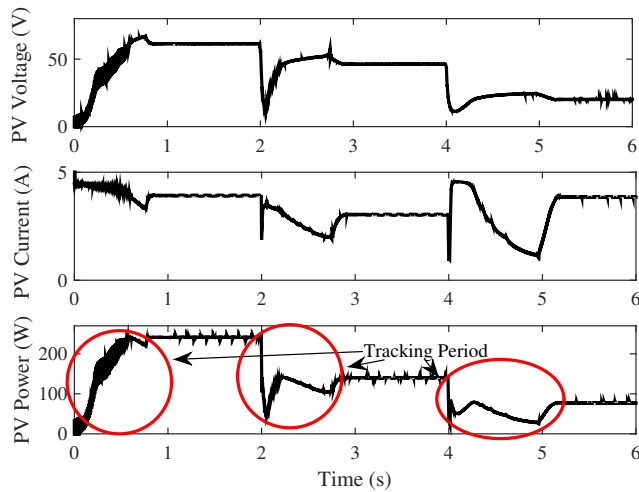
Figure 3.6: PV voltage, PV current, PV power for (a) Proposed Method (b) method in (Wang et al., 2016)

3.5(b) and Fig. 3.5(c) respectively. Shading pattern-1 is applied with irradiance of [900 900 900 900 900 900 900 900] W/m^2 for eight modules. It is applied from time t=0 to 2s. Shading pattern-2 is applied from t=2s to t=4s. The irradiance for this pattern is [900 900 700 700 700 700 400 400] W/m^2. Shading pattern-3 is applied from t=4s to t=6s. The irradiance for this pattern is [950 950 950 250 200 175 160 170] W/m^2. PV voltage (V), PV current (I) and PV power (P) obtained using proposed algorithm is presented in Fig.3.6(a). PV voltage (V), PV current (I) and PV power

(P) obtained for (Wang et al., 2016) is presented in Fig.3.6(b). The pre-specified value of critical power (P_{crit}) is chosen as 10W.

At t=0s, shading pattern-1 is applied. The initial reference current (I_{ref}) of the algorithm is 1A(I_1). At this I_{ref}, the values of (V, I, P) are (76.17V, 1A, 76.17W). The value of $V_{\min}$ obtained from (3.6) is 17.31V. As the value of $V_{\min}$ is greater than $0.9V_{\mathrm{ocm}}$, next condition $V < V_{\min}$ is checked. As $V > V_{min}$, the algorithm moves to backward phase. The current reference is assigned in the backward direction as per (3.8). As it is moved in the backward direction, the value of I_{ref} increases. It can be noticed from Fig. 3.5(a) that the movement of the operating point in the backward direction from A will have an increase in maximum power($P_{\max}$) which is continued until B. The (V, I, P) at B are (61.3V, 3.93A, 240.9W). This point occurs at t=0.58s in Fig. 3.6(a). At this point the updated values of $V_{\min}$ and $I_{\min}$ are 54.75V and 3.06A. The next perturbation of I_{ref} done using (3.8) is 4.35A(C in Fig.3.5(a)). In the process of moving towards 4.35A, the algorithm detects voltage less than $V_{\min}$ at t=0.067s (in Fig.3.6(a)). The value of the voltage at this point is 47.6V. So the backward phase is terminated. The condition $I_1 < I_{\min}$, which decides whether the algorithm should operate in forward phase or global peak tracking termination criteria is checked. The condition gets satisfied as I_1 is 1A and $I_{\min}$ is 3.05A. So the global peak tracking is terminated, and current at maximum power(3.93A) is assigned to I_{ref}. From this point, conventional perturb and observe method is used to retain the operating point at MPP. It takes 0.62s to track the peak while the algorithm in (Wang et al., 2016) takes 0.8s.

The shading pattern-2 is applied at t=2s. The operating point is shifted to (62.75V, 2A, 125.5W). As the change in power is greater than P_{crit} (10W), the global peak tracking algorithm is activated with an initial current(I_1) of 2A(point A in Fig. 3.5(b)). The same procedure is followed to track the peak. It can be noticed from Fig. 3.5(b) and Fig. 3.6(a) that for this pattern both backward phase(A to C in Fig. 3.5(b)) and forward phase(A to D in Fig. 3.5(b)) are activated. The global peak is at B, and it is tracked as presented in Fig.3.6(a). The values of (V, I, P) is (45.9V, 3.05A, 140W). The tracking time is 0.29s. The tracking time for the method proposed in (Wang et al., 2016) is 0.88s, and it can be noticed from Fig.3.6(b). The shading pattern-3 is applied at t=0.8s in Fig. 3.6(a). The operating point immediately after the change in the shading pattern is (44.5V, 0.824A, 36.68W). As the change in power is greater than P_{crit} (10W), the global peak tracking is initiated with an initial

Table 3.1: Comparison of Tracking Time in Simulations

	Tracking Time (s)		
Algorithm	P1	P2	P3
Proposed	0.62	0.29	0.33
Wang et al. (2016)	0.8	0.88	1.17

current(I_1) of 0.824A. The global peak is tracked at (19.43V, 4.04A, 78.5W). It can be noticed from Fig. 3.5(c) that for this pattern only backward phase is activated (A to C). The maximum power is tracked at C and B is the operating point preceding to C. The tracking time of the proposed method is 0.33s while the method presented in (Wang et al., 2016) takes 1.17s to track the peak. Comparison of tracking time in simulations for the proposed method and method in (Wang et al., 2016) is presented in Table 3.1. The proposed algorithm tracks the global peak faster than the existing method.

3.5   Hardware Implementation

The hardware setup used is presented in the appendix. Three different shading patterns used in simulations are used for validation in this section. The corresponding tracked PV voltage, PV current and PV power for P1, P2 and P3 are shown in Fig. 3.7(a), Fig. 3.7(b) and Fig. 3.7(c) respectively. For shading pattern-1 (P1), it takes 9.8s to track the global peak. For shading pattern-2 (P2), the proposed algorithm takes 7.6s to track the peak. For shading pattern-3 (P3), the proposed algorithm takes 12s to track the peak.

In Fig. 3.7, global peak tracking of all the three shading patterns are done separately. In order to check the real-time performance of the proposed algorithm in hardware, dynamic tracking is implemented using all three shading patterns (P1, P2, P3). The PV voltage, PV current and PV power of the proposed algorithm is presented in Fig. 3.8(a). At time(t)=0s, P1 is activated. The value of I_1 for P1 is 2.5A. The time taken to track the peak is 9.8s. In this case, the backward phase is initiated. The value of GP is at (60V, 4A, 240W). The value of I_{min} at this point is 3.05A. After the backward phase is terminated, the algorithm will not go to forward phase because of $I_1 < I_{min}$. In Fig. 3.8(a), P2 is activated at t=77s. The change in power is greater than P_{crit} (10W). So the global peak tracking algorithm is activated.
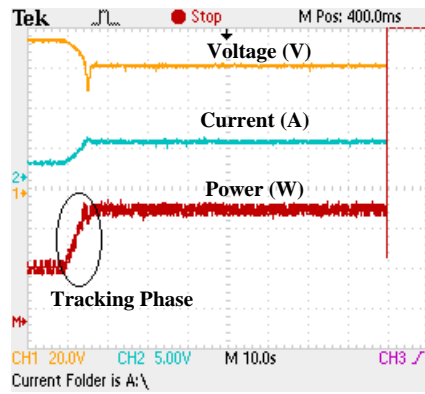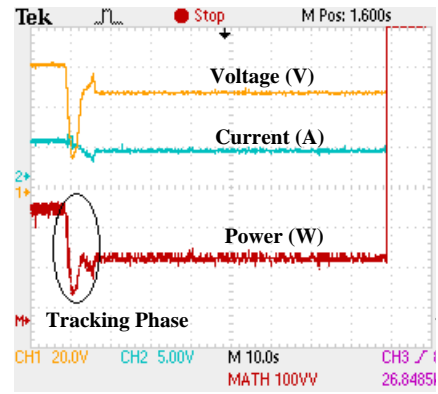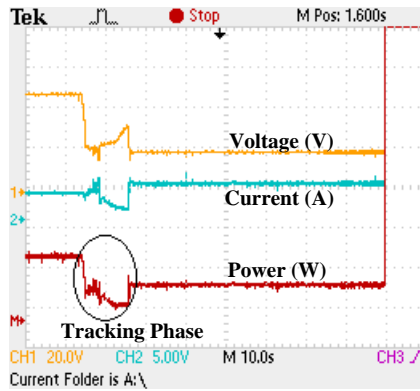
Figure 3.7: PV voltage, PV current, PV power obtained from hardware prototype of proposed method for (a) P1 (b) P2 (c) P3
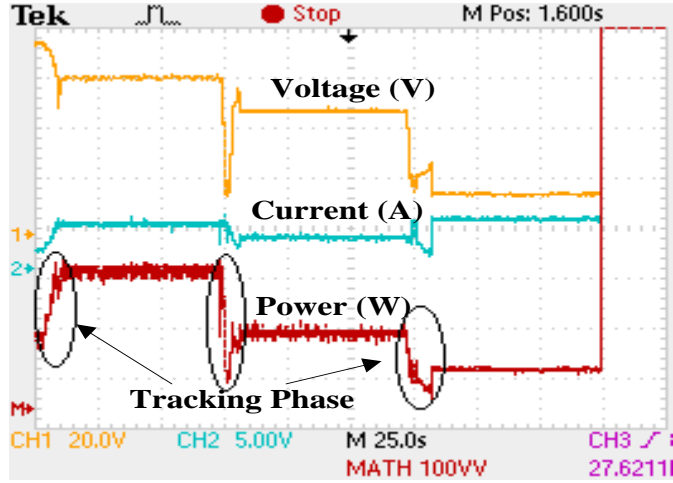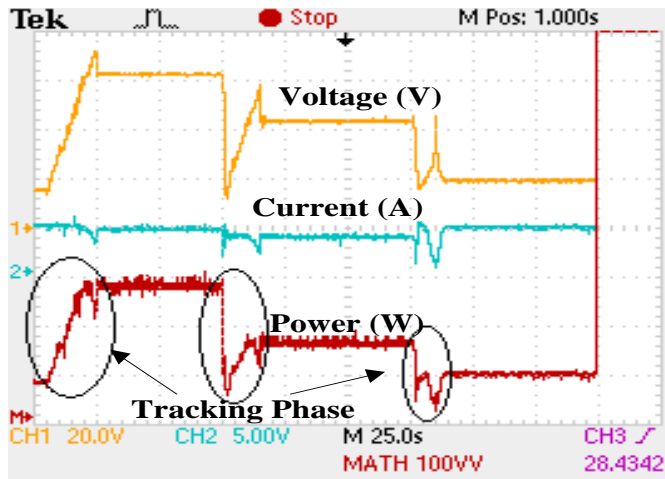
Figure 3.8: PV voltage, PV current and PV power of P1, P2 and P3 obtained from (a) proposed method (b) method in (Wang et al., 2016)

It took 7.8s to track the peak. P3 is activated at t=144s in Fig. 3.8. It took 13s to track the global peak. The values of PV voltage, PV current and PV power for all the three shading patterns obtained using (Wang et al., 2016) is presented in Fig. 3.8(b). The algorithm proposed in (Wang et al., 2016) takes 24s for tracking global peak of P1, 18s for tracking GP of P2 and 15s for tracking GP of P3. The tracking time in hardware for the proposed method and method in (Wang et al., 2016) are summarized in Table 3.2. It can be noticed that the proposed method performs better than the existing method in terms of tracking time.

The tracking time in hardware implementation is more than the simulation time.

Table 3.2: Comparison of Tracking Time in Hardware

Algorithm	Tracking Time (s)		
	P1	P2	P3
Proposed	9.8	7.8	13
(Wang et al., 2016)	24	18	15

This is because the hardware system is rated for a higher power (2KW). Because of the higher values of inductance and capacitance than those used in the simulation, the time constant of the system is more. Apart from this, the equivalent series resistance of inductors and capacitors, sampling and acquisition time in analog to digital converters also lead to an increase in tracking time. It can be validated by the experimental results that the proposed method tracks the global peak accurately.

3.6   Conclusion

A global peak tracking algorithm based on current control for tracking global peak is proposed in this chapter. The algorithm operates in two phases. They are the backward phase and the forward phase. Initially, the reference current is moved in the backward direction by dividing PV current with 0.9. The movement is continued in the backward direction until a termination criterion is met. Then the reference current is moved in the forward direction, from the initial value of current by multiplying PV current with 0.9. The movement is continued until a particular termination criterion is met. The maximum power obtained in this search process is the global peak. The performance of the proposed method is analyzed using simulations in MATLAB. Experimental validation is done using a solar array simulator, the boost converter, resistive load, and dSPACE controller. The proposed method accurately tracks the global peak with less computational time.

Chapter 4

Global Peak Tracking Algorithm Using Voltage and Current Conrol

Contents

4.1 Introduction

A global peak tracking algorithm based on voltage and current control is presented in this chapter. Three modes viz., initialization mode, voltage control, and current control mode are used for tracking the global peak. Initialization mode will be activated immediately after the change in shading pattern. The initial parameters required are specified in this mode. The algorithm operates in either voltage control mode or current control mode for tracking the global peak. The choice to operate in either voltage control mode or current control mode is made using a decision variable.

Current control mode identifies the succeeding maximum power point. Voltage control mode identifies the succeeding inflection point. The operation of these modes will continue until the condition for terminating the global peak is satisfied. The conventional MPPT is used to retain the operating point at MPP.

The following assumptions are considered in this chapter.

- The value of cell temperature is considered constant

- The ratio of V_{mp} to V_{oc} and I_{mp} to I_{sc} will not exceed 0.9.

- The minimum irradiance falling on the PV panel is $100\text{W}/\text{m}^2$ and the maximum irradiance falling on the PV panel is $1000\text{W}/\text{m}^2$.

- The effects of degradation on PV modules are not considered.

4.2 Crucial Parameters for Implementing Proposed Algorithm

The proposed algorithm is based on the observation presented in section 3.2 related PV module characteristics. The critical parameters used in the proposed approach are the same as that of section 3.2. They are V_{min} and I_{min}. However, the proposed algorithm in chapter 3 is based on current control and the proposed algorithm in this chapter is based on voltage and current control.

The proposed algorithm operates in either voltage control mode or current control mode in the process of tracking the GP. The choice to use voltage or current control mode is based on a decision variable (dec). If the value of dec is zero, the current control mode is activated, else voltage control mode is activated. In the current control mode, succeeding peak from the present operating point is determined. The reference current (I_{ref}) in this mode is given by (4.1).

$$I_{\text{ref}} = 0.9 \times I \tag{4.1}$$

In voltage control mode, succeeding inflection point to the current operating point is determined. The reference voltage (V_{ref}) in this mode is given by (4.2).

$$V_{\text{ref}} = V + V_{\text{step}} \tag{4.2}$$

76

where V_{step} is a small increment in the value of voltage.

Apart from these parameters, there is a condition which serves as the criteria for terminating the algorithm from global peak tracking. The condition is given by (4.3)

$$0.9 \times I < I_{\text{min}} \qquad (4.3)$$

If the value of $0.9I$ is less than I_{min}, there is no chance of occurrence of the global peak at a value less than $0.9I$. In current control, I_{ref} is given by (4.1). It means that the subsequent peak will be occurring at $0.9 \times I$. If $0.9 \times I$ is less than I_{min}, then it indicates that the current at next peak is less than I_{min} indicating that there is no possibility of occurrence of the global peak beyond that point.

The algorithm will operate in voltage control mode when the operating point is in the constant voltage region. The algorithm retains in voltage control mode until an inflection point is achieved. At any point in the constant voltage region, the operating point corresponding to $0.9 \times I$ will lie between two adjacent peaks. If the value $0.9 \times I < I_{\text{min}}$, then there is no chance that GP lies after $0.9 \times I$.

4.3   Proposed Algorithm

4.3.1   Methodology

The description of the proposed voltage and current control algorithm is presented as a flowchart in Fig. 4.1. The proposed algorithm operates in three modes viz., initialization, voltage control, and current control.

After the change in the shading pattern is detected, initialization mode is activated. The values of V and I are measured and the value of P is computed. The value of maximum power (P_{max}) is updated to P and the voltage at maximum power (V_{mp}) is updated to V. V_{min} and I_{min} are calculated using (3.6) and (3.7). The value of V and I obtained are initial values of voltage and current and are assigned to V_1 and I_1 respectively.

In this mode, initially voltage control is operated by initializing V_{min} and V_{ref}. If the value of V_{ref} is less than voltage at MPP of single module ($0.9 \times V_{\text{ocm}}$) connected in a string, then reference voltage is assigned as 0.9 x V_{ocm} . After V_{ref} is reached, current mode is activated by assigning zero to *dec*. Before calculation of reference current, the termination criteria is searched. If $0.9 \times I$ is less than I_{min}, then global peak tracking

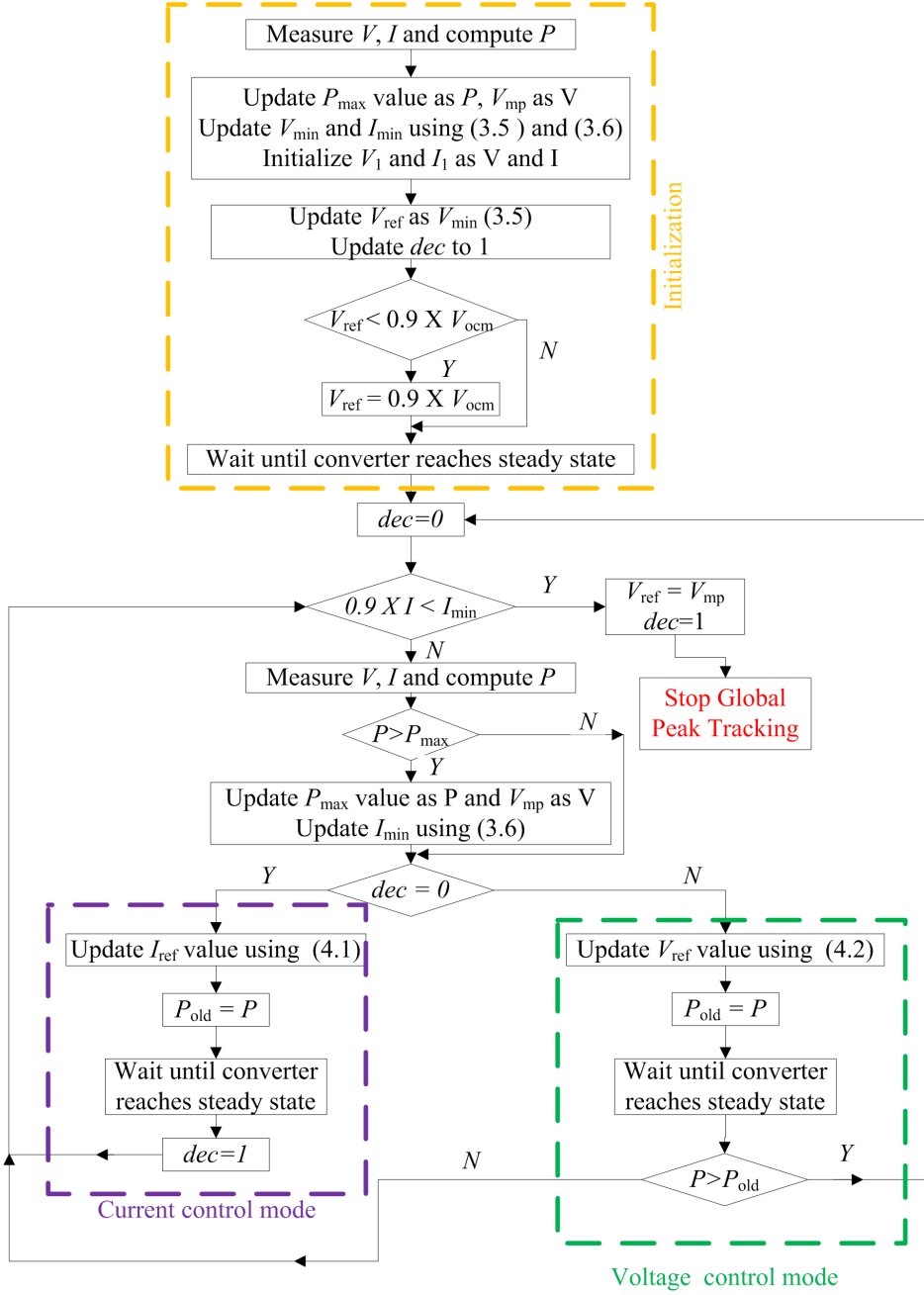**Figure 4.1:** Flowchart of Proposed Method

is terminated and the algorithm operates in local mode with conventional MPPT algorithm. If $0.9 \times I$ is greater than I_{min}, the values of V and I are obtained and P are computed. The value of P_{max} is updated if the power is greater than present value of maximum power (P_{max}). V_{mp}, I_{min} are also updated. Then, the value of

78

the previous value of power (P_{old}) is updated as P and the voltage control mode is activated. Before finding the reference voltage, the termination criteria is checked. If it is not satisfied, the value of P_{max} is updated if there is an increase in power. As the voltage control mode is on, *dec* will be 1. So the voltage control mode is activated and the reference voltage (V_{ref}) is updated using (4.2) by giving a small step in the value of voltage. The value of P_{old} is updated. After a steady state is reached with voltage (V) equal to V_{ref}, the values of V and I are obtained and P are computed. If the value of P is less than P_{old}, it indicates that the operating point has crossed the local MPP. The algorithm will continue to perform in voltage control mode until an inflection point is detected. The inflection point is obtained when P are greater than P_{old}. Then current control mode is activated. The process is continued until any one of the termination criteria is satisfied.

Once the termination criterion is satisfied, the algorithm operates in the local mode with voltage control. The algorithm will be in local mode until there is a change in the shading pattern. The change in shading pattern will be detected if the change in power is greater than P_{crit}.

4.3.2 Illustration

In order to demonstrate the working of the proposed algorithm, a shading pattern is considered. The *I-V* and *P-V* characteristics of the shading pattern is presented in Fig.4.2.
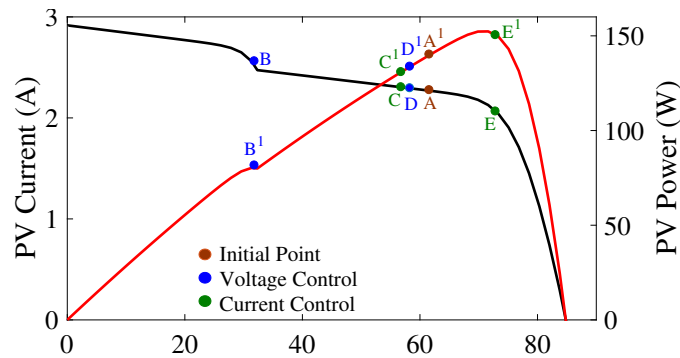

Figure 4.2: *I-V* and *P-V* curves of PV module of a shading pattern to illustrate the proposed algorithm

In Fig. 4.2 the points on *I-V* curve are presented from A to E and the values on *P-V* curve are presented from A^1 to E^1. The initial operating point after the change

in shading pattern is at A in *I-V* curve and A[1] in the *P-V*. The operating point is at (61.6V, 2.275A, 140.14W). The value of P_{max} is updated to 140.14W. The value of V_{mp} is 61.6V and the values of V_{min} and I_{min} are 31.85 V and 1.91 A respectively. In the initialization mode, the reference voltage is made equal to V_{min}. So the value of V_{ref} is 31.85 V which is less than 9.72V (V_{mp} of the single module). After reaching the steady state, the operating point will be at (31.85V, 2.561 A, 81.56V). This point is represented by B in *I-V* curve and B[1] in *P-V* curve. As the current control mode is activated, the reference current is calculated and is found to be 2.304A. After the steady state is reached the operating point will be (56.8V, 2.304A, 130.8672W) which is represented by point C in *I-V* curve and C[1] in *P-V* curve. The value of P_{max} and I_{min} are updated. The value of I_{min} is 1.78A. After the current control mode, the voltage control mode is activated by making *dec* to 1. A V_{step} of 1.5V is given. The updated value of V_{ref} is 58.3V. After the steady state is reached, the operating point is at (58.3V, 2.294A, 133.74W) denoted by D and D[1] in *I-V* and *P-V* curves respectively. The value power is greater than the previous values of power (P_{old}). So the current control mode is activated and the reference current is initialized after updating the values of V_{mp}, V_{ref}, I_{min}.

After a steady state is reached, the reference current is at point E in *I-V* curve and E[1] in *P-V* curve. The operating point is (72.86V, 2.064A, 150.38W). The value of P_{max} is updated 150.38W, V_{mp} to 72.86V and I_{min} to 2.04 A. In this case, $0.9I$ is 1.85 A which is less than I_{min}. So the global peak tracking is terminated and the algorithm will operate in the voltage control mode in local mode. The value of V_{ref} is updated to 72.86V and conventional P and O MPPT algorithm are used to retain the operating point at MPP.

4.4 Simulations

The performance of the proposed algorithm is verified using simulations in MATLAB. The circuit diagram used in this chapter is presented in Fig. 4.3. Fig. 4.3(a) is the power circuit comprising of PV modules, boost converter and a resistive load. PV module comprises eight PV submodules connected in series. Each PV submodule is equipped with a bypass diode. C_i is the input capacitor, C_o is the output capacitor of the boost converter, L is boost inductor, S_1 is controlled switch of the boost converter, S_2 is the uncontrolled switch of the boost converter. The datasheet parameters of
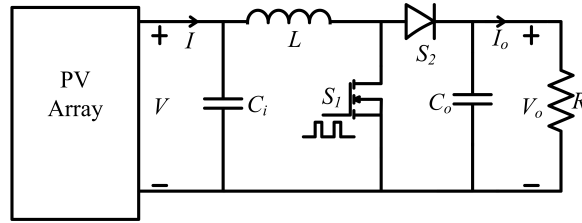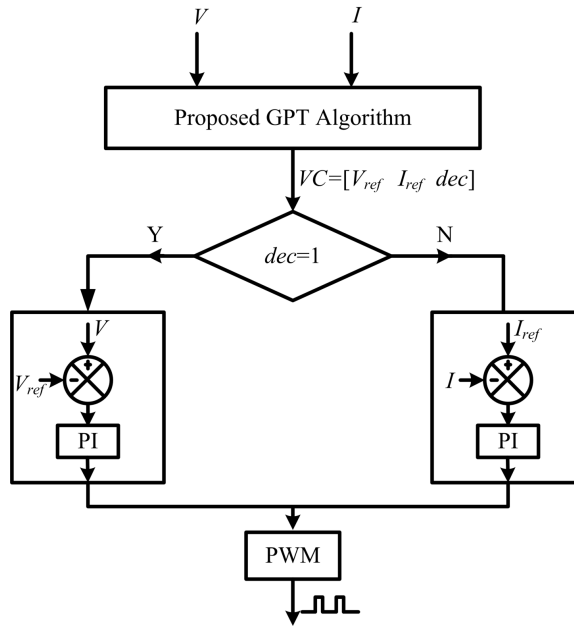
Figure 4.3: (a) Power circuit (b) Control circuit

the module used are presented in Table 2.1. The parameters of the boost converter used are presented in Table 2.2. Fig. 4.3(b) depicts the control circuit. It basically consists of a proposed global peak tracking (GPT) algorithm. The inputs to the GPT algorithm are PV Voltage (V) and PV current (I). The output is an array comprising of reference voltage(V_{ref}), reference current(I_{ref}) and a decision variable (dec). There are two control modes: voltage control mode and current control mode. Only one mode is activated for an instant. The decision to chose voltage or current mode is done by the decision variable dec. If the value of dec is 1, voltage control is activated. Else current control is activated. Depending on the control, the respective PI controller is used for generating duty ratio which is given to PWM for the generation of pulses to the boost converter.

Table 4.1: Comparison of Tracking Time in Simulations

|	Tracking Time (s)		
Algorithm	P1	P2	P3
Proposed	0.18	0.42	0.55
(Boztepe et al., 2014)	0.484	0.82	0.68

The proposed algorithm is compared with the voltage window search algorithm presented in (Boztepe et al., 2014). Three different shading patterns are used for verifying the effectiveness of the proposed algorithm. The curves are plotted in such a way that the peaks occur in three different regions. The regions are rightmost part of the P-V Curve, leftmost part of the P-V curve and center of the *P-V* Curve. The data in the plots are obtained by the simulations using single diode PV model. Shading pattern-1 is applied with an irradiance of [850 850 850 850 850 850 850 850] W/m^2 for eight modules. It is applied from time $t=0$ to 2s. Shading pattern-2 is applied from $t=2$s to $t=4$s. The irradiance for this pattern is [900 900 700 700 700 700 400 400] W/m^2. Shading pattern-3 is applied from t=4s to t=6s. The irradiance for this pattern is [950 950 950 250 250 250 250 250] W/m^2. The *I-V* and *P-V* characteristics obtained for three different shading patterns are presented in Fig. 4.4. PV voltage (V), PV current (I) and PV power (P) obtained using proposed algorithm is presented in Fig.4.5(a). PV voltage (V), PV current (I) and PV power (P) obtained for (Boztepe et al., 2014) is presented in Fig.4.5(b). The pre-specified value of critical power (P_{crit}) is chosen as 10W.

At t=0s, shading pattern-1 (P1) is applied to the power converter. The proposed algorithm takes 0.18s to track the GP. But the proposed algorithm in (Boztepe et al., 2014) takes 0.484s to track the peak. The shading pattern-2 (P2) is applied at t=2s. The proposed algorithm takes 0.42s to track the peak. The algorithm in (Boztepe et al., 2014) takes 0.82s to track the global peak. The shading pattern-3 is applied at t=4s. It takes 0.55s for the prosed algorithm to track the peak. The algorithm in (Boztepe et al., 2014) takes 0.68s to track the peak. The comparison of tracking time in simulations is presented in Table 4.1. It can be noticed that the proposed algorithm tracks the global peak accurately with reduced oscillation at steady state.

However, the saving in time is not much in P3. This scenario arises in a group of eight modules where three modules are highly irradiated and other five receives less irradiance. Then the peak occurs at the leftmost part of the curve. The number of
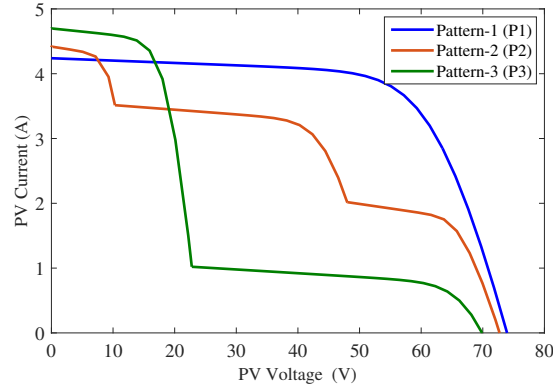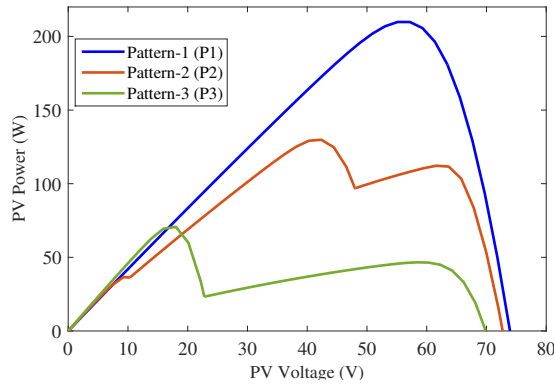
Figure 4.4: (a)*I-V* and (b)*P-V* curves of three different shading patterns

points to be scanned according to the algorithm are more in this scenario. So there is no much difference between the existing method and the proposed method. However, the proposed method yields the best results than the existing methods when the peak occurs at the center and to the right of the *P-V* curve. Also, the tracking time depends on the initial operating point after a change in shading pattern is observed.

4.5   Hardware Implementation

The experimental setup used to validate the proposed model is presented in the Appendix. Three different shading patterns used in simulations are used for validating the proposed approach in hardware. The proposed algorithm is compared with (Boztepe et al., 2014). The PV voltage (V), PV current (I) and PV power tracked using the proposed method and the method presented in (Boztepe et al., 2014) are
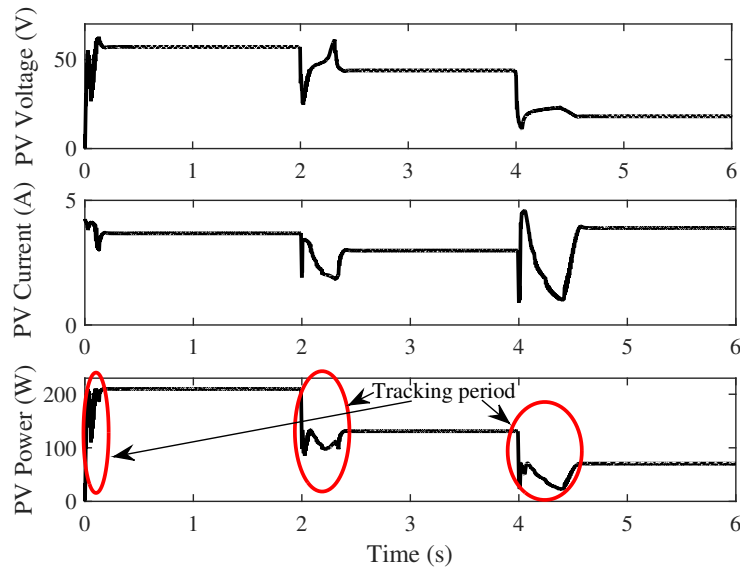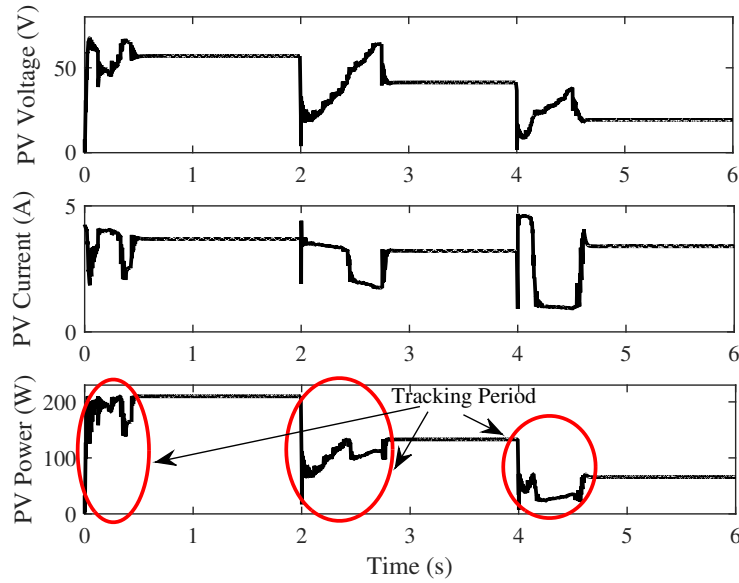
Figure 4.5: Simulation values of PV Voltage, PV current and PV power of three different shading patterns of (a) proposed approach (b) method proposed in (Boztepe et al., 2014)

presented in 4.6. The proposed algorithm takes 4.4s, 7.6s, and 8.8s for tracking the global peak for shading patterns P1, P2, and P3 respectively. The algorithm in (Boztepe et al., 2014) takes 10s, 12s, and 9.8s for tracking the global peak. The

(a)

(b)

Figure 4.6: Experimental values of PV Voltage, PV current and PV power of three different shading patterns of (a) proposed approach (b) method proposed in (Boztepe et al., 2014)

comparison of tracking time is presented in Table 4.2. It can be noticed that the proposed algorithm takes lesser time for tracking global peak compared to the existing method. The simulation time is very much lesser than hardware time. This is because
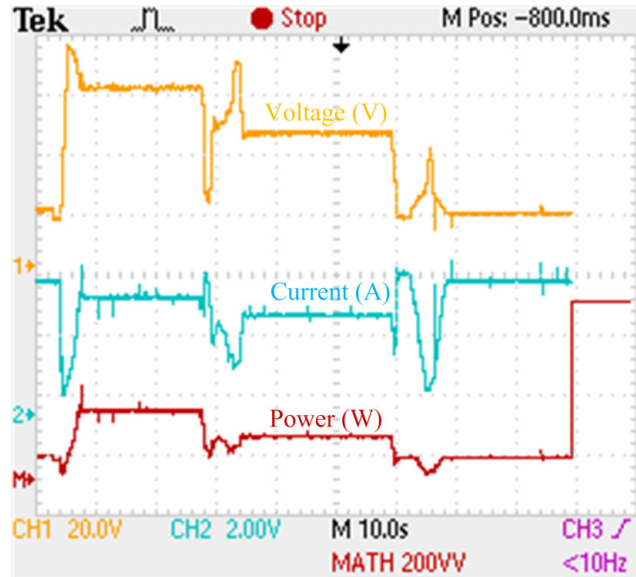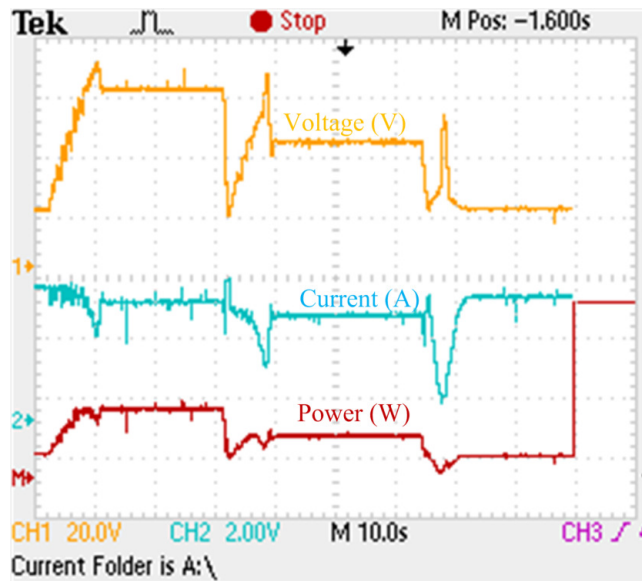
the hardware system is rated for a higher power (2KW). Because of the higher values of inductance and capacitance than those used in the simulation, the time constant of the system is more. Apart from this, the equivalent series resistance of inductors and capacitors, sampling and acquisition time in analog to digital converters also lead to an increase in tracking time. It can be validated from the experimental results that the proposed method tracks the global peak accurately. Also, the step time taken for performing each iteration in hardware is more than in simulation which led to an increase in tracking time.

Table 4.2: Comparison of Tracking Time in Hardware

	Tracking Time (s)		
Algorithm	P1	P2	P3
Proposed	6	7.6	8.8
(Boztepe et al., 2014)	10	12	9.8

4.6   Conclusion

A global peak tracking algorithm based on voltage and current control is proposed in this chapter. The algorithm operates in three modes. Those are initialization mode, voltage control mode, current control mode. After a change in shading, the pattern is detected, the initialization mode is activated. The minimum reference voltage is calculated in this mode and is assigned as the reference voltage. Then the algorithm operates in the current control mode to find the nearest peak. Once the peak is detected, the algorithm will continue in voltage control mode until an inflection point is detected. Once the inflection point is identified, the current control mode is activated. This process is continued until the operating PV current is less than the minimum possible current which is calculated by necessary equations. The proposed algorithm is verified with simulations and compared with existing methods in the literature. Experimental validation is performed using solar array simulator, resistive load, the boost converter, and dSPACE controller. The proposed method accurately tracks the global peak with less computational time. This algorithm is most suitable for module level converter.

Chapter 5

Global Peak Tracking Using Capacitor Charging Method

Contents

5.1 Introduction

An MPPT algorithm based on the step change in duty ratio is proposed in this chapter. The proposed algorithm operates in three stages viz., (i) detection of maximum power and voltage at maximum power using the scanning procedure by giving step change in duty ratio, (ii) varying the value of duty ratio to make PV voltage equal to voltage at maximum power point, and (iii) operation of conventional P and O method to retain the operating point around the MPP. In this algorithm, a step change in duty ratio is considered to reduce the tracking time. Even though the algorithm operates in three stages, it is of reduced complexity and has improved tracking speed than all the existing algorithms. The algorithm is presented for different types of working conditions.

The following assumptions are considered in this chapter.

- The value of cell temperature is considered constant

- The ratio of V_{mp} to V_{oc} and I_{mp} to I_{sc} will not exceed 0.9.

- The minimum irradiance falling on the PV panel is $100\mathrm{W/m}^2$ and the maximum irradiance falling on the PV panel is $1000\mathrm{W/m}^2$.

- The effects of degradation on PV modules are not considered.

5.2 Scanning Based MPPT

A comprehensive analysis of PV panel for tracking global peak under mismatching conditions is performed by using simulations in MATLAB. A boost converter is used as a power interface between source and load. The parameters of the PV module at standard test conditions used in this chapter are presented in Table 5.1.

Table 5.1: Datasheet Parameters

Open Circuit Voltage(V_{oc})	:	23.3 V
Short Circuit Current(I_{sc})	:	2.68A
Voltage at maximum power(V_{mp})	:	16.6V
Current at maximum power(I_{mp})	:	2.41A
Number of cells in module	:	36

5.2.1 Determination of Global peak point

In this chapter, the global peak is tracked during the time of charging of input capacitor of the boost converter. For demonstrating it, the following explanation is considered. PV Panel is used as s source. Load is resistive. DC-DC boost converter is used as interface between source and load for performing the maximum power point tracking. In this demonstration, it is assumed that there is no change in the shading pattern.

Initially, the duty ratio of the boost converter is made equal to 0.6. This can be noticed from Fig. 5.1. The values of PV voltage, PV current, PV power, and duty ratio are presented in Fig. 5.1(a), 5.1(b), 5.1(c) and 5.1(d) respectively. The duty ratio is maintained at 0.6 from time, $t=0$to 0.5s. At the time,$t=0.5$s, the value of duty ratio is changed from 0.6 to 0.8. As the duty ratio is increased, PV Voltage decreases. At time,$t=0.6$s, the value of duty ratio is changed from 0.8 to 0.2 as shown in Fig. 5.1(d). As the duty ratio is decreased the value of PV voltage starts increasing. The PV Voltage cannot change instantaneously as the capacitor is connected across the PV panel. For every change in PV Voltage, the corresponding PV current will be obtained. During the transition of duty ratio from 0.8 to 0.2, the value of maximum power is detected at t=0.603s. The zoomed view of PV Voltage and PV Current and the corresponding PV Power are presented in Fig.5.1(a), Fig. 5.1 (b) Fig.5.1(c) respectively. The value of maximum power and voltage at maximum power are recorded for tracking the global peak.
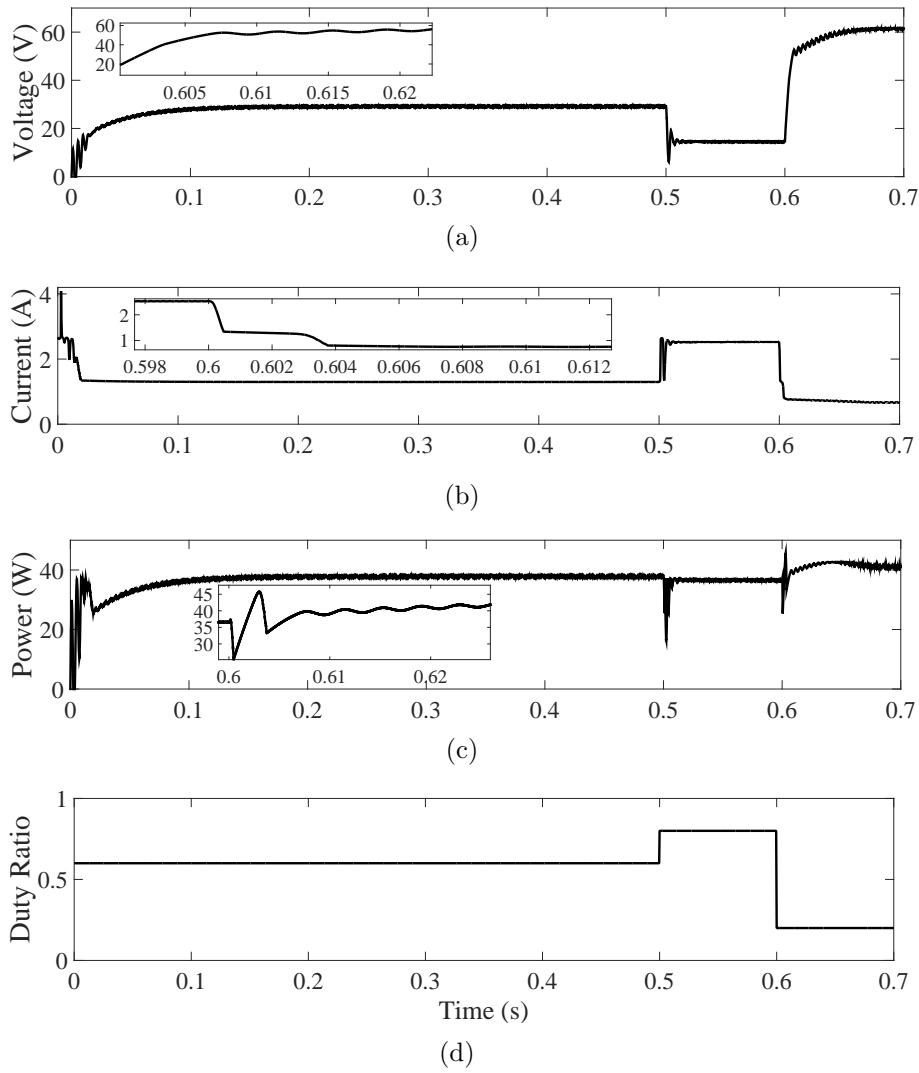
Figure 5.1: (a) PV Voltage (b) Current (c) Power (d) Duty ratio for demonstrating the detection of GP using scanning
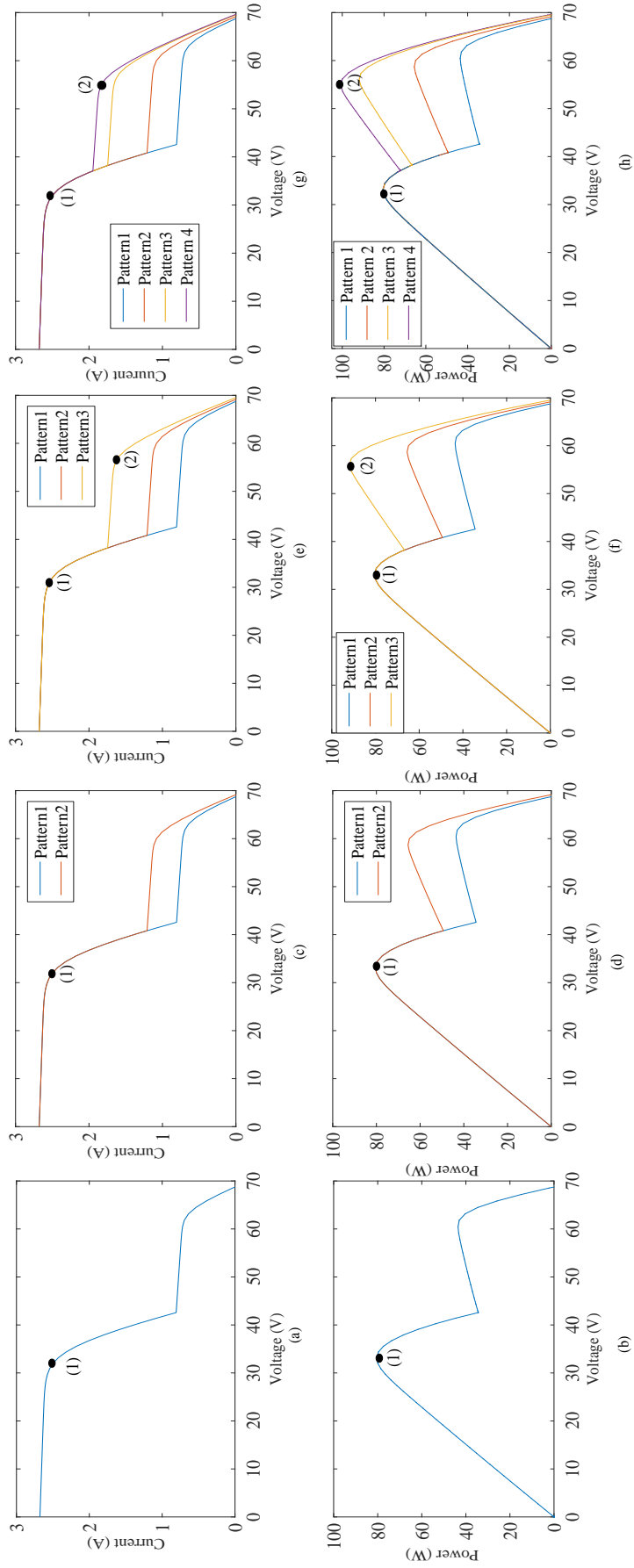
Figure 5.2: *I-V* and *P-V* characteristics at different shading patterns

5.2.2 Detection Criterion for Change in Shading Pattern

Change in the shading pattern is mainly because of environmental factors like irradiance and temperature. Under uniformly shaded conditions, there is a single peak. In this situation, P and O method is sufficient to track the maximum power point. For mismatching condition, if P and O are used, the operating point gets trapped at the local peak. So an algorithm for tracking global peak is inevitable. The detection of the change in irradiance is crucial especially in case of mismatching condition for tracking the global peak.

Usage of irradiance and temperature sensors for every module increases the cost of the system (Karatepe et al., 2009). An alternative to this can be the usage of panel parameters like panel voltage and panel current. The authors in (Nguyen and Low, 2010b), have used the change in power i.e., the difference between present power and power in the previous iteration for detecting the change in irradiance pattern. Apart from this, they have proposed an approach for differentiating uniform and mismatching conditions. However, the identification of mismatching condition proposed in (Nguyen and Low, 2010b) fails in situations when there is a drastic change in irradiance. Similar approaches are presented in (Ishaque et al., 2012a, Ishaque and Salam, 2013a) for differentiating global and local peaks. In this regard, it is proposed to use change in power as the detection criterion. As the proposed algorithm is intended to have faster-tracking speed (discussed and proved in subsequent sections), no algorithm is proposed for differentiating uniform and mismatching conditions.

5.2.3 Non-detection of change in shading pattern

There are some operating conditions under mismatching conditions during which the change in irradiance cannot be detected with the change in power, change in voltage and change in current. Consider *I-V* and *P-V* curves presented in Fig. 5.3. Initially, the operating point is at point (1) as shown in Fig. 5.2(a) and 5.2 (b) which is at GP, i.e., at 33.4V. If the irradiance is changed to pattern 2 as in Fig. 5.2(c) and Fig. 5.2(d), the operating point does not change. This is because the change in power is not detected. In the present scenario, there is no power loss as the operating point is at GP. When the irradiance is changed from pattern 2 to pattern 3 in Fig.5.2(e) and Fig. 5.2(f), the operating point does not alter, but the global peak changes. A similar situation prevails when the operating point is moved from pattern 3 to pattern 4 (Fig.5.2(g) and Fig.5.2(h)). The operating point does not change as there

is no change in power detected, thereby leading to a considerable loss of power. Although the detection procedures mentioned in (Karatepe et al., 2009) can solve the problem, the usage of these can be evaded because of their demerits (discussed in section 5.2.2). There can be many other issues apart from the one discussed in this section which may lead to non-detection of change in shading pattern. To avoid all the issues related to non-detection of change in shading pattern, it is proposed to use a timer that operates for a given set period (t_a). The process of tracking re-initializes once the timer reaches the pre-specified time (t_a). If the value of t_a is less, then tracking re-initializes frequently leading to severe transients, if the value of t_a is more, then there are chances of loss of power. In this regard, the value of t_a should be selected optimally depending on the panel configuration.

5.3   Proposed Algorithm for Tracking GP

The proposed algorithm operates in three stages: 1) scanning stage: detection of maximum power and voltage at maximum power by varying the value of duty ratio, 2) correcting stage: varying the duty ratio to make PV voltage equal to voltage at a maximum power point, and 3) retaining stage: retaining the operating point at global peak using conventional P and O. Fig. 5.3 presents the flowchart of the proposed algorithm. The values of critical power (P_{crit}), critical voltage (V_{crit}), voltage limit (V_{limit}), change in power (ΔP) and global peak value (GPV) are initialized. Initially, the algorithm operates in the scanning stage, i.e., $GPV=1$. After initialization, clock time is checked. If the value of clock time is greater than t_a seconds (pre-specified time for which the global peak tracking is initiated), the algorithm needs to reset the process, i.e., the values of all initial parameters and reinitialized. If the value of the clock time is less than t_a seconds, the algorithm measures the value of PV voltage, PV current, and corresponding PV power is calculated. The condition for global peak mode is checked. If $GPV=1$, the algorithm is in the scanning stage. It indicates either the change in shading pattern or clock time has reached t_a seconds. In this stage, the value of duty ratio is initialized to d_{max} and then changed to d_{min}. The values of d_{max} and d_{min} are duty ratios chosen based on the procedure mentioned in section 2.2.1. In the process of change in duty ratio from d_{max}, to d_{min}, the maximum power and voltage at which maximum power occurs are recorded. The algorithm stays in global mode until V_{limit} is reached. The value of V_{limit} is presented in equation (5.1).
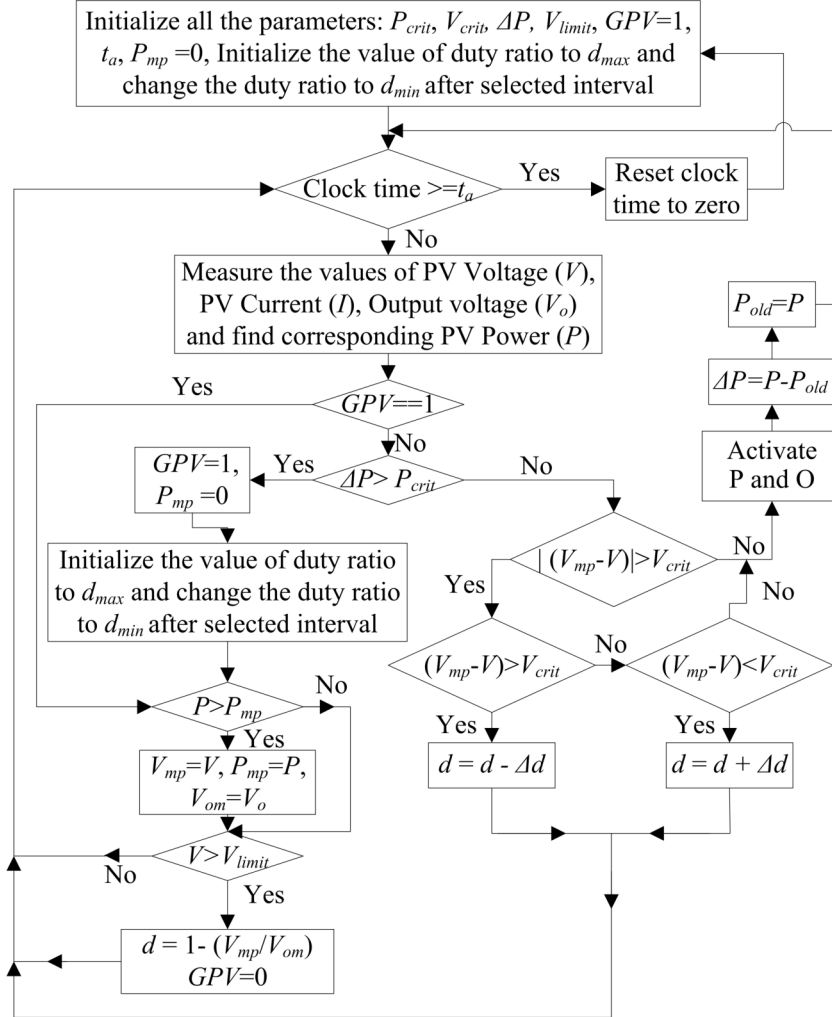
Figure 5.3: Flowchart of Proposed Algorithm

$$V_{\text{limit}} = \delta_{\text{V}} \times V_{\text{oct}} \tag{5.1}$$

V_{oct} is open circuit voltage of entire array. Beyond V_{limit} there is no chance of occurrence of MPP. Once the value of V_{limit} is reached the approximate value of duty ratio at MPP is calculated using equation (5.2) (Taghvaee et al., 2013b).

$$d = 1 - \frac{V_{\text{mp}}}{V_{\text{om}}} \tag{5.2}$$

where V_{mp} is the voltage at MPP obtained during the scanning stage. V_{om} is the output voltage of the boost converter at MPP and it varies with the change in irradiance in the case of a resistive load. After calculating the duty ratio, GPV is

made equal to zero and the change in power (ΔP) is checked. If the difference in power (ΔP) is greater than critical power (P_{crit}), the algorithm switches back to the scanning stage. The critical power is set to detect the change in irradiance. If the change in power is less than critical power, the difference between the voltage at maximum power (V_{mp}) and panel voltage (V_{pv}) checked. If it is greater than V_{crit}, the algorithm shifts to correcting stage. The value of V_{crit} depends on the panel and is user-defined. At this point, the value of duty ratio is perturbed in steps until the difference between V_{mp} and V_{pv} becomes less than V_{crit}. If the difference between the voltage at maximum power (V_{mp}) and panel voltage (V_{pv}) is less than V_{crit}, then retaining stage is operated to maintain the operating point at MPP (stage 3). Perturb and observe method retains the operating point at MPP until the irradiance pattern is changed or clock time becomes greater than t_{a} seconds. The third stage of the algorithm occurs when the operating point is near the global peak. So the disadvantages of oscillations around the MPP can be greatly reduced by selecting the small step size of duty ratio which is used only for retaining the operating point at the maximum power point.

5.4   Simulation Results

For evaluating the performance of the proposed scanning based MPPT algorithm, simulation studies are performed. The circuit diagram for implementing the proposed approach is presented in Fig. 5.4. Three modules connected with bypass diodes across each of them are connected in series to form a PV panel. The specifications of the modules used are presented in Table 5.1. All the values presented are at standard test conditions. The rheostat is used as a resistive load. A boost converter is used as an interface between source and load. Specifications of the boost converter used are presented in Table 5.2. The proposed maximum power point algorithm is implemented in partial shading MPPT block. This MPPT block takes PV voltage (V), PV current (I) and output voltage (V_o) of boost converter as input and generates duty cycle (d) as output. Pulse width modulator (PWM) converts the duty ratio into pulses required for the boost converter. Simulations are performed in MATLAB with a personal computer of 8 GB RAM, i7-4720HQ CPU.

The initial parameters viz., clock time, P_{crit}, V_{crit}, ΔP, V_{limit}, GPV, and t_{a} are set to 0, 3.2W, 1V, 10W, $(0.8 \times V_{\text{oct}})$, 1, and 5s respectively.
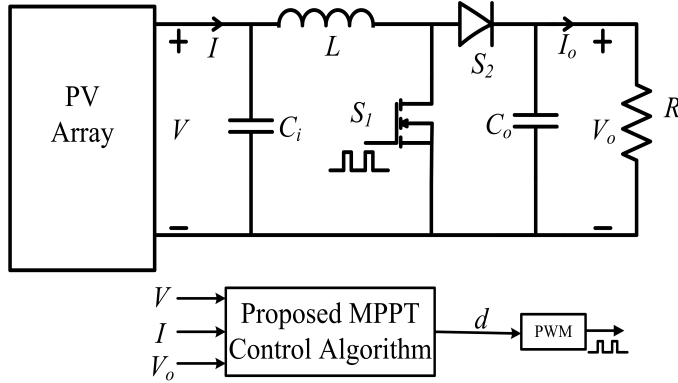
Figure 5.4: Circuit Diagram for implementing proposed approach

Table 5.2: Simulation Parameters of Boost Converter

Input capacitance	:	$170\mu F$
Output capacitance	:	$270\mu F$
Inductance	:	1mH
Switching Frequency	:	25kHz

5.4.1   Uniform Irradiance Conditions

The proposed algorithm is compared with conventional perturb and observe method for rapid change in environmental conditions. The proposed algorithm is validated with two different shading patterns. From t=0 to 0.5s, an irradiance of 1000 W/m^2 and from t=0.5s to 1s an irradiance of 300 W/m^2 is executed. The simulation results comprising of PV voltage (V), PV current (I) and PV power (P) are presented in Fig. 5.5 (a), (b) and (c) respectively. At t=0s, the duty ratio is changed from $d_{\max}$ to $d_{\min}$ (0.85 to 0.2) according to proposed algorithm. The proposed method takes 0.06s to track the peak. But P and O takes 0.22s to track the peak.At t=0.5s, the irradiance is changed to $300W/m^2$. According to the proposed method, the global peak tracking algorithm is initiated and the proposed method has taken 0.05s to track the peak. But P and O takes more time (0.4s) to track the peak because it is based on perturbation and more samples are required to identify the peak. But the proposed method uses step change in duty ratio to track the peak. This feature of the proposed algorithm makes it best suitable to be implemented in varying environmental conditions.

96
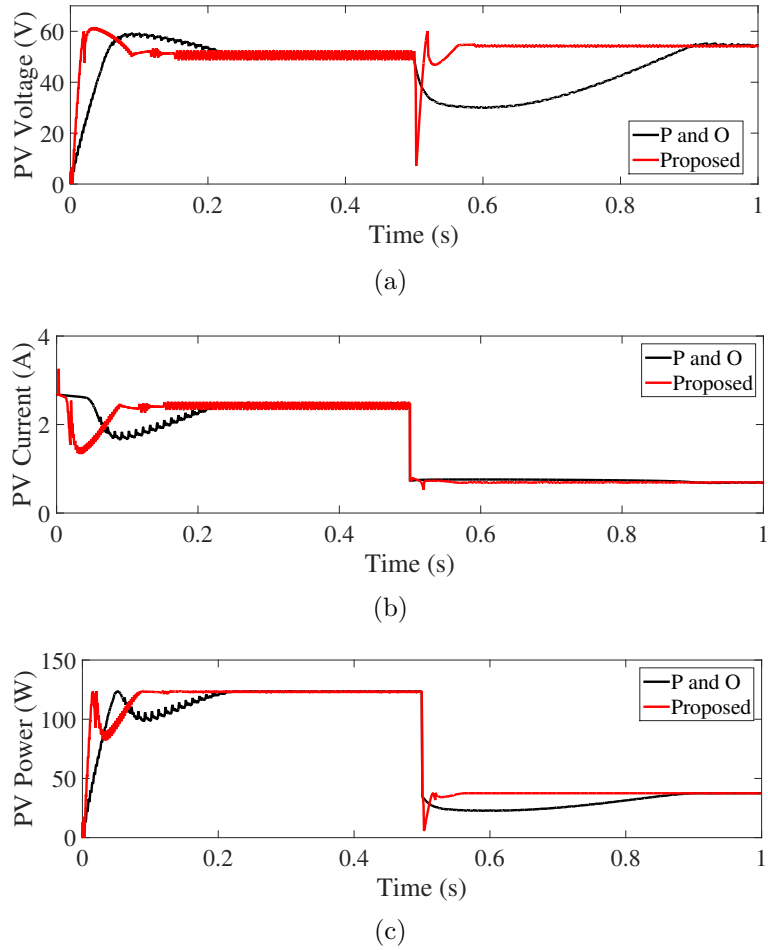
Figure 5.5: (a) PV Voltage, (b) PV Current, (c) PV Power for uniform irradiance conditions

5.4.2 Mismatching Conditions

Four different shading patterns are considered to validate the proposed algorithm. The *P-V* curves of four different shading patterns are presented in Fig. 5.6. The proposed algorithm is validated with the existing algorithms like perturb and observe, step-based scanning MPPT (Kotti and Shireen, 2015), ramp based scanning MPPT (Ghasemi et al., 2016). The PV Voltage, PV Current and PV power for four different shading patterns for all the four methods are presented in Fig. 5.7 (a), (b), (c) and (d). The shading pattern-1 is applied at $t=0.1$s and shading pattern is changed for each 0.7s. For the first two shading patterns i.e., from $t=0.1$s to 0.8s and from $t=0.8$s to 1.5s, all the four algorithms track the global peak. It is observed that P

and O, (Ghasemi et al., 2016), the proposed method and (Kotti and Shireen, 2015) have decreasing order of settling time. Whenever there is a change in the shading pattern, according to (Kotti and Shireen, 2015), the duty cycle is set to one. Since the time constant becomes very low, the tracking speed is high. However, this leads to considerable undershoots and overshoots in PV voltage which can be noticed from Fig. 5.7 (c). The proposed method traverses the P-V curve between d_{max} and d_{min}. The over/under voltages and currents can thus be controlled within the limits. Since the converter operates within the duty cycle boundary, the time constant is little more than the method presented in (Kotti and Shireen, 2015). The advantage of the proposed method is that more samples of V and I can be obtained leading to accurate tracking of maximum power. For shading pattern-3, the algorithms proposed in (Kotti and Shireen, 2015), (Ghasemi et al., 2016) and the proposed algorithm track peak accurately. But perturb and observe method tracks the local peak leading to considerable loss of power. At t=2.2s, shading pattern 4 is activated. Results from Fig. 5.7 (a), (b), (c) and (d) shows that the proposed method, (Ghasemi et al., 2016) and perturb and observe method tracks the global peak. Whereas the algorithm presented in Kotti and Shireen (2015) could not track the GP. This is because when the shading pattern is changed, the duty ratio of the boost converter is made one, which leads to a decrease in PV voltage. The PV voltage for previous shading pattern is 16V and for a change in shading pattern voltage is decreased, the algorithm in (Kotti and Shireen, 2015) scans for voltages less than 16V. But the MPP voltage for shading pattern 4 is around 56V. So there is no chance that the algorithm in (Kotti and Shireen, 2015) scans 56V as the voltage at MPP is greater than the operating voltage of the previous shading pattern. This is the major drawback of the method proposed in (Kotti and Shireen, 2015). For all shading patterns, the tracking speed of (Ghasemi et al., 2016) is less than the proposed method. Overall, the proposed method is more efficient with high tracking speed and tracks the global peak in all the cases.

5.4.3   Combination of uniform and mismatching conditions

The effectiveness of the proposed approach is further verified using eight different shading patterns. The shading patterns along with corresponding maximum power (P_a) and voltage at maximum power (V_a) for resistive load are presented in Table 5.3.
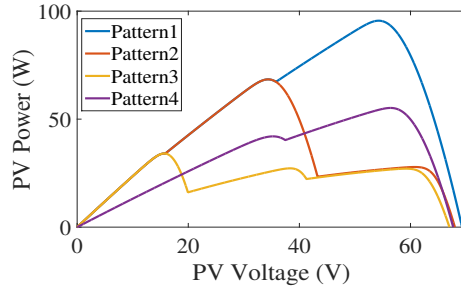
Figure 5.6: *P-V* curves under mismatching conditions
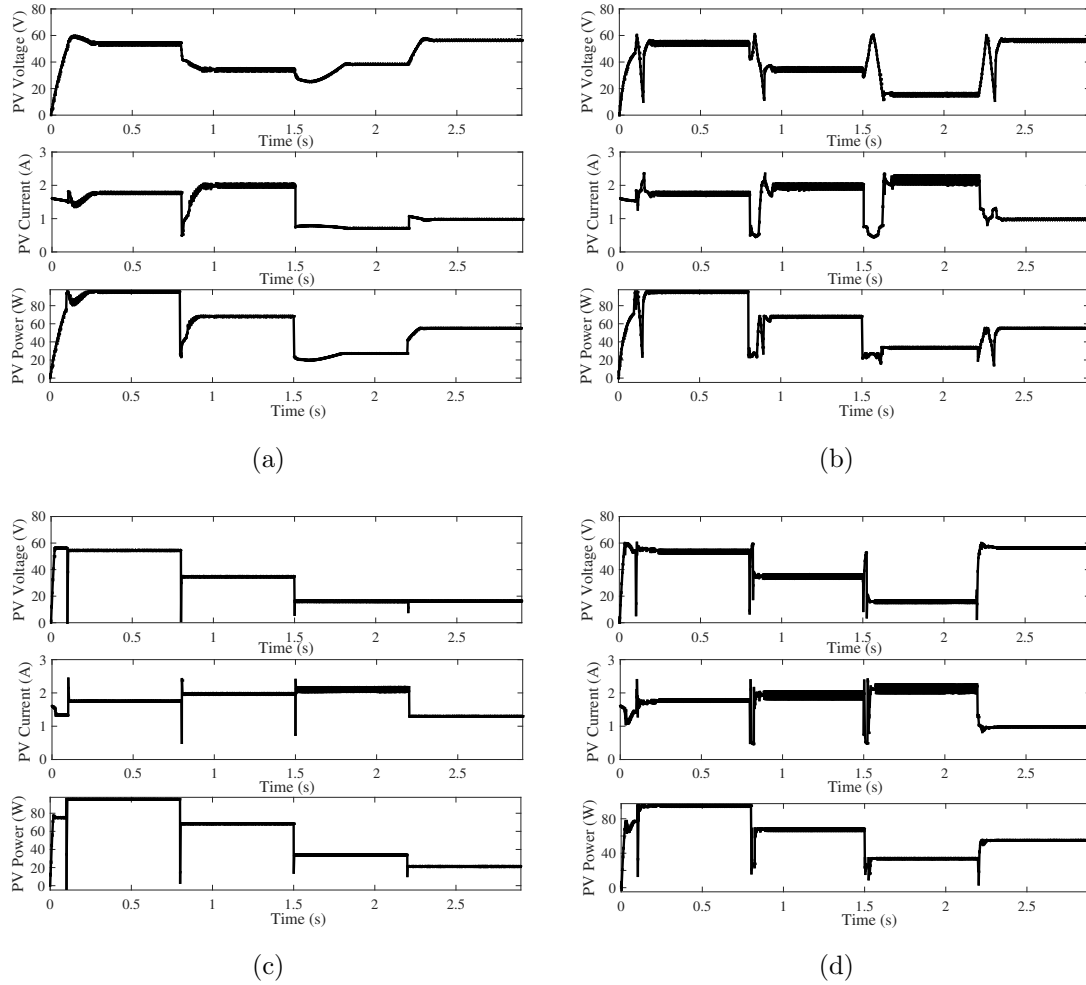
Figure 5.7: PV Voltage, PV Current, and PV Power under mismatching conditions for (a) perturb and observe method (b) method presented in (Ghasemi et al., 2016) (c) method presented in (Kotti and Shireen, 2015) (d) proposed Method

In Table 5.3, G_1, G_2 and G_3 are irradiance of three modules connected in series, P_{a} is maximum power obtained from *P-V* curve, and V_{a} is voltage at maximum power
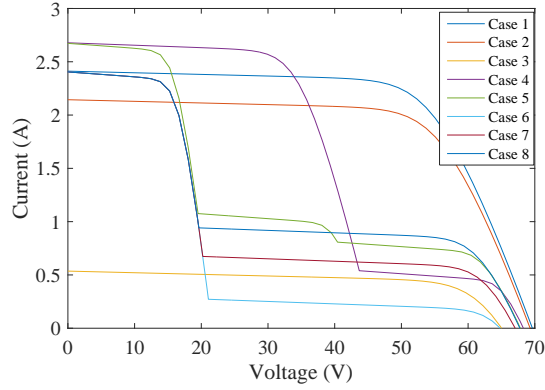
(a)
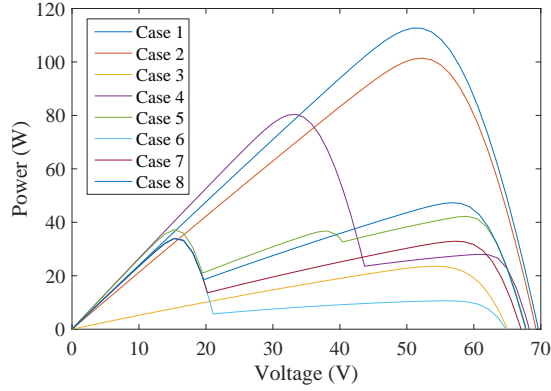
(b)

Figure 5.8: *I-V* and *P-V* characteristics at different shading patterns of 5.3

point obtained from *P-V* curve, *P*, *V* and T_t indicates tracked power, tracked voltage and tracking time for proposed method. The *I-V* curves and *P-V* curves of all the shading patterns presented in Table 5.3 are shown in Fig. 5.8(a) and Fig. 5.8(b).

The PV voltage, PV current, PV power, and duty ratio are shown in Fig. 5.9. Consider Case 1 of Table 5.3. The PV panel is uniformly irradiated with 900 W/m^2. The algorithm tracks the maximum power point using stage 1 (scanning stage) and retains at that point using P and O algorithm (retaining stage of the proposed algorithm). The tracking time of the proposed method for Case 1 is 0.09 seconds. After the change in irradiance from Case 1 to Case 2, i.e., from 900 W/m^2 to 800 W/m^2, the proposed algorithm takes 0.03s to track the peak. It is because, whenever a change in power is detected greater than P_{crit}, the proposed algorithm re-initializes and tracks for the global peak. When the shading pattern of the panel is changed from Case 2 to Case 3, i.e., 800 W/m^2 to 200 W/m^2 (uniformly irradiated), the tracking time of
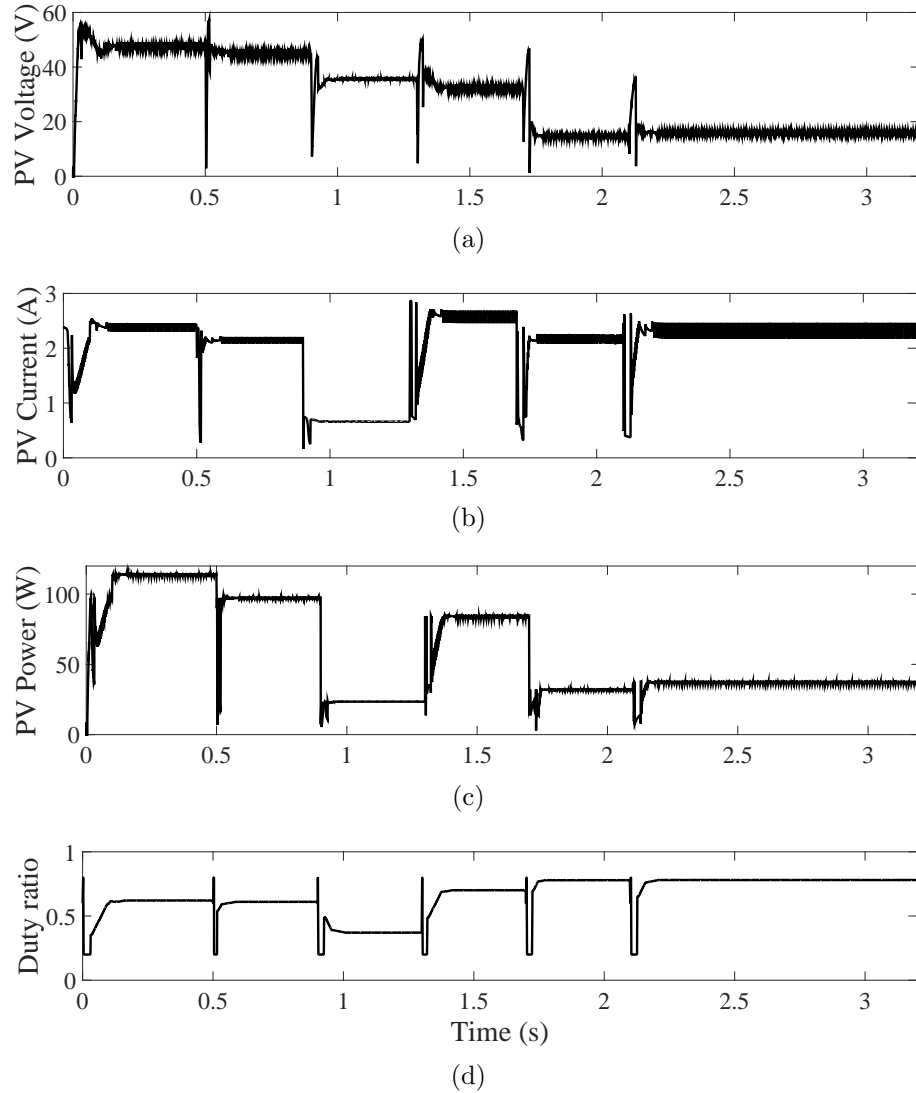
Figure 5.9: (a) PV Voltage, (b) PV Current, (c) PV Power (d) Duty ratio of Table 5.3

the proposed algorithm is 0.04s.

The irradiance pattern changes from uniform (Case 3) to mismatching (Case 4). The algorithm tracks the GP (84.43W) in 0.035s. The peaks corresponding to Case 4 are evident from the *P-V* curve in Fig 5.8(b). Similarly, GP is tracked when the irradiance is changed from Case 4 to Case 5 and Case 5 to Case 6. During the shift in shading pattern from Case 6 to Case 7, there is no change in power detected (because of the phenomena discussed in section 5.2.3). There is no loss in power, as the operating point is a global peak. When the shading pattern is changed from Case 7 to Case 8, the global peak is changed, but the operating point cannot move as there
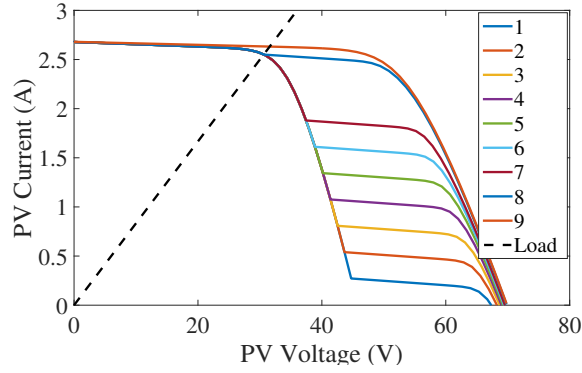
(a)
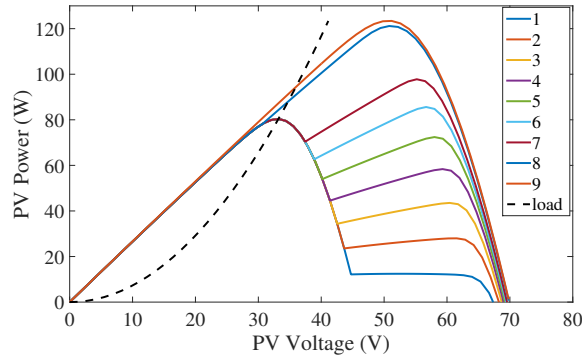
(b)

Figure 5.10: *I-V* and *P-V* characteristics for demonstrating timer

Table 5.3: Shading patterns and their corresponding values

Case	G_1 (W/m^2)	G_2 (W/m^2)	G_3 (W/m^2)	P_a (W)	V_a (V)	Proposed Method		
						P (W)	V (V)	T_t (s)
1	900	900	900	114.1	47.33	114.05	47.2	0.09
2	800	800	800	97.35	45.03	97.2	45.6	0.03
3	200	200	200	25.533	35.68	23.48	35.6	0.04
4	200	1000	1000	84.43	32.03	84.4	32.1	0.035
5	300	400	1000	32.04	14.83	32.08	15.1	0.03
6	100	100	900	37.57	15.59	37.52	15.9	0.03
7	250	250	900	37.57	15.59	37.52	15.9	-
8	350	350	900	47.28	56.58	37.52	15.9	-

is no change in power detected. The algorithm gets trapped in the present operating point. In this situation, it is proposed to use a timer. However, the timer does not get operated because the time for the timer to act (t_a) is kept as 5s.
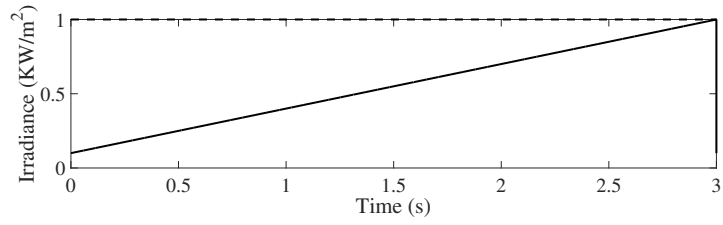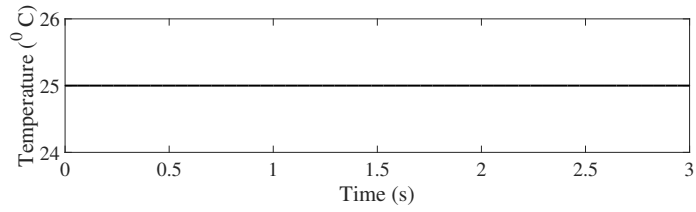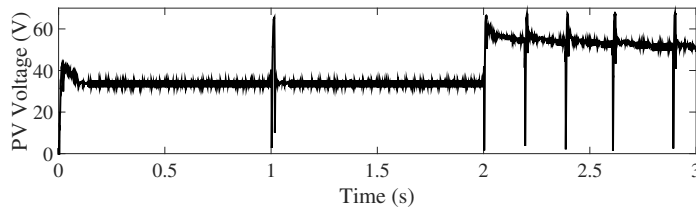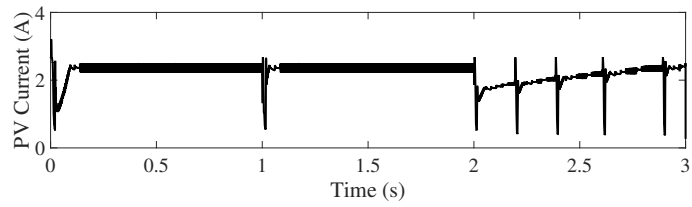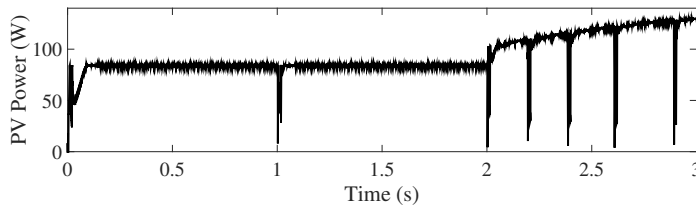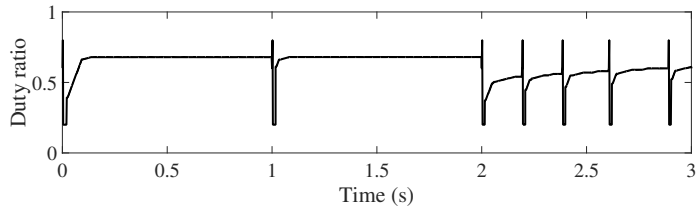
Figure 5.11: Irradiance, Temperature, PV Voltage, PV Current, PV Power and Duty ratio with timer

Table 5.4: Performance Comparison of different algorithms

Algorithm	TS	IC	TR	SSR	GPT
P and O	Less	Less	Poor	Good	No
Scanning based (Kotti and Shireen, 2015)	High	Less	Poor	Good	No
Scanning based (Ghasemi et al., 2016)	Medium	Medium	Good	Good	Yes
Proposed method	High	Less	Good	Good	Yes

'

To prove the effectiveness of the timer in the proposed algorithm, the irradiance and temperature profiles shown in Fig. 5.11(a) and Fig. 5.11 (b) respectively are simulated. The irradiance showed in Fig. 5.11(a) is only for one module i.e., G_1 is operating from $100W/m^2$ to 1000 W/m^2. Rest two modules viz., G_2 and G_3 are operating at $1000W/m^2$. The temperature is maintained constant at $25°$ C. The corresponding I-V and P-V curves are presented in 5.10(a) and 5.10(b). With all the initial parameters being the same, the value of t_a alone is set to 1s. The corresponding PV voltage, current, power, and duty ratio are presented in Fig. 5.11(c), Fig. 5.11(d), Fig. 5.11(e) and Fig. 5.11(f) respectively. The timer is operated for the first time at t=1sec as clock time becomes greater than 1 second. During this period, the irradiance of the varying module is around $400$ W/m^2. From Fig. 5.10(b), the MPP of this particular condition lies at 33V. Hence the MPP is retained at the same point. Whenever the timer acts at 2s, the value of irradiance is around 750 W/m^2. For this shading pattern, the voltage at the maximum power point lies at 55V. This change can be noticed from I-V and P-V curve 7 in Fig. 5.10(a) and 5.10(b). As the timer is operated at t=2s, the algorithm re-initializes all the parameters, and the tracking of GP is initiated. The global peak is tracked as shown in Fig. 5.11(e). From this point, for every change in power (ΔP) greater than P_{crit}, the algorithm acts and tracks the global peak.

The proposed algorithm is compared with other algorithms in Table 5.4 regarding tracking speed (TS), implementation complexity (IC), transient response (TR), steady state response (SSR) and ability to track GP (GPT). It is found that the proposed method performs better than all the compared existing methods.
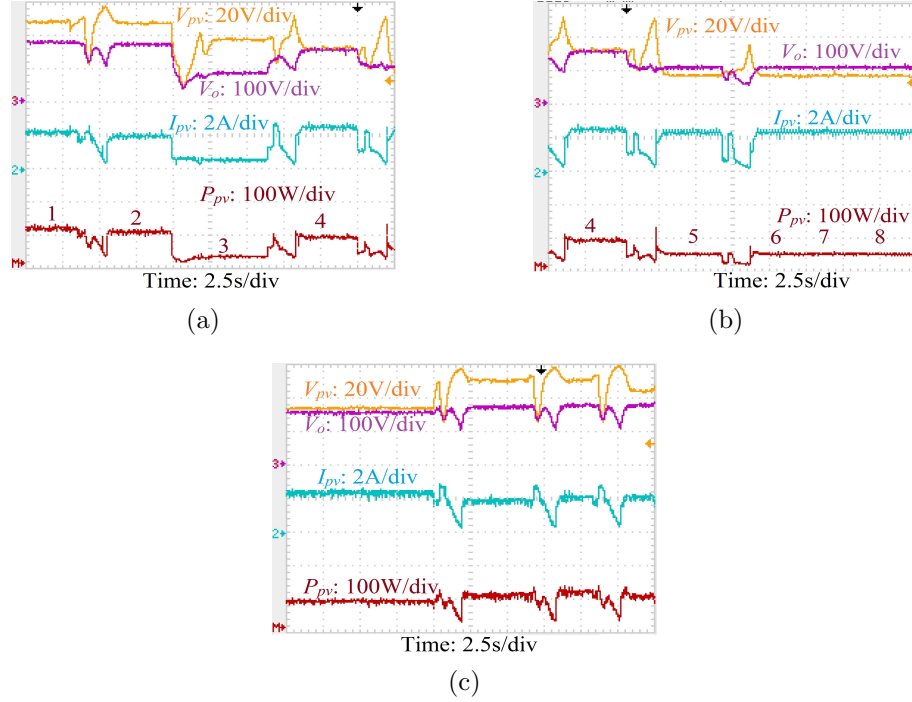
Figure 5.12: PV Voltage, PV Current, PV Power, Output Voltage from (a) Case 1 to Case 4 (b) Case 4 to Case 8 (c) for demonstrating timer

5.5 Experimental Validations

The hardware setup is presented in the Appendix. The sampling frequency for acquiring PV Voltage(V) and PV current (I) is calculated using the procedure mentioned in (Ghasemi et al., 2016). The open circuit voltage of the array at STC used in this paper is approximately 70V. The minimum value of tracking time from simulations is 30ms. Theoretically, the rate of change of voltage is 2.3KV/s (70V/30ms). If the sampling is done for every 2V, then the sampling frequency will be 1.16kHz (2.3kV/s/2V). The dSPACE 1206 controller used for implementing the proposed algorithm has a sampling frequency greater than 1.16kHz. This facilitates the accurate measurement of voltage and current in the process of tracking the global peak.

The irradiance patterns presented in Table 5.3 are used for validation in this section using experimental setup. As discussed in the previous section, the algorithm is implemented for eight different shading patterns. The corresponding plots of PV voltage (V_{pv}), PV current (I_{pv}) and PV power (P_{pv}) and output voltage V_{o} are presented in Fig. 5.12 (a) and Fig. 5.12 (b). The case numbers are indicated on the top of the power characteristics.
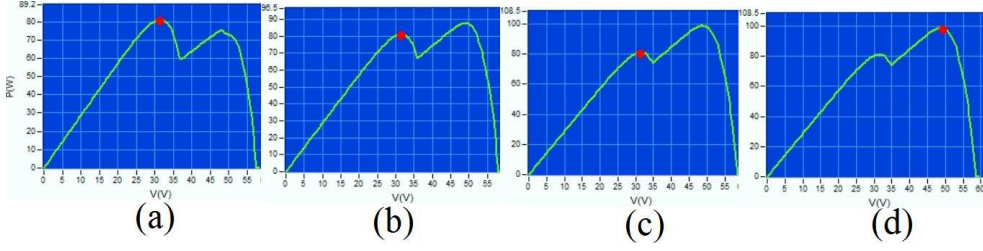
Figure 5.13: *P-V* Curves from simulator at (a) (1000,1000,500) W/m^2, (b) (1000,1000,600) W/m^2, (c) (1000,1000,700) W/m^2 (before timer activation), (d) (1000,1000,700) W/m^2 (after timer activation)

Table 5.5: Comparison of simulated and experimental results

Case	G_1 (W/m^2)	G_2 (W/m^2)	G_3 (W/m^2)	Simulated Power(W)	Experimental Power(W)
1	900	900	900	114.05	108.09
2	800	800	800	97.2	97.15
3	200	200	200	23.48	22.26
4	200	1000	1000	84.4	81.06
5	300	400	1000	32.08	31.99
6	100	100	900	37.52	36.4
7	250	250	900	37.52	36.4
8	350	350	900	37.52	36.4

From Fig. 5.12 (a) and 5.12(b), it is evident that the proposed algorithm tracks the power for all the patterns in Table 5.3 except for pattern 8. This is because the operating point cannot detect the change in irradiance pattern. To overcome this problem, a timer is proposed to operate at equal intervals of time. To show the effectiveness of the proposed timer, two modules are equally irradiated at 1000 W/m^2, and the other one is varied at steps of 100 W/m^2 starting from 400 W/m^2. The purpose of the timer is to reset the algorithm so that the tracking process starts. The timer is operated for every 12s. The irradiance pattern is varied for every 2.5s (approx.). The corresponding plots are presented in Fig. 5.12 (c).

At 5 seconds, when the value of irradiance is (1000, 1000, 500) W/m^2 (Fig. 5.13 (a)) global peak lies at around 31 V. For next change in shading pattern when the irradiance changes to (1000, 1000, 600) W/m^2 (Fig. 5.13 (b)), the value of global peak shifts, but the operating point does not shift as the change in power does not occur. For the next pattern when the irradiance changes to (1000, 1000, 700) W/m^2,

106

change in power is not detected (Fig. 5.13 (c)). However, the timer is activated in this condition, and actual power is tracked (Fig. 5.13 (d)).

The tracking time in hardware implementation is more than the simulation time. This is because the hardware system is rated for a higher power (2KW). Because of the higher values of inductance and capacitance than those used in the simulation, the time constant of the system is more. Apart from this, the equivalent series resistance of inductors and capacitors, sampling and acquisition time in analog to digital converters also lead to an increase in tracking time. It can be validated from the experimental results that the proposed method tracks the global peak accurately.

A comparison between simulated values and experimental values is presented in Table 5.5. It can be noticed that the simulated and experimental values are almost close to each other.

5.6 Comparison of Proposed Algorithms

- Algorithm in Chapter-2

  - Duty ratio based control, so the effort of tuning controllers can be eliminated.

  - During tracking of GP, the voltage range covered will be more.

- Algorithm in Chapter-3

  - Employs current control

  - Uses perturbation of current to track GP. So a change in shading pattern can be detected in the first stage of the GP tracking algorithm if the change in current is used as detection criteria.

- Algorithm in Chapter-4

  - based on voltage and current control

  - Tracks global peak faster under uniform irradiation cannot track GP faster when the local peaks have almost the same values of power.

- Algorithm in Chapter-5

  - Uses duty ratio control, so the tuning of controller gains can be eliminated.

– Can track GP faster than all algorithms

– The tracking of GP depends on the ADC of the microcontroller.

5.7 Conclusion

In this chapter, a maximum power point tracking algorithm is proposed for mismatching conditions. The proposed algorithm tracks the global peak by sampling variations in the transient period. The algorithm operates in three stages viz., scanning, correcting and retaining the operating point at MPP. A case is discussed wherein the conventional detection techniques fail to detect the change in irradiance. It is proposed to use a timer to minimize power loss. The algorithm is tested with boost converter as a power interface between source and load. The proposed algorithm is compared with perturb and observe method and scanning based algorithms w.r.t. tracking speed, implementation complexity, tracking accuracy, transient and steady-state response. Experimental validation is performed with solar array simulator, resistive load, boost converter and a dSPACE 1206 controller. The proposed algorithm is found to be more reliable and efficient. Towards the end of the chapter, a comparison is made among all the proposed algorithms in this chapter.

Chapter 6

CONCLUSION AND FUTURE SCOPE

6.1 Conclusion

Maximum power point tracking algorithm is crucial for extracting the maximum power from the PV source. Under mismatching condition there exist multiple peaks in power-voltage characteristics. Maximum among all the peaks is the global peak. It is imperative to track the global peak in order to utilize the complete energy generated from the PV source. The main contributions of this thesis are the development of a global peak tracking algorithm using modified perturbation algorithms and scanning based algorithms. The generalized conclusions of each chapter are presented below.

Chapter 1 presents the background of the thesis. The generalized block diagram of the photovoltaic system is presented. A brief description of PV modeling is presented. From the PV model, the characteristics of the PV source under uniform conditions are deduced. The characteristics of the PV source under mismatching conditions are presented. The major causes of mismatching conditions viz., shading, soiling, module degradation are explained in greater detail. The concept of maximum power point tracking is presented. A detailed literature review on maximum power point tracking techniques is presented. Based on the research gaps, the objectives of this thesis are identified.

Chapter 2 presents a global peak tracking algorithm based on direct duty ratio control. The proposed algorithm is based on searching technique and a bisection

method. For implementing the proposed algorithm, the minimum and maximum limits of duty ratio are calculated. In the global mode, the searching for the peak is performed by dividing the panel characteristics. The subdivisions are referred to as zones. Apart from this, an estimation of current and power values is done by approximating the current-voltage curve using the concept of slope of the line. Using this estimation, the possibility of occurrence of the global peak in each zone is checked. If the possibility of occurrence of the global peak in the zones is at most one, then global peak tracking is terminated and the algorithm operates in the local mode for retaining the operating point at MPP. Else bisection method is used to find out the next value of duty ratio. The proposed algorithm is validated with four different shading patterns and compared with two recent similar algorithms in the literature. It tracks the global peak faster when compared to both the existing algorithms.

Chapter 3 presents a global peak tracking algorithm based on current control. The proposed algorithm is based on perturbing the value of the reference current. It operates in backward mode and forward mode to track the global peak. After the change in shading pattern, the backward phase is initiated in which the reference current is divided by 0.9 until the operating voltage is less than minimum voltage below which there is no chance of occurrence of the global peak. After that, the algorithm is operated in forward phase until the operating current is less than the minimum value of current below which there is no chance of occurrence of the global peak. Once this point is reached, the global peak tracking is stopped and the algorithm operates in the local mode to retain the operating point at MPP. The algorithm tracks the global peak faster when compared with the similar existing algorithm in the literature.

Chapter 4 presents a global peak tracking algorithm based on voltage and current control. The choice to operate voltage or current control is made using a decision variable. If the value of the decision variable is zero, current control is employed. Else voltage control is employed. The algorithm operates in initialization mode, voltage control mode and current control mode to track the global peak. After the change in shading pattern, the initialization mode is operated where the minimum value of voltage is given as reference voltage. Then the algorithm is operated in the current control mode or voltage control mode depending on the requirement. The algorithm is operated in voltage control mode to identify the succeeding maximum power point. The algorithm is operated in voltage control mode to identify succeeding inflection point. The algorithm will be operating in any of these two modes until the

110

termination criterion is met. Then a conventional MPPT algorithm is used to retain the operating point at GP. The algorithm tracks global peak faster, especially under uniform irradiance conditions.

Chapter 5 presents a global peak tracking algorithm based on capacitor charging. The algorithm operates in three modes to track the global peak. They are scanning stage, correcting stage and retaining stage. In the scanning stage, the value of duty ratio is changed from its maximum value to the minimum value. With the change of duty ratio, the operating PV voltage will change. But the value of the capacitor voltage does not change instantaneously. During the charging of the capacitor, the values of voltage and current are obtained and the maximum power and voltage at the maximum power point are determined during the charging period. In the correcting stage, the operating point is brought to the vicinity of the global peak by varying the value of duty ratio. In the retaining stage, the operating point is retained at MPP using a conventional MPPT algorithm. The proposed algorithm tracks the global peak faster compared to all other MPPT algorithms. The tracking time also depends on the ADC of microcontroller and the size of the input capacitor.

All four algorithms are successfully implemented in simulations and hardware and are found to be better than existing methods in the literature.

6.2 Future scope

Based on the research carried out in this thesis, the recommendations for future research are as presented. The proposed global peak tracking algorithms are implemented to resistive loads. They can be implemented for battery loads and grid-connected systems. The proposed algorithms are intervened for PV string. These algorithms can be extended to PV arrays and they can be applied to PV modules. For large PV arrays, where there is a chance of occurrence of many peaks in P-V curves, the proposed algorithms can be modified for that particular condition. An intelligent algorithm can be developed which identifies one among the four proposed algorithms for a particular ambient condition and panel requirements.

Appendix-A: Experimental Setup

In this section, the experimental setup used to validate the simulation studies is presented. Chroma solar array simulator 62020H-150S is used as a PV source. It takes irradiance (G), temperature (T), datasheet parameters viz., open circuit voltage (V_{oc}), short-circuit current (I_{sc}), the voltage at maximum power (V_{mp}) and current at maximum power (I_{mp}) as input in order to get the I-V and P-V characteristics. The simulator is used in shadow test mode.

Figure 6.1: Hardware Setup

Eight modules connected in series is used as a source chapter 2, 3 and 4. Three modules connected in series are used as a source in chapter 5. Rheostat of rating (5A, 100 Ω) is used as a load. The boost converter is used as an interface between source and load. dSPACE 1206 is used as a controller for implementing the proposed MPPT algorithm. Three ADC pins in dSPACE 1206 are used for sensing PV Voltage (V), PV current (I), and output voltage (V_o). One DAC pin of dSPACE 1206 is used to get the duty ratio (d). PWM circuit converts the duty ratio into the required pulses. As the ADC pins of dSPACE 1206 cannot accept more than 10V, the voltage and current sensors are scaled down using a scaling circuit. The value of the voltage is scaled down from 230V to 3.3V and given to the controller. Similarly, the value of the current is converted into an equivalent voltage, i.e., 2V is equal to 2A. The entire hardware setup is presented in Fig. 6.1.

Appendix-B: IV Tracer

This device is manufactured by HT instruments. This I-V tracer I-V400V is used for measurement of I-V Curve of one or more modules or of one whole string. It is used for measurement of open circuit voltage and short circuit current. The database of 30 selectable photovoltaic modules is embedded in this device. IV tracer is presented in Fig.6.2.

Figure 6.2: Hardware Setup

The characteristics of IV Tracer are presented in Table 6.1.

Table 6.1: Specifications of IV Tracer

Maximum Open Circuit Voltage	:	1000V
Maximum Short Circuit Current	:	15A
Measurement category	:	CAT III 300V
Internal memory capacity	:	200 *I-V* curves
Size (L X W X H)	:	235 X 165 X 75mm
Weight	:	1.2kg

Appendix-C: Model for plotting PV Characteristics

The *I-V* and *P-V* curves plotted are using MATLAB-Simulink presented in 6.3. Four PV modules are shown in the figure. Each PV module contains two sub-modules. So there are eight sub-modules each connected with bypass diodes in anti-parallel. The datasheet parameters of these modules are presented in Table 2.1. PV panel. The modelling is done using the method presented in (Villalva et al., 2009). The algorithm is presented inside each PV block. The inputs to the block are given by double-clicking each PV sub-module. The inputs are presented in Fig. 6.4. There are 11 different datasheets incorporated in these models. These datasheets are named in the order of 1 to 11. The details of the datasheets can be found in the initialization section of the PV module mask. The irradiance refers to the irradiance of the single sub-module. The cell temperature is given in Temperature tab. Nss is the number of modules in series. Npp is the number of series connected modules in parallel. The output of the PV modules is connected to the controlled voltage source. A ramp signal with a slope of open circuit voltage is given as input to the controlled voltage source. The simulation time is kept as 1s. The value of PV voltage, PV current, and PV power are obtained at the end of the simulation. These values are used for plotting the *I-V* and *P-V* characteristics.
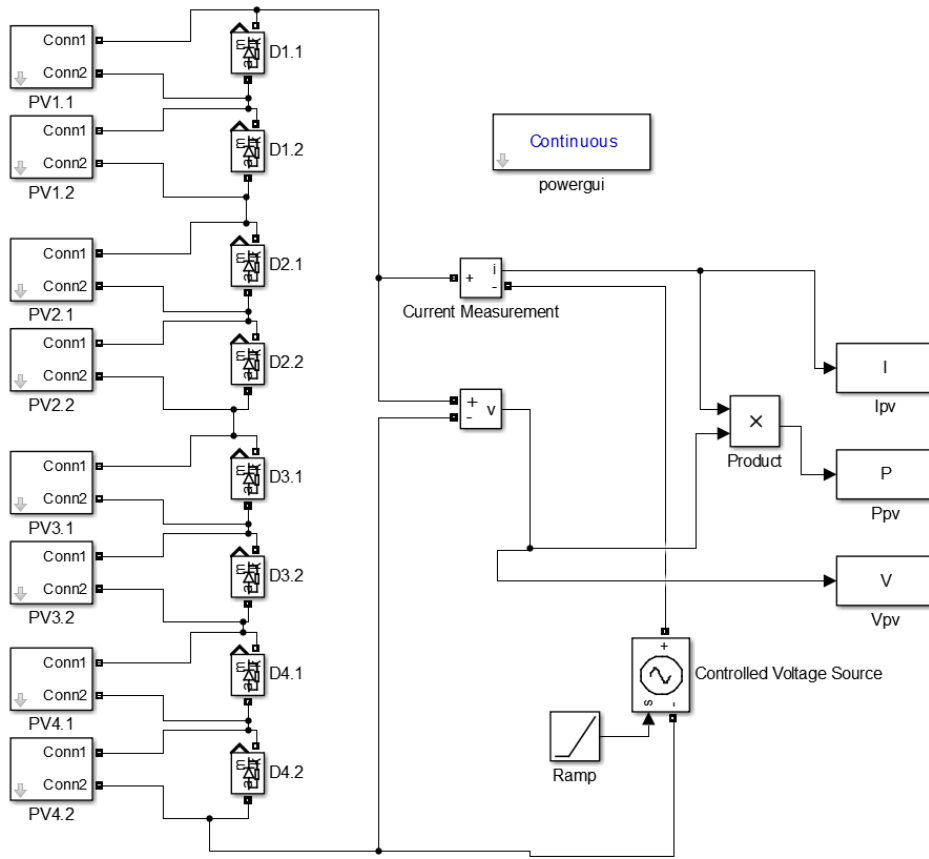
Figure 6.3: Simulink model for obtaining PV characteristics
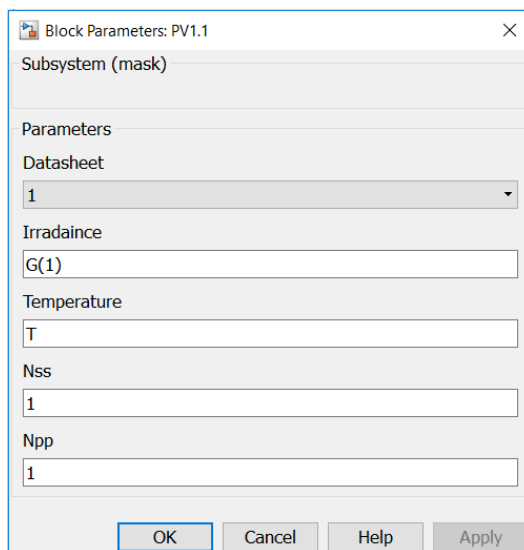
Figure 6.4: Inputs of each PV sub-module

118

Appendix-D: MicroLabBox

MicroLabBox is designed for use in a laboratory environment which can be used for control prototyping. It contains a DS1202 base board. The baseboard contains a real-time dual-core processor and a separate co-processor that manages host PC communications. The MicroLabBox contains an RTI blockset for modeling the custom control algorithms and access them virtually through I/O and the capabilities of the MicroLabBox in Simulink. The MicroLabBox is presented in Fig. 6.5.

Figure 6.5: MicroLabBox

The specificaytions of MicroLabBox are as follows:

- NXP (Freescale) dual-core processor

- 1GB DRAM 128MB flash memory

- Autonomous booting of applications from flash (depending on application size)

- Integrated Gigabit Ethernet host interface

- USB 2.0 interface for data logging

- 2 CAN channels

- 2 x UART (RS232/422/485) interface

- 1 x LVDS interface to connect with the Programmable Generic Interface PGI1

- Xilinx Kintex-7 XC7K325T FPGA

- 8 14-bit Analog input channels, 10 Msps

- Input voltage range from -10V to 10V

- 16 16-bit Analog output channels, 1 Msps, settling time: 1 s

- Output voltage range from -10V to 10V

- output current is $\pm$8mA

- 48 bidirectional Digital I/O channels, 2.5/3.3/5 V (single-ended); functionality: bit I/O, PWM generation and measurement (10 ns resolution), pulse generation and measurement (10 ns resolution), 4 x SPI Master 12 bidirectional channels (RS422/485 type) to connect sensors with differential interfaces

Bibliography

Adly, M. and Besheer, A. (2012). An optimized fuzzy maximum power point tracker for stand alone photovoltaic systems: Ant colony approach. In *Industrial Electronics and Applications (ICIEA), 2012 7th IEEE Conference on*, pages 113–119. IEEE.

Ahmed, J. and Salam, Z. (2015). An improved method to predict the position of maximum power point during partial shading for pv arrays. *IEEE Transactions on Industrial Informatics*, 11(6):1378–1387.

Ahmed, N. A. and Miyatake, M. (2008). A novel maximum power point tracking for photovoltaic applications under partially shaded insolation conditions. *Electric Power Systems Research*, 78(5):777–784.

Al-Amoudi, A. and Zhang, L. (1998). Optimal control of a grid-connected pv system for maximum power point tracking and unity power factor. In *IEE conference publication*, pages 80–85. IET.

Alajmi, B. N., Ahmed, K. H., Finney, S. J., and Williams, B. W. (2013). A maximum power point tracking technique for partially shaded photovoltaic systems in microgrids. *IEEE Transactions on Industrial Electronics*, 60(4):1596–1606.

Alik, R. and Jusoh, A. (2017). Modified perturb and observe (p&o) with checking algorithm under various solar irradiation. *Solar Energy*, 148:128–139.

Babu, T. S., Rajasekar, N., and Sangeetha, K. (2015). Modified particle swarm optimization technique based maximum power point tracking for uniform and under partial shading condition. *Applied Soft Computing*, 34:613–624.

Balasankar, R., Arasu, G. T., and Raj, J. C. M. (2017). A global mppt technique invoking partitioned estimation and strategic deployment of p&o to tackle partial shading conditions. *Solar Energy*, 143:73–85.

Bastidas-Rodrguez, J. D., Franco, E., Petrone, G., Ramos-Paja, C. A., and Spagnuolo, G. (2015). Model-based degradation analysis of photovoltaic modules through series resistance estimation. *IEEE Transactions on Industrial Electronics*, 62(11):7256–7265.

Boehringer, A. F. (1968). Self-adapting dc converter for solar spacecraft power supply selbstanpassender gleichstromwandler für die energieversorgung eines sonnensatelliten. *IEEE Transactions on Aerospace and electronic Systems*, (1):102–111.

Boukenoui, R., Salhi, H., Bradai, R., and Mellit, A. (2016). A new intelligent mppt method for stand-alone photovoltaic systems operating under fast transient variations of shading patterns. *Solar Energy*, 124:124–142.

Boztepe, M., Guinjoan, F., Velasco-Quesada, G., Silvestre, S., Chouder, A., and Karatepe, E. (2014). Global mppt scheme for photovoltaic string inverters based on restricted voltage window search algorithm. *IEEE Transactions on Industrial Electronics*, 61(7):3302–3312.

Bucciarelli, L., Grossman, B., Lyon, E., and Rasmussen, N. (1980). Energy balance associated with the use of a maximum power tracer in a 100-kw-peak power system. Technical report, Massachusetts Inst. of Tech., Lexington (USA). Lincoln Lab.

Carannante, G., Fraddanno, C., Pagano, M., and Piegari, L. (2009). Experimental performance of mppt algorithm for photovoltaic sources subject to inhomogeneous insolation. *IEEE Transactions on Industrial Electronics*, 56(11):4374–4380.

Chao, K.-H., Lin, Y.-S., and Lai, U.-D. (2015). Improved particle swarm optimization for maximum power point tracking in photovoltaic module arrays. *Applied Energy*, 158:609–618.

Chen, K., Tian, S., Cheng, Y., and Bai, L. (2014). An improved mppt controller for photovoltaic system under partial shading condition. *IEEE transactions on sustainable energy*, 5(3):978–985.

Chen, Y.-T., Jhang, Y.-C., Kuo, T.-H., Liang, R.-H., and Hung, C.-W. (2016). Jumping maximum power point tracking method for pv array under partially shaded conditions. *Solar Energy*, 132:617–627.

Chiu, C.-S. (2010). Ts fuzzy maximum power point tracking control of solar power generation systems. *IEEE Transactions on Energy Conversion*, 25(4):1123–1132.

Costogue, E. and Lindena, S. (1976). Comparison of candidate solar array maximum power utilization approaches.[for spacecraft propulsion].

Cristaldi, L., Faifer, M., Rossi, M., and Toscani, S. (2012). A simplified model of photovoltaic panel. In *2012 IEEE International Instrumentation and Measurement Technology Conference Proceedings*, pages 431–436.

Cristaldi, L., Faifer, M., Rossi, M., and Toscani, S. (2014). An improved model-based maximum power point tracker for photovoltaic panels. *IEEE Transactions on Instrumentation and Measurement*, 63(1):63–71.

Das, S. and Suganthan, P. N. (2011). Differential evolution: A survey of the state-of-the-art. *IEEE transactions on evolutionary computation*, 15(1):4–31.

Dorigo, M., Birattari, M., and Stutzle, T. (2006). Ant colony optimization. *IEEE computational intelligence magazine*, 1(4):28–39.

Dorigo, M. and Gambardella, L. M. (1997). Ant colony system: a cooperative learning approach to the traveling salesman problem. *IEEE Transactions on evolutionary computation*, 1(1):53–66.

D'Souza, N. S., Lopes, L. A., and Liu, X. (2005). An intelligent maximum power point tracker using peak current control. In *2005 IEEE 36th Power Electronics Specialists Conference*, page 172. IEEE.

Eberhart, R. and Kennedy, J. (1995). A new optimizer using particle swarm theory. In *Micro Machine and Human Science, 1995. MHS'95., Proceedings of the Sixth International Symposium on*, pages 39–43. IEEE.

El-Helw, H. M., Magdy, A., and Marei, M. I. (2017). A hybrid maximum power point tracking technique for partially shaded photovoltaic arrays. *IEEE Access*, 5:11900–11908.

Enrique, J., Andújar, J., and Bohorquez, M. (2010). A reliable, fast and low cost maximum power point tracker for photovoltaic applications. *Solar Energy*, 84(1):79–89.

Fathy, A. (2015). Reliable and efficient approach for mitigating the shading effect on photovoltaic module based on modified artificial bee colony algorithm. *Renewable Energy*, 81:78–88.

Femia, N., Petrone, G., Spagnuolo, G., and Vitelli, M. (2005). Optimization of perturb and observe maximum power point tracking method. *IEEE transactions on power electronics*, 20(4):963–973.

Ghasemi, M. A., Forushani, H. M., and Parniani, M. (2016). Partial shading detection and smooth maximum power point tracking of pv arrays under psc. *IEEE Transactions on Power Electronics*, 31(9):6281–6292.

Ghasemi, M. A., Ramyar, A., and Iman-Eini, H. (2018). Mppt method for pv systems under partially shaded conditions by approximating iv curve. *IEEE Transactions on Industrial Electronics*, 65(5):3966–3975.

Harada, K. and Zhao, G. (1993). Controlled power interface between solar cells and ac source. *IEEE transactions on Power Electronics*, 8(4):654–662.

Hart, G., Branz, H., and Cox, C. (1984). Experimental tests of open-loop maximum-power-point tracking techniques for photovoltaic arrays. *Solar cells*, 13(2):185–195.

Hartmann, L. V., Vitorino, M. A., d. R. Correa, M. B., and Lima, A. M. N. (2013). Combining model-based and heuristic techniques for fast tracking the maximum-power point of photovoltaic systems. *IEEE Transactions on Power Electronics*, 28(6):2875–2885.

Hashimoto, O., Shimizu, T., and Kimura, G. (2000). A novel high performance utility interactive photovoltaic inverter system. In *Conference Record of the 2000 IEEE Industry Applications Conference. Thirty-Fifth IAS Annual Meeting and World Conference on Industrial Applications of Electrical Energy (Cat. No. 00CH37129)*, volume 4, pages 2255–2260. IEEE.

Hsiao, Y.-T. and Chen, C.-H. (2002). Maximum power tracking for photovoltaic power system. In *Conference Record of the 2002 IEEE Industry Applications Conference. 37th IAS Annual Meeting (Cat. No. 02CH37344)*, volume 2, pages 1035–1040. IEEE.

Hu, Y., Cao, W., Wu, J., Ji, B., and Holliday, D. (2014). Thermography-based virtual mppt scheme for improving pv energy efficiency under partial shading conditions. *IEEE Transactions on Power Electronics*, 29(11):5667–5672.

Hua, C., Lin, J., and Shen, C. (1998). Implementation of a dsp-controlled photovoltaic system with peak power tracking. *IEEE Transactions on Industrial Electronics*, 45(1):99–107.

Hua, C. and Lin, J. R. (1996). Dsp-based controller application in battery storage of photovoltaic system. In *Proceedings of the 1996 IEEE IECON. 22nd International Conference on Industrial Electronics, Control, and Instrumentation*, volume 3, pages 1705–1710. IEEE.

Hua, C.-C. and Lin, J.-R. (2001). Fully digital control of distributed photovoltaic power systems. In *ISIE 2001. 2001 IEEE International Symposium on Industrial Electronics Proceedings (Cat. No. 01TH8570)*, volume 1, pages 1–6. IEEE.

Hussein, K., Muta, I., Hoshino, T., and Osakada, M. (1995). Maximum photovoltaic power tracking: an algorithm for rapidly changing atmospheric conditions. *IEE Proceedings-Generation, Transmission and Distribution*, 142(1):59–64.

Ishaque, K. and Salam, Z. (2013a). A deterministic particle swarm optimization maximum power point tracker for photovoltaic system under partial shading condition. *IEEE transactions on industrial electronics*, 60(8):3195–3206.

Ishaque, K. and Salam, Z. (2013b). A deterministic particle swarm optimization maximum power point tracker for photovoltaic system under partial shading condition. *IEEE transactions on industrial electronics*, 60(8):3195–3206.

Ishaque, K., Salam, Z., Amjad, M., and Mekhilef, S. (2012a). An improved particle swarm optimization (pso)–based mppt for pv with reduced steady-state oscillation. *IEEE transactions on Power Electronics*, 27(8):3627–3638.

Ishaque, K., Salam, Z., Shamsudin, A., and Amjad, M. (2012b). A direct control based maximum power point tracking method for photovoltaic system under partial shading conditions using particle swarm optimization algorithm. *Applied Energy*, 99:414–422.

Jain, S. and Agarwal, V. (2004). A new algorithm for rapid tracking of approximate maximum power point in photovoltaic systems. *IEEE power electronics letters*, 2(1):16–19.

Jedari, M. and Fathi, S. H. (2017). A new approach for photovoltaic arrays modeling and maximum power point estimation in real operating conditions. *IEEE Transactions on Industrial Electronics*, PP(99):1–1.

Jena, D. and Ramana, V. V. (2015). Modeling of photovoltaic system for uniform and non-uniform irradiance: A critical review. *Renewable and Sustainable Energy Reviews*, 52:400–417.

Jiang, L. L., Maskell, D. L., and Patra, J. C. (2013). A novel ant colony optimization-based maximum power point tracking for photovoltaic systems under partially shaded conditions. *Energy and Buildings*, 58:227–236.

Karatepe, E., Hiyama, T., et al. (2009). Artificial neural network-polar coordinated fuzzy controller based maximum power point tracking control under partially shaded conditions. *IET Renewable Power Generation*, 3(2):239–253.

Kasa, N., Iida, T., and Chen, L. (2005). Flyback inverter controlled by sensorless current mppt for photovoltaic power system. *IEEE Transactions on Industrial Electronics*, 52(4):1145–1152.

Kasa, N., Iida, T., and Iwamoto, H. (2000). Maximum power point tracking with capacitor identificator for photovoltaic power system.

Killi, M. and Samanta, S. (2015). Modified perturb and observe mppt algorithm for drift avoidance in photovoltaic systems. *IEEE Transactions on Industrial Electronics*, 62(9):5549–5559.

Kim, Y., Jo, H., and Kim, D. (1996). A new peak power tracker for cost-effective photovoltaic power system. In *IECEC 96. Proceedings of the 31st Intersociety Energy Conversion Engineering Conference*, volume 3, pages 1673–1678. IEEE.

Kobayashi, K., Takano, I., and Sawada, Y. (2006). A study of a two stage maximum power point tracking control of a photovoltaic system under partially shaded insolation conditions. *Solar energy materials and solar cells*, 90(18):2975–2988.

Kotti, R. and Shireen, W. (2015). Efficient mppt control for pv systems adaptive to fast changing irradiation and partial shading conditions. *Solar Energy*, 114(Supplement C):397 – 407.

Koutroulis, E. and Blaabjerg, F. (2012). A new technique for tracking the global maximum power point of pv arrays operating under partial-shading conditions. *IEEE Journal of Photovoltaics*, 2(2):184–190.

Koutroulis, E., Kalaitzakis, K., and Voulgaris, N. C. (2001). Development of a microcontroller-based, photovoltaic maximum power point tracking control system. *IEEE Transactions on power electronics*, 16(1):46–54.

Kumar, N., Hussain, I., Panigrahi, B., et al. (2017a). Mppt in dynamic condition of partially shaded pv system by using wode technique. *IEEE Transactions on Sustainable Energy*.

Kumar, N., Hussain, I., Singh, B., and Panigrahi, B. (2017b). Rapid mppt for uniformly and partial shaded pv system by using jayade algorithm in highly fluctuating atmospheric conditions. *IEEE Transactions on Industrial Informatics*.

Lei, M., Yaojie, S., Yandan, L., Zhifeng, B., Liqin, T., and Jieqiong, S. (2011). A high performance mppt control method. In *Materials for Renewable Energy & Environment (ICMREE), 2011 International Conference on*, volume 1, pages 195–199. IEEE.

Liu, F., Duan, S., Liu, F., Liu, B., and Kang, Y. (2008). A variable step size inc mppt method for pv systems. *IEEE Transactions on industrial electronics*, 55(7):2622–2628.

Maghami, M. R., Hizam, H., Gomes, C., Radzi, M. A., Rezadad, M. I., and Hajighorbani, S. (2016). Power loss due to soiling on solar panel: A review. *Renewable and Sustainable Energy Reviews*, 59:1307–1316.

Mahmoud, Y. and El-Saadany, E. F. (2016). Fast power-peaks estimator for partially shaded pv systems. *IEEE Transactions on Energy Conversion*, 31(1):206–217.

Mahmoud, Y. and El-Saadany, E. F. (2017). A novel mppt technique based on an image of pv modules. *IEEE Transactions on Energy Conversion*, 32(1):213–221.

Manickam, C., Raman, G. R., Raman, G. P., Ganesan, S. I., and Nagamani, C. (2016). A hybrid algorithm for tracking of gmpp based on p o and pso with reduced power oscillation in string inverters. *IEEE Transactions on Industrial Electronics*, 63(10):6097–6106.

Masoum, M. A., Dehbonei, H., and Fuchs, E. F. (2002a). Theoretical and experimental analyses of photovoltaic systems with voltage and current-based maximum power-point tracking. *IEEE Transactions on Energy Conversion*, 17(4):514–522.

Masoum, M. A., Dehbonei, H., and Fuchs, E. F. (2002b). Theoretical and experimental analyses of photovoltaic systems with voltageand current-based maximum power-point tracking. *IEEE Transactions on energy conversion*, 17(4):514–522.

Mohan, N. and Undeland, T. M. (2007). *Power electronics: converters, applications, and design.* John Wiley & Sons.

Nguyen, T. L. and Low, K. S. (2010a). A global maximum power point tracking scheme employing direct search algorithm for photovoltaic systems. *IEEE Transactions on Industrial Electronics*, 57(10):3456–3467.

Nguyen, T. L. and Low, K.-S. (2010b). A global maximum power point tracking scheme employing direct search algorithm for photovoltaic systems. *IEEE transactions on Industrial Electronics*, 57(10):3456–3467.

Oshaba, A., Ali, E., and Abd-Elazim, S. (2015). Artificial bee colony algorithm based maximum power point tracking in photovoltaic system. *WSEAS Trans. Power Syst*, 10(123134):22.

Parlak, K. S. (2014). Fpga based new mppt (maximum power point tracking) method for pv (photovoltaic) array system operating partially shaded conditions. *Energy*, 68(Supplement C):399 – 410.

Patel, H. and Agarwal, V. (2008). Matlab-based modeling to study the effects of partial shading on pv array characteristics. *IEEE transactions on energy conversion*, 23(1):302–310.

Piegari, L. and Rizzo, R. (2010). Adaptive perturb and observe algorithm for photovoltaic maximum power point tracking. *IET Renewable Power Generation*, 4(4):317–328.

Pragallapati, N., Sen, T., and Agarwal, V. (2017). Adaptive velocity pso for global maximum power control of a pv array under nonuniform irradiation conditions. *IEEE Journal of Photovoltaics*, 7(2):624–639.

Punitha, K., Devaraj, D., and Sakthivel, S. (2013). Development and analysis of adaptive fuzzy controllers for photovoltaic system under varying atmospheric and partial shading condition. *Applied Soft Computing*, 13(11):4320–4332.

Rakhshan, M., Vafamand, N., Khooban, M. H., et al. (2017). Maximum power point tracking control of photovoltaic systems: A polynomial fuzzy model-based approach. *IEEE Journal of Emerging and Selected Topics in Power Electronics*.

Ram, J. P. and Rajasekar, N. (2017). A new robust, mutated and fast tracking lpso method for solar pv maximum power point tracking under partial shaded conditions. *Applied Energy*, 201:45–59.

Ramaprabha, R., Balaji, M., and Mathur, B. (2012). Maximum power point tracking of partially shaded solar pv system using modified fibonacci search method with fuzzy controller. *International Journal of Electrical Power & Energy Systems*, 43(1):754–765.

Ramli, M. A., Ishaque, K., Jawaid, F., Al-Turki, Y. A., and Salam, Z. (2015). A modified differential evolution based maximum power point tracker for photovoltaic system under partial shading condition. *Energy and Buildings*, 103:175–184.

Ramyar, A., Iman-Eini, H., and Farhangi, S. (2017). Global maximum power point tracking method for photovoltaic arrays under partial shading conditions. *IEEE Transactions on Industrial Electronics*, 64(4):2855–2864.

Schellnhuber, H.-J. (2004). *World in transition: Towards sustainable energy systems*, volume 3. Earthscan.

Schoeman, J. J. and Wyk, J. D. V. (1982). A simplified maximal power controller for terrestrial photovoltaic panel arrays. In *1982 IEEE Power Electronics Specialists conference*, pages 361–367.

Sedra, A. S. and Smith, K. C. (1998). *Microelectronic circuits*, volume 1. New York: Oxford University Press.

Sekhar, P. C. and Mishra, S. (2014). Takagi–sugeno fuzzy-based incremental conductance algorithm for maximum power point tracking of a photovoltaic generating system. *IET Renewable Power Generation*, 8(8):900–914.

Shen, Q., Jiang, J.-H., Tao, J.-c., Shen, G.-l., and Yu, R.-Q. (2005). Modified ant colony optimization algorithm for variable selection in qsar modeling: Qsar studies of cyclooxygenase inhibitors. *Journal of chemical information and modeling*, 45(4):1024–1029.

Skoplaki, E. and Palyvos, J. A. (2009). On the temperature dependence of photovoltaic module electrical performance: A review of efficiency/power correlations. *Solar energy*, 83(5):614–624.

Spertino, F., Ahmad, J., Ciocia, A., Leo, P. D., Murtaza, A. F., and Chiaberge, M. (2015). Capacitor charging method for iv curve tracer and mppt in photovoltaic systems. *Solar Energy*, 119(Supplement C):461 – 473.

Subiyanto, S., Mohamed, A., and Hannan, M. (2012). Intelligent maximum power point tracking for pv system using hopfield neural network optimized fuzzy logic controller. *Energy and Buildings*, 51:29–38.

Subudhi, B. and Pradhan, R. (2013). A comparative study on maximum power point tracking techniques for photovoltaic power systems. *IEEE Transactions on sustainable energy*, 4(1):89–98.

Sundareswaran, K., Peddapati, S., and Palani, S. (2014). Mppt of pv systems under partial shaded conditions through a colony of flashing fireflies. *IEEE Transactions on Energy Conversion*, 29(2):463–472.

Sundareswaran, K., Sankar, P., Nayak, P., Simon, S. P., and Palani, S. (2015). Enhanced energy output from a pv system under partial shaded conditions through artificial bee colony. *IEEE transactions on sustainable energy*, 6(1):198–209.

Taghvaee, M., Radzi, M., Moosavain, S., Hizam, H., and Marhaban, M. H. (2013a). A current and future study on non-isolated dc–dc converters for photovoltaic applications. *Renewable and Sustainable Energy Reviews*, 17:216–227.

Taghvaee, M., Radzi, M., Moosavain, S., Hizam, H., and Marhaban, M. H. (2013b). A current and future study on non-isolated dc–dc converters for photovoltaic applications. *Renewable and Sustainable Energy Reviews*, 17:216–227.

Taheri, H., Salam, Z., Ishaque, K., et al. (2010). A novel maximum power point tracking control of photovoltaic system under partial and rapidly fluctuating shadow conditions using differential evolution. In *Industrial Electronics & Applications (ISIEA), 2010 IEEE Symposium on*, pages 82–87. IEEE.

Tang, S., Sun, Y., Chen, Y., Zhao, Y., Yang, Y., and Szeto, W. (2017). An enhanced mppt method combining fractional-order and fuzzy logic control. *IEEE Journal of Photovoltaics*, 7(2):640–650.

Teulings, W., Marpinard, J., Capel, A., and O'sullivan, D. (1993). A new maximum power point tracking system. In *Proceedings of IEEE Power Electronics Specialist Conference-PESC'93*, pages 833–838. IEEE.

Tey, K. S., Mekhilef, S., Yang, H.-T., and Chuang, M.-K. (2014). A differential evolution based mppt method for photovoltaic modules under partial shading conditions. *International Journal of Photoenergy*, 2014.

Titri, S., Larbes, C., Toumi, K. Y., and Benatchba, K. (2017). A new mppt controller based on the ant colony optimization algorithm for photovoltaic systems under partial shading conditions. *Applied Soft Computing*, 58:465–479.

Tsang, K. and Chan, W. (2013). Model based rapid maximum power point tracking for photovoltaic systems. *Energy conversion and management*, 70:83–89.

Veerachary, M., Senjyu, T., and Uezato, K. (2001). Maximum power point tracking control of idb converter supplied pv system. *IEE Proceedings-Electric Power Applications*, 148(6):494–502.

Veerachary, M., Senjyu, T., and Uezato, K. (2002). Voltage-based maximum power point tracking control of pv system. *IEEE Transactions on aerospace and electronic systems*, 38(1):262–270.

Villalva, M. G., Gazoli, J. R., and Filho, E. R. (2009). Comprehensive approach to modeling and simulation of photovoltaic arrays. *IEEE Transactions on Power Electronics*, 24(5):1198–1208.

Wang, Y., Li, Y., and Ruan, X. (2016). High-accuracy and fast-speed mppt methods for pv string under partially shaded conditions. *IEEE Transactions on Industrial Electronics*, 63(1):235–245.

Wasynezuk, O. (1983). Dynamic behavior of a class of photovoltaic power systems. *IEEE transactions on power apparatus and systems*, (9):3031–3037.

Wolfs, P. J. and Tang, L. (2005). A single cell maximum power point tracking converter without a current sensor for high performance vehicle solar arrays. In *2005 IEEE 36th Power Electronics Specialists Conference*, pages 165–171. IEEE.

Xiao, W. and Dunford, W. G. (2004). A modified adaptive hill climbing mppt method for photovoltaic power systems. In *Power Electronics Specialists Conference, 2004. PESC 04. 2004 IEEE 35th Annual*, volume 3, pages 1957–1963. Ieee.

Yang, X.-S. (2009). Firefly algorithms for multimodal optimization. In *International symposium on stochastic algorithms*, pages 169–178. Springer.

Yang, X.-S. (2010). *Nature-inspired metaheuristic algorithms*. Luniver press.

Zhang, L., Al-Amoudi, A., and Bai, Y. (2000). Real-time maximum power point tracking for grid-connected photovoltaic systems. In *2000 Eighth International Conference on Power Electronics and Variable Speed Drives (IEE Conf. Publ. No. 475)*, pages 124–129.

PUBLICATIONS BASED ON THE THESIS

Papers in refereed journals

1. **Vanjari Venkata Ramana**, Arjun Mudlapur, Roopa Viswadev Damodaran, B Venkatesaperumal and Sukumar Mishra., "Global Peak Tracking of Photovoltaic Array Under Mismatching Conditions Using Current Control.", *IEEE Transactions on Energy Conversion.*

Papers published in referred conference proceedings

1. **Vanjari Venkata Ramana**, Arjun M, Roopa Viswadev Damodaran, B.Venkatesaperumal, and Sukumar Mishra., "Efficient global peak tracking of PV system under mismatching conditions using searching technique and bisection method" in Proc. *IEEE IEEMA Engineer Infinite Conference (eTechNxT), Noida, India.*

Bio-data

Name : Vanjari Venkata Ramana

Date of birth: 04-08-1990

Marital status: Unmarried

E-mail: venkat.vr90@gmail.com

Mobile: +91-9632238998

Education

- **M.Tech (Research).**, Power and Energy Systems, National Institute of Technology Karnataka, Surathkal, 2014.

- **B.Tech.**, Electrical & Electronics Engineering, Gokula Krishna College of Engineering, Sullurupeta, 2011.

Experience

- **Research Associate** in Department of Electrical and Electronics Engineering, National Institute of Technology Karnataka for CPRI funded project " FPGA based Maximum Power Point Tracking (MPPT) of Photovoltaic System Using Artificial Intelligence" from April 2015 to July 2016.

Awards

- Received POSOCO Power System Award (PPSA)-2015 for research work in Master's Programme organized by Power System Operation Corporation Ltd. (POSOCO) in association with Foundation for Innovation and Technology Transfer (FIIT) at IIT Delhi.

Address

Plot No. 3

Gayatri Nagar Extension, Kotapolur Road

Sullurupeta, Andhra Pradesh -524121, India.